

1971

Fatigue behavior of rolled and welded beams, PhD. dissertation, October 1971

Manfred A. Hirt

Follow this and additional works at: <http://preserve.lehigh.edu/engr-civil-environmental-fritz-lab-reports>

Recommended Citation

Hirt, Manfred A., "Fatigue behavior of rolled and welded beams, PhD. dissertation, October 1971" (1971). *Fritz Laboratory Reports*. Paper 324.
<http://preserve.lehigh.edu/engr-civil-environmental-fritz-lab-reports/324>

This Technical Report is brought to you for free and open access by the Civil and Environmental Engineering at Lehigh Preserve. It has been accepted for inclusion in Fritz Laboratory Reports by an authorized administrator of Lehigh Preserve. For more information, please contact preserve@lehigh.edu.

FATIGUE BEHAVIOR OF ROLLED AND WELDED BEAMS

by

Manfred A. Hirt

A Dissertation
Presented to the Graduate Committee
of Lehigh University
in Candidacy for the Degree of
Doctor of Philosophy
in the
Department of Civil Engineering

FRITZ ENGINEERING
LABORATORY LIBRARY

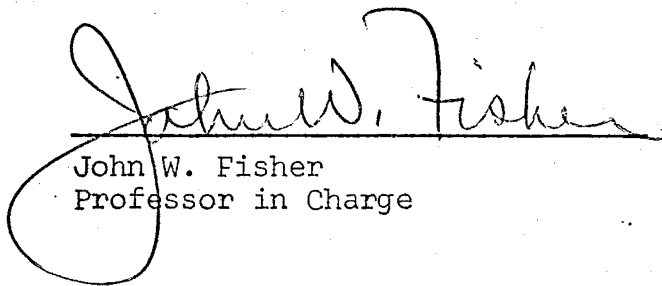
Lehigh University
Bethlehem, Pennsylvania

October 1971

CERTIFICATE OF APPROVAL

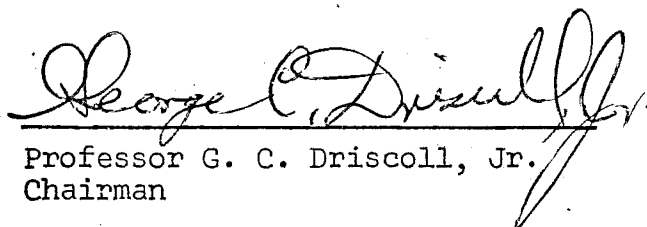
Approved and recommended for acceptance as a dissertation in partial fulfillment of the requirements for the degree of Doctor of Philosophy.

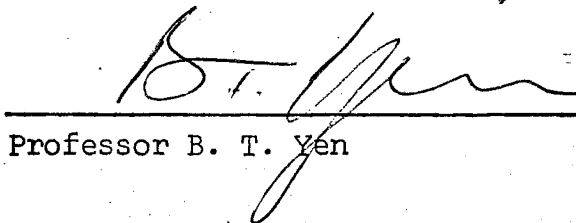
July 14, 1971
(date)

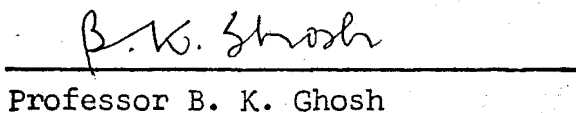

John W. Fisher
Professor in Charge

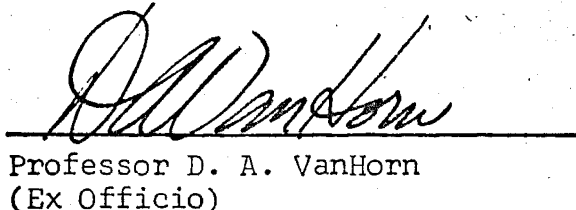
Accepted July 23, 1971
(date)

Special committee directing
the doctoral work of
Mr. Manfred A. Hirt


Professor G. C. Driscoll, Jr.
Chairman


Professor B. T. Yen


Professor B. K. Ghosh


Professor D. A. VanHorn
(Ex Officio)

ACKNOWLEDGEMENTS

This dissertation is based in part on the experimental and theoretical investigations made during the course of a research program on the effect of weldments on the fatigue strength of steel beams. The research was performed under National Highway Research Program Project 12-7 at Fritz Engineering Laboratory, Department of Civil Engineering, Lehigh University, Bethlehem. Dr. Lynn S. Beedle is the Director of the Laboratory and Dr. D. A. VanHorn is Chairman of the Department of Civil Engineering.

The author wishes to thank Professor John W. Fisher, supervisor of the doctoral and research work, for his advice, encouragement, and patience. The guidance of Professors George C. Driscoll, Ben T. Yen, Bhaskar K. Ghosh and David A. VanHorn, members of the Special Committee directing the author's doctoral work, is gratefully acknowledged.

The author wishes to express his appreciation for the helpful suggestions made by Professors G. R. Irwin, A. W. Pense, and R. W. Hertzberg on the fracture mechanics and metallurgical aspects of this work. Special thanks are due his colleague, Mr. Karl H. Frank, for the cooperation and challenging discussions during the progress of this study.

Sincere thanks are due Mrs. Charlotte Yost for the careful typing, Mr. Richard Sopko for the outstanding photographic work, and Mr. John Gera and his staff for the line drawings.

Finally, the author wishes to express his keen appreciation and thanks to his wife, Hanneliese, for her understanding and encouragement throughout the preparation of this dissertation.

TABLE OF CONTENTS

	<u>Page</u>
ABSTRACT	1
1. INTRODUCTION	3
1.1 Background	3
1.2 Objectives	5
1.3 Outline of Work	6
2. TEST PROGRAM	10
2.1 Experiment Variables	10
2.2 Fabrication	11
2.3 Testing Procedures	12
2.4 Additional Investigations	13
3. DISCUSSION OF TEST RESULTS	15
3.1 Summary of Findings	15
3.2 Description and Characterization of Flaws	19
3.3 Distribution of Residual Stresses	26
3.4 Crack Growth Observation on a Plain-Welded Beam	29
4. FATIGUE STRENGTH OF WELDED AND ROLLED BEAMS	33
4.1 The Influence of Flaws on the Fatigue Strength	33
4.2 Crack Distribution in Welded Beams	43
5. EVALUATION OF FATIGUE BEHAVIOR USING FRACTURE MECHANICS CONCEPTS	48
5.1 Summary of Fracture Mechanics Concepts	48
5.2 Application to the Plain-Welded Beam	53
5.3 Comparison of Crack Growth in Beams with Crack Propagation Studies	67

	<u>Page</u>
5.4 Influence of Geometrical and Material Factors on Crack Growth in Welded Beams	76
5.5 Applicability of Crack Model and Predictions of Fatigue Life	80
6. INITIAL FLAWS AND FABRICATION OF ROLLED AND WELDED BEAMS WITHOUT ATTACHMENTS	89
6.1 Plain-Welded Beams	89
6.2 Plain-Rolled Beams	91
7. CONCLUSIONS	93
NOMENCLATURE	98
FIGURES	104
REFERENCES	143
VITA	150

LIST OF FIGURES

<u>Figure</u>		<u>Page</u>
1	Loading geometry and cross-sections of plain-welded and plain-rolled beams	105
2	Examples of porosity from the root of the longitudinal fillet weld	106
	(a) Typical gas pore	106
	(b) Pore elongated and perpendicular to the weld surface	106
3	Schematic of possible locations for crack initiation in welded beams	107
4	Small fatigue cracks originating from porosity in the flange-to-web fillet weld, and growing perpendicular to the axis of the weld	108
	(a) Location and distribution of shapes and sizes of pores in the longitudinal fillet weld	108
	(b) Small fatigue crack completely inside the fillet weld	108
5	Crack initiation from lack of fusion of the fillet weld in the flange	109
6	Local undercut in the flange at the location of the continuous weld passing over a tack weld	109
7	Initiation of a crack at the start of a weld repair placed to fill insufficient weld profile	110
8	Crack initiation from a flaw in the rolled surface of a plain-rolled beam	110
9	Examples for crack-initiation from the flange-tip	111
	(a) Lamination at the flange-tip of a rolled beam	111
	(b) Severe notch at the flame-cut flange-tip of a welded beam	111

<u>Figure</u>		<u>Page</u>
10	Schematic of distribution and redistribution of residual stresses in welded beams	112
11	Summary of crack-growth study on a plain-welded beam	113
12	Measurements of crack sizes of a three-ended crack in the test beam	114
13	Schematic of the stages of crack growth from a pore in the fillet weld	115
14	Fatigue test data of plain-welded beams failing from porosity	116
15	Comparison of all welded beams failing from porosity in the fillet weld with beams failing from other defects	117
16	Comparison of beams failing from weld-repair defects with the mean for porosity	118
17	Comparison of weld-repair failures with failures from stop-start positions or weld craters	119
18	Fatigue test data from welded beams with cracks originating from the flame-cut flange-tip	120
19	Comparison of rolled-beam test data with previous results of beams that developed cracks from the rolled surface	121
20	Comparison of plain-rolled and plain-welded beams with cracks originating at the flange-tip	122
21	Summary of rolled-beam data from this study and other investigations	123
22	Comparison of the frequency distribution of cracks with the stress distribution in the tension flange of plain-welded beams	124
	(a) Frequency distribution (cracks per inch)	124
	(b) Correction for load influence	124
	(c) Total bending stress at web-flange junction	124

<u>Figure</u>		<u>Page</u>
23	Two small fatigue cracks that initiated from pores in the longitudinal fillet-weld and grew perpendicular to the axis of the weld	125
24	Small crack with penetration to the fillet-weld surface	126
25	Crack in flange-to-web junction approaching the extreme fibre of the tension flange	126
26	Estimates of K-values for disc-like cracks in an infinite body	127
27	Example for the estimates of K-values of an arbitrarily shaped pore	128
28	Distribution of estimated K-values and equivalent crack-radii	129
29	Crack-growth rates computed from measurements on a plain-welded beam	130
30	Various stages of crack growth and corresponding growth rates for a crack in a plain-welded beam starting from a pore in the fillet weld	131
31	Ranges for crack growth as a penny-shaped crack. Scatterbands and an upper bound estimate from other crack growth studies	132
32	Comparison of theoretical crack-growth curve with Gurney's test data on a range of steel	133
33	Variation of exponent m with yield strength	134
34	Approximate mean line of Paris' data for very slow growth, and Harrison's limiting ΔK -values for non-propagating cracks	135
35	Effect of flange thickness on the fatigue life of plain-welded beams	136
36	Number of cycles required to grow a penny-shaped crack from the size a_i to size a_j	137
37	Comparison of the scatter of measured equivalent flaw-sizes with the scatter of flaw-sizes derived from fatigue data	138

<u>Figure</u>		<u>Page</u>
38	Prediction of fatigue life using various crack-models	139
39	Comparison of a predicted lower bound and a mean line with mean life and scatterband from test data	140
40	Prediction of fatigue life based on Paris' data, and comparison with observed fatigue data	141
41	Comparison of scatterband derived from beam tests with scatter of measurements from crack-growth studies on notched specimens	142

ABSTRACT

The main objective of this dissertation was to analyze and evaluate the influence of stress conditions, grade of steel, and flaw conditions on the fatigue behavior of welded and rolled beams without attachments.

The first part of this dissertation summarizes the relevant portions of the test program that provided the basis for part of this study. The observed fatigue lives of the beams were related to the flaw condition that causes crack initiation and growth. The stress-life relationship of welded beams failing from internal pores in the web-to-flange fillet weld is used as a reference for other weld defects yielding shorter fatigue lives. Rolled beam failures are shown to provide an upper bound condition for the welded beams.

A fracture mechanics model for cracks originating from pores in the web-flange connection is developed. Estimates of crack stress-intensity-factors are made that numerically describe the initial flaw condition. A crack growth equation was derived from the welded beam fatigue test data.

The derived crack growth equation is compared to crack growth measurements on a welded beam and available data from crack growth studies. Most of the fatigue life of the welded

beams was spent growing a crack from its initial size to a visible crack. This corresponded to growth rates below 10^{-6} in. per cycle where little information is available from crack growth studies.

Criteria for the design and fabrication of welded beams are outlined and related to the internal defects and existing specification provisions. It is shown for example that an increase in flange thickness and weld size should not permit an increase in allowable defect size. The initial crack size is shown to be the controlling factor for the fatigue life of the beams.

It is concluded that the fracture mechanics concepts of stable crack growth can be used to analyze welded and rolled beams. More information is needed outside the regions of available growth rate data, and on the statistical variation of the individual parameters that influence crack growth rates and hence the fatigue behavior of welded joints.

1. INTRODUCTION

1.1 BACKGROUND

The investigations of Lea and Whitman,⁽³⁷⁾ Graf,^(17,18) and Wilson⁽⁶⁴⁾ in the 1930's provided an indication of the importance of various welded details on the fatigue strength of steel beams. Large reductions in fatigue strength were observed for beams with partial-length cover plates, stiffeners, and other welded details.

The earlier fatigue studies were not very extensive. Many small studies were made with no coordination of the experiment designs. This did not permit an unbiased evaluation of the various design factors. In addition, no attempt was made to determine the experimental error.

A study^{(11)*} was initiated to investigate the effect of weldments on the fatigue strength of steel beams. Plain-rolled, plain-welded, partial-length cover-plated, and flange-spliced beams were tested. The experiment design provided for appropriate measurement of experimental error and the ability to deduce the significance of controlled variable effects.^(9,43)

* Ref. 11 contains the detailed test data relevant to a part of this dissertation.

Cover-plated beams are known to contain defects at the toe of the weld at the end of the cover plate. All weld toes were shown to have microscopic defects that were directly comparable to cracks.^(57,60) Fractographic examination of cracks from plain-welded beams revealed that gas pores in the web-to-flange fillet welds were the most frequent location of crack initiation. Other crack-initiation sites were found at weld repairs, tack welds, and at the flame-cut flange-tips.

Plain-rolled beams do not usually contain internal flaws which result in crack initiation and growth. Most cracks in this study were observed to originate from flaws at arbitrary locations on the rolled surface of the flange. Slight irregularities at the flange-tip corners were also found to cause crack initiation and growth.

Paris⁽⁴⁶⁾ introduced the concepts of fracture mechanics to rationally evaluate the fatigue life of metal elements containing a crack. Much work followed to establish crack-growth rate curves from studies on crack-growth specimens of different shapes, sizes and material. Crooker and Lange⁽⁸⁾ showed these data to fall within a common scatterband for a large group of steels.

Most crack-growth work has concentrated on the generation of crack-growth data for aluminum alloys and high strength steels. Only recently have data become available on the rate of

crack propagation in steels of various yield strengths below 100 ksi.^(4,20,24,34) Several studies examined the influence of weld material and heat affected zone on crack-growth behavior.^(24,41) Little work has been done to integrate this information into civil engineering applications.

Fracture mechanics concepts have provided an explanation for the influence of various defects and geometry on the fatigue life of cover-plated beams.⁽¹¹⁾ Harrison⁽²²⁾ has used fracture mechanics to describe a variety of flaw conditions in butt-welds. Maddox⁽⁴²⁾ successfully predicted the fatigue life of a structural specimen based on information from crack-growth rate data. Lawrence and Radziminski⁽³⁶⁾ used fracture mechanics to evaluate crack initiation and propagation in butt-welded joints.

It was observed in these earlier studies^(22,36) that the size and geometry of the defects were the controlling factors in the fatigue behavior of the welded details. Pores in the web-to-flange fillet weld of beams constitute a similar defect.

1.2 OBJECTIVES

The main objective of this dissertation was to analyze and evaluate the influence of stress, grade of steel, and flaw conditions on the fatigue behavior of welded and rolled beams. This included the following evaluations and study:

- (1) Analysis of fatigue test data from rolled and welded beams.
- (2) Description and characterization of the flaw conditions that exist in plain-welded and plain-rolled beams without attachments.
- (3) The integration of fracture mechanics concepts for fatigue into civil engineering application.
- (4) Examination of the influence of geometry and material factors using fracture mechanics and an appropriate model to describe the behavior of the welded beams.
- (5) Discussion of crack-growth data and its applicability for estimates of the fatigue life of structural elements.
- (6) Suggestion of fabrication and design criteria for welded and rolled beams. This includes an evaluation of critical design factors and initial defect conditions.

1.3 OUTLINE OF WORK

The first part of this dissertation summarizes the relevant portions of the test program⁽¹¹⁾ that provided a basis for part of this study. Findings from the statistically evaluated test data including the influence of grade of steel and the major stress variables on the fatigue strength of welded and rolled beams are summarized.

Earlier studies had indicated that various flaw conditions existed in welded and rolled beams. These flaw conditions are examined and discussed in more detail in this dissertation. Both internal and external weld defects in the web-to-flange fillet weld of welded beams were evaluated. Internal pores caused by entrapped gas in the weldment are known to form a common defect and these are examined in detail. Weld repairs, tack welds, and other weld discontinuities are discussed and related to the behavior of beams with porosity.

Micro-flaws in the rolled surface were observed to be the controlling defects for crack initiation and growth in rolled beams. Cracks were also observed to originate from the flange-tips of both rolled and welded beams. The flange-tip flaws in rolled beams are believed to be introduced by the rolling operation. The notch condition at the flange-tips of the welded beams resulted from the flame-cut flange-edge.

Chapter 4 relates the observed fatigue lives of the test beams to the observed flaw conditions. The stress-life relationship of welded beams failing from internal pores in the fillet weld is established and used as a reference for other weld defects and rolled beam failures. The data are also used to develop a fracture mechanics model of the crack. The scatter in the data is discussed, and mean lines and confidence limits are introduced where appropriate.

The application of fracture mechanics concepts to characterize the fatigue behavior of rolled and welded beams without attachments is introduced in Chapter 5. A fracture mechanics model for cracks originating from pores in the web-to-flange fillet weld is compared with the test data. Estimates of the stress-intensity factor are made that correspond to the initial flaw condition. Since the final crack size was known, a theoretical crack-growth equation is derived from the welded beam test data.

The derived crack-growth equation is also compared to other crack-growth measurements including a welded beam and special crack-growth specimens. The correlation is discussed and the influence of parameters such as specimen shape, thickness, and material on crack growth is evaluated. The regime where most of the time is spent growing a fatigue crack in a structural element is shown to have little experimental crack-growth data available. The problems connected with extrapolation into regions outside the crack-growth data are discussed.

Deviations from the assumed straight-line model at the lower and upper end of the crack-growth curve are noted and discussed. Crack growth under various stress conditions is compared with the welded-beam behavior under the influence of welding residual stresses. Very slow growth rates are discussed and related to the observed run-out test data from welded and rolled beams.

The evaluation of the influence of geometrical and material factors on the fatigue life of welded beams is based on the fracture mechanics model of a penny-shaped crack. The scatter of the beam fatigue-test data is compared to the variation in measured defect size and variations in the fatigue crack-growth rate.

The relationship between the fatigue strength of rolled and welded beams and various defects is reviewed in Chapter 6. An upper bound condition for the life of all welded beams is discussed. Criteria for the design and fabrication of welded beams are outlined and related to the initial defect.

2. TEST PROGRAM

2.1 EXPERIMENT VARIABLES

The major objective of the study on the "effect of weldments on the fatigue strength of steel beams"⁽¹¹⁾ was to develop suitable mathematical design relationships between applied stresses and fatigue life. The principal variables were grouped into the three categories: (1) type of steel, (2) type of beams and details, and (3) stress variables. The discussion in this dissertation is concentrated on the fatigue behavior of rolled and welded beams without attachments. The relevant data are reported in detail in Ref. 11.

Three grades of steel were included in the welded beam study: ASTM A36, A441, and A514 representing material with yield strengths between 36 ksi and 100 ksi. All plate material for the fabrication of the welded beams (Fig. 1) for each grade of steel came from the same heat.

Only A36 and A441 steel rolled beams (W14x30) were included in the original test program.⁽¹¹⁾ A514 steel rolled beams (W14x30 and W10x25) were tested during the continuing study and the test data are included in this dissertation. The steel for the rolling of the beams came from the same heat for each grade of steel, except for the smaller A514 section where steel from two heats was used.

The primary stress variables were selected as minimum stress S_{\min} , and stress range S_r , in a factorial experiment design. (9,11) All stresses, unless otherwise noted, refer to the bending stress at the extreme fibre of the tension flange of the beam. For different levels of minimum stress various stress ranges were examined. This had the advantage that one variable could be changed while the other was kept constant, as compared to stress ratio where both, minimum and maximum stress have to be adjusted simultaneously for a given value of stress ratio. The arrangement in the factorial also permitted an evaluation of the influence of maximum stress.

2.2 FABRICATION

All welded beams were fabricated using the same technique. The flange and web plates were flame cut to size and the weld areas blast cleaned. The components were then assembled in a jig and tack welded at about 10 inch intervals. The 3/16 inch web-to-flange fillet welds were placed by the automatic submerged arc process. L60 electrodes of 5/64 inch diameter were used for the A36 and A441 grade steel, and L61 electrodes of the same diameter for A514 grade steel. The other weld parameters were 350A, 30V at a weld speed of 23 in./minute. A Lincoln No. 780 flux was used.

The fabricator was instructed to use fabrication

procedures, workmanship and inspection requirements in common use by state highway departments for bridge construction. Tack welds and weld repairs were noted by paint marks on the web to facilitate the test evaluation. The burned edges of the flange plates were kept to a roughness of approximately 1000 or less according to ASA (American Standard ASA B46.1-1962, Surface Texture). The roughness of the rolled beam flanges was about 250 or less and was highest on the inside edge of the flange tip.

2.3 TESTING PROCEDURES

All welded and the A36 and A441 steel rolled beams were tested on a ten-foot span with the two point loading shown in Fig. 1. The load was applied by a hydraulic jack through a spreader beam. The distance between the load points was 42 inches. The constant moment region was reduced to 24 inches and 18 inches for the A514 steel W14x30 and W10x25 sections, respectively. This became necessary because the limits of the load and stroke capacity of the equipment were reached when testing at higher stresses.

The pulsator activating the jack operated at between 200 and 800 cycles of load applications per minute. When reversal of loading was required, a constant upward load at the two load points was applied by a hydraulic accumulator-load system.

When the downward deflection had increased by 20/1000

inch the beams were considered to have failed. Loading was automatically discontinued through a microswitch. This usually occurred when the crack had propagated through enough of the flange for net-section yielding to occur. At this stage, most of the fatigue life of the beam was exhausted. The crack generally had destroyed 15% to 75% of the flange area.

At least two beams were tested under identical stress conditions to provide replication within the cells of the experiment factorials.⁽¹¹⁾ Random assignment of the beams to cells in the factorial and randomization of the testing sequence was used to minimize the influence of uncontrolled variables, such as temperature, humidity, laboratory and testing personnel.

2.4 ADDITIONAL INVESTIGATIONS

The residual stress distribution in the plain-welded beams was measured for all three grades of steel. Only A36 and A441 steel rolled beams were available at the time of the investigation. All data for the residual stresses measured after cyclic loading are given in Ref. 11 together with the stress distribution of a previously unloaded beam.

Redistribution of residual stress due to stepwise increased cyclic loads was further investigated in an independent program.⁽³⁹⁾ A change from a symmetric residual stress pattern to an unsymmetric pattern with respect to the neutral axis was reported.

Data was also obtained from a special study on crack propagation in a plain-welded beam. A beam that had failed prematurely from a flange-tip defect was repaired. The fillet weld was then closely examined during the continuation of testing and at intervals under static loads. After first detection of a very small crack on the surface of the fillet weld, subsequent crack growth was monitored with a 10 power magnifying glass.

3. DISCUSSION OF TEST RESULTS

3.1 SUMMARY OF FINDINGS

3.1.1 Plain-Welded Beams

A total of more than 115 welded beams were tested. This included plain-welded beams from the basic experiment and welded beams from the continuing study on the effect of stiffeners and attachments. Thirteen beams containing stiffeners or short attachments failed in the same manner as plain-welded beams.

The 56 plain-welded beams from the basic experiment covered the three grades of steel - ASTM A36, A441, and A514. The factorials for the three grades of steel were identical with the exception of two cells for the A36 grade steel. The test data are documented in Ref. 11. None of the factorials were complete because of known boundary conditions, such as yield stress or expected fatigue life outside the region of interest.

The cracks causing failure initiated in most cases at a flaw in the fillet welds of the flange-to-web junction. Most flaws were found in the vicinity of tack welds or at weld repairs. The flaw itself was usually a gas pocket or blow hole in the weld. Typical examples are shown in Fig. 2. The relatively smooth crack surface characterizes the fatigue crack which had grown

from the pore through the web-flange junction into both sides of the flange and up into the web. The portion of the junction without weld penetration, the deposited weld material and heat affected zone are apparent in the photographs of the fracture surface.

A few cracks were found to have initiated from other weld defects or from the flame-cut flange-tip. The original analysis of the data reported in Ref. 11 was based on the observed fatigue lives of the beams. A detailed examination of the various flaw conditions that caused cracking was not undertaken. In this dissertation emphasis is placed on the characterization and analysis of the different flaw conditions.

Statistical methods were used to analyze the effects of the grade of steel, and the primary stress variables of minimum stress and stress range for each grade of steel. Detailed discussion of the analysis is found in Refs. 11 and 26 and showed stress range to be the dominant variable for each grade of steel. Minimum stress and grade of steel were not significant for design purposes.

Multiple regression analysis indicated that the regression model using the logarithmic transformation of both stress range and number of cycles to failure resulted in the best fit to the data. The correlation coefficient was usually largest and the standard error smallest for this model.

However, statistical evaluations did not reveal a significantly better fit than obtained for the semi-logarithmic model. The proposed log-log model best described the data at the extreme stress range levels and was compatible with the theoretical concepts of fracture mechanics.

A comparison of the fatigue test data from earlier work with the results obtained in the welded-beam study yielded good agreement. Other studies^(10,19,50,51) also indicated that welded beams fabricated according to current procedures can be expected to exhibit crack growth from flaws in the continuously fillet-welded web-flange connection.

3.1.2 Plain-Rolled Beams

Twenty-two rolled W14x30 beams of the A36 and A441 grade steels were tested in the original test program.⁽¹¹⁾ The experiment factorials were not as extensive as used for the welded beam study and reflected the limitations in stresses because of yield strength or excessive cycle life. A514 steel rolled beams were tested during the continuation of the test program. Nine W14x30 and twenty W10x25 beams were tested. The data are summarized in Chapter 4 and are compared with earlier studies on lower strength and T-1 steels.

The cracks in the plain-rolled beams always originated from the rolled surface of the tension flange. Cracks some

distance from the load points generally initiated from a small surface flaw. This flaw occurred at random on the surface of the flange or at the inside or outside corner of the flange-tip. The flaws were always smaller than the flaws detected in the fillet-welded beams. Most beams experienced only one crack, and a number of run-out data were obtained when testing was terminated at 10 million cycles.

For rolled beams tested under partial reversal of loading, cracks tended to form at locations of high stress concentration on the contact area between the loading jack and the tension flange. A similar condition existed underneath the wooden stiffeners that were inserted at the load points (Fig. 1). The wooden stiffeners kept the flanges parallel and prevented lateral instability during testing.

The original data⁽¹¹⁾ was analyzed regardless of the different crack initiation sites. No significant effect due to type of steel or minimum stress was apparent from the data, and stress range accounted for most of the variation in cycle life. The experimental data compared well with the results from other experimental work within the region of the stresses tested.

The tests also reflected the strong sensitivity of the fatigue life of rolled beams to the initial flaw condition. At every stress range level a large scatter was observed, and one or more beams exhibited long life. In these cases, the life

approached the value reported for plain plate-specimens.

3.2 DESCRIPTION AND CHARACTERIZATION OF FLAWS

3.2.1 Locations of Crack Initiation

It was observed that cracks in the plain-welded beams always originated from a flaw in the fillet weld unless a severe notch existed at the flame-cut flange-tip. It is common knowledge⁽³⁸⁾ that a perfect weld cannot be made. Some imperfections always exist in weldments. A number of such imperfections in fillet and butt-welds are illustrated for example in Ref. 25. Their cause and prevention, effect on strength, and proposed correction are also outlined.

The term defect is defined in Ref. 38 as an imperfection or discontinuity that is judged damaging to the function of the material or weldment. The term flaw is generally used in this dissertation to indicate an imperfection or discontinuity in the base material, in the weldment, or introduced by the weld. A flaw may become a defect under certain stress conditions.

Typical conditions that may become critical and result in crack growth in a welded beam are schematically shown in Fig. 3. The flaws can be classified into three groups according to their general location in the cross-section:

1. Internal Weld Flaws (a) porosity and slab inclusions
(b) lack of fusion
(c) partial penetration
2. External Weld Flaws (a) undercut
(b) weld repair
(c) stop-start position
(d) weld spatter
(e) micro-flaws at weld toe
3. Surface Flaws (a) flange tip irregularities
(b) rolled surface

More than 180 cracks were found in the 56 plain-welded beams of the basic experiment design. Seventy-five cracks were cut open for fractographic examination. It was found that about 80% of the cracks had originated from porosity, 10% from the start of weld repairs, and the remaining 10% from various other weld discontinuities or the flange-tip. Other flaws such as cracks due to cooling of the weldment were not observed in this study.

3.2.2 Internal Weld Flaws

The term porosity is used in this dissertation to describe the presence of cavities in the weld metal caused by the entrapment of gas. In general, porosity took the form of small cavities completely inside the weld. The gas pores appeared on

the fracture surface as rounded cavities with a smooth and shiny surface as shown in Fig. 2(a). A few pipe or blow holes extended to the surface of the weld.

Except for blow holes extending to the surface of the fillet weld, these small pores cannot be detected by visual inspection and only with great difficulty using modern non-destructive inspection techniques. Radziminski and Lawrence⁽⁴⁹⁾ observed under favorable inspection conditions on polished butt welds that defects causing crack initiation were not always the ones which appeared to be most severe from radiographic inspection.

A collection of pores over a 1-1/2 inch length of weldment from the longitudinal fillet-weld of a welded beam is shown in Fig. 4(a). The weld was mechanically opened on a 45 degree plane between flange and web. The flat surface on the bottom of the web segment shown is the unfused portion of the faying surface between web and flange. Various shapes and sizes of pores at random intervals are seen to originate from the root of the weld. Various shapes, such as elongated pores and worm-holes (a pore consisting of a series of small voids) were found inside the weld.

It is also interesting to observe that small cracks existed in most of the pores perpendicular to the axis of the weld [Fig. 4(a)]. The large, elongated pore in the center of the specimen was carefully opened. A fatigue crack with less

than 1/4 inch diameter was found as illustrated in Fig. 4(b). This crack had not penetrated to the surface of the fillet weld and was completely inside the weld.

The beams in the original test series were welded by individual weld-runs, that is, welds were not placed simultaneously on both sides of the web. This was necessary for the A514 grade beams because of restrictions on the heat input. Besides some distortion of the cross-section, more porosity (gas pockets) was found in the second weld. This is believed due to impurities that were caught between the web-edge and the flange during the first weld pass. In addition, gases could be trapped easily at the same location during the placement of the second weld especially when approaching a tack weld. More uniform flaw sizes were found in a specimen where simultaneous welding was used.

The center of the flange and the edge of the flame-cut web were blast cleaned prior to welding to insure good fusion. Only one case of lack of fusion was found (Fig. 5), and had caused a premature failure of a beam.

Partial penetration did not influence crack initiation and growth. This gap at the faying surface was parallel to the applied bending-stress direction and continuous along the span. No cracks were found to initiate at this location. Gurney⁽¹⁹⁾ observed no difference between beams welded with partial or complete penetration. Reemsnyder⁽⁵⁰⁾ reported that cracks initiated

from the corners of the gap in the shear span. The principal stress in the shear span is no longer parallel to the longitudinal direction of the gap and the sharp corner at the gap may lead to crack initiation and growth.

Several cracks originated at or under the applied loads in the shear span. Initiation of the crack proper was however from porosity in the fillet weld. Very little influence on crack growth was observed when this occurred.

3.2.3 External Weld Flaws

Most external flaws in manually placed welds are introduced by ripples on the weld surface, or at locations of change of electrode. Automatic welding reduces the surface ripples and generally eliminates many restart positions. Undercut may still occur as shown in Fig. 6. Only one crack was observed in this study to have initiated from undercutting. Current practice⁽²⁵⁾ recommends that weld metal be added at the point where undercutting occurs. Weld repairs were usually placed in this study at such locations.

Another suggested reason for repair is insufficient weld profile. The convexity of the profile is repaired by adding more weld metal. Unfortunately, a weld repair may constitute a severe notch. In most cases when a weld repair was placed, a crack initiated from the start of the repair as illustrated in

Fig. 7. The fatigue crack is recognized by the fine grained fracture surface with a circular boundary in the web-flange junction. The coarser grained surface near the circular boundary was caused by mechanical tearing of the remaining cross-section after saw-cuts had been introduced. These saw-cuts are visible in the outstanding legs of the flange and web.

Other discontinuities introduced by the automatic welding process are caused by accidental stop-start positions. These restarts are equivalent to weld repairs and the common discontinuities in manually welded beams. Weld spatter was sometimes found in the vicinity of tack welds. Only one crack was found that had originated from a small weld drop.

Micro-flaws generally exist at the weld periphery. They were described as directly comparable to cracks.^(57,60) These microscopic defects are much smaller than acceptable undercut. The orientation of these toe-flaws was parallel to the applied stresses in the welded-beams and no cracks were observed to initiate from these locations.

3.2.4 Surface Flaws

Cracks in rolled beams generally initiated from small flaws in the flange surface that were apparently introduced by the normal rolling operation or by locally adhered mill-scale. These flaws were much smaller than the porosity observed in the

plain-welded beams. A typical crack starting from a surface flaw is shown in Fig. 8. The region where slow growth had prevailed over a large portion of the life is apparent from the smooth fracture appearance.

Many cracks in the A36 and A441 steel rolled beams originated at locations of high local stresses at the load points. Fretting⁽³³⁾ contributed to the initiation of these cracks. It was difficult to judge the influence of fretting and local stresses. This was also true for cracks that originated underneath the wooden stiffeners that were inserted at the load points.

Cracks initiated from the flange-tip of plain-rolled beams at the inside or outside corner. This location probably constitutes an exposed part in the rolling process. A few laminations in the flange-edge were also found to cause crack initiation and growth as illustrated in Fig. 9(a).

The only surface flaws that were critical in plain-welded beams were at the flame-cut flange-tip. During flame-cutting accidental discontinuities may occur in the advancement of the machine. Notches in the flange tip as shown in Fig. 9(b) can result and are deeper than the usual surface roughness. A severe condition can result from the sharp notch in locally embrittled material. In addition, high residual tensile stresses exist at the flame-cut flange-tip.

3.3 DISTRIBUTION OF RESIDUAL STRESSES

One welded beam of each grade of steel and one rolled beam of A36 and A441 grade steel were used for residual stress measurements. The residual stress specimens were taken from the region between the support reaction and the load point. The method of sectioning⁽⁵⁸⁾ was used to determine the distribution and the magnitude of residual stresses.

Strains were measured on both inside and outside surface of the flanges and on both sides of the web. The residual stress distributions for typical welded beams measured after completion of fatigue testing are given in Ref. 11. These studies indicated very high tensile residual stresses at the fillet weld and at the flame-cut flange-tips. The tensile residual stresses were of the order of the yield strength of the weld material at the fillet weld, and about half the yield strength at the heat-influenced flange-tip. The compressive residual stresses were about 20 ksi to 30 ksi for all three grades of steel.

Much smaller residual stresses were found in rolled beams. The normal cooling residual stress pattern was not present because the rolled beams were straightened by the rotarizing process. The resulting residual stresses were usually less than + 15 ksi.⁽¹¹⁾

It was also observed that the residual stresses in the two adjacent fillet-welds at the same flange-to-web junction were not equal. Since the fillet welds were not simultaneously placed, the welding and subsequent cooling of the second weld relieved part of the residual stresses in the first weld, and at the extreme fibre opposite the second weld.

A small reduction of residual stress was also observed after fatigue testing when compared to the as-welded state. The primary residual stress pattern was not greatly influenced and the reduction could be correlated to normal redistribution due to applied loading. An investigation⁽³⁹⁾ to further evaluate the redistribution in welded shapes was undertaken on two beams. The two A36 and A514 shapes came from the same lot of specimens used in the fatigue study.⁽¹¹⁾

A schematic of the residual stress distributions in an A36 and an A514 welded beam is shown in Fig. 10. The residual stresses in the tension and compression flanges before loading are shown by the heavy lines, and the stress patterns after loading and redistribution are indicated by the shaded areas.

A fictitious load application equivalent to 30 ksi nominal tension and compression stress in the flanges and subsequent unloading may cause a redistribution of residual stresses. A number of observations can be made from the comparison of the as-welded (heavy lines) and redistributed residual stress-

patterns (shaded areas) shown in Fig. 10.

- (1) The residual stress pattern in the tension flange of both A36 and A514 steel was likely to change because of yielding at the fillet weld. Higher applied stress may also cause the flange tip region to yield.
- (2) No changes were observed in the compression flange of the A514 steel beam because the compressive residual stresses were small when compared to the yield point. Redistribution did occur in the A36 steel beam because the compressive residual stress was much closer to the yield point of the base metal.
- (3) The residual stress patterns are no longer symmetric with respect to the nominal neutral axis after the load application. This observation was confirmed in Ref. 39.

A repetition of the applied load will cause very little additional change. Constant amplitude cyclic loading will cause fluctuations in the stresses in both flanges. The nominal stress range, $\Delta\sigma$, in the tension flange of both shapes is shown in Fig. 10. It varies between the residual stress and some maximum less than or equal to the yield stress. Hence, the full applied stress range is effective.

In the compression flange of the A514 steel, the stress fluctuation at the weld is between the yield stress and some

lower tensile stress ($\sigma_y - \Delta\sigma$). In the A36 steel beam the residual stress at the fillet weld is less than the yield point because of redistribution. The fluctuation is hence between this reduced residual stress and some lower tensile or even compressive stress ($\sigma_r - \Delta\sigma$). Hence, the full applied stress range may not always be effective. The yield level will be reached in the compressive part of the compression flange for the A36 steel beam.

3.4 CRACK GROWTH OBSERVATION ON A PLAIN-WELDED BEAM

A plain-welded beam was tested and closely observed in order to investigate crack formation and growth on the surfaces of the fillet weld, web, and flange. Measurements of crack length and load were made so that crack growth could be determined for the structural element.

Beam PRB-341 was selected for this study since it had failed prematurely after 192,000 cycles of stress from a flange-tip crack. Replicate beams tested at the same stress range of 36 ksi indicated that a crack from a gas pore could be expected to become visible within an additional 200,000 cycles. The flange-tip crack was gouged and carefully repaired with a multiple-pass butt-weld. The reinforcement was removed and the surface ground flush. The beam and especially the fillet welds were whitewashed to help detect small surface cracks.

Testing was resumed under the same stress conditions

(Fig. 1). The stresses in the extreme fibre were used to set the loads and were measured with electrical strain-gauges. The fillet welds were searched for cracks using a regular hand magnifying-glass while testing at 250 cycles per minute. A length of more than 42 inches of weld on both sides of the web was observed. The maximum vertical movement of the beam in this region was approximately 0.35 in. Testing was interrupted after 103,000 and 150,000 additional cycles so that the weld could be examined under static load. Suspicious locations were further examined with a 50-power microscope.

After the second static loading, a hairline crack was detected on the weld surface after an additional 9,000 cycles was applied. Testing was temporarily discontinued at that time after 351,700 applied stress cycles. The apparent crack size on the weld surface was found to measure about 0.05 inch when the load was removed from the beam. This increased to 0.25 in. under maximum stress of 50 ksi in the extreme fibre.

A reference grid was placed on the inside surfaces and the extreme fibre of the flange as well as on both faces of the web. The grids were placed close to the cross section containing the hairline crack. It was possible to estimate the crack-tip to within $1/5$ of a grid line (± 0.01 inch) using 50-power magnification. The hand magnifying-glass permitted about $1/2$ the grid distance to be estimated (± 0.025 inch). The crack length "a"

on the inside surface of the flange is plotted as a function of the total applied cycles in Fig. 11.

At intervals of about 18,000 cycles, testing was interrupted and the crack was measured under a statically applied maximum load. These measurements are indicated by crosses in Fig. 11. There was good agreement between the crack length measurements under dynamic and static loading.

At 402,000 cycles, a flange-tip crack occurred at the repair and testing was again halted. The crack size in the fillet weld was measured when the load was removed and is indicated by the circle in Fig. 11. The region around the flange-tip crack was removed by saw-cut and replaced by a piece of sound metal groove-welded to the three inside edges. The weld repair of the second flange-tip crack introduced considerable deformation into the beam. Hence, further testing was conducted at a reduced maximum stress of 38 ksi. The stress range was maintained at 36 ksi. Since the crack was expected to penetrate the opposite fillet weld and the extreme fibre (Fig. 11), much attention was given to the observation of these locations.

It was difficult to pinpoint the exact time at which the crack reached the extreme fibre. After about 435,000 cycles the crack was detected on the bottom surface of the flange. This was confirmed under a static load at 440,000 cycles. It was also observed that the crack had penetrated through the other fillet

weld. This was not detected under dynamically applied loads.

A first set of measurements under static maximum load was taken to establish the crack on the inside and outside of the flange, as well as in the web. This three-ended crack is schematically shown in Fig. 12. The data points for the measured dimensions, a and c , on the inside surface of the flange are plotted. Also plotted is the length, ef , of the three-ended crack on the extreme fibre of the flange. Measurements taken under static maximum load are indicated by a cross on top of the symbols.

It is apparent from Figs. 11 and 12 that the increase in crack size was very rapid after the crack had penetrated the bottom flange surface. The cross-section of the flange fractured at 567,000 cycles as the crack tip reached the flange-tip. A schematic of the advancement of the crack after it had penetrated the extreme fibre is shown in Fig. 13 and indicates a transition from a penny-shaped crack in the flange-web junction to a three-ended crack. A detailed discussion of the stages in crack growth will follow in Chapter 5.

4. FATIGUE STRENGTH OF WELDED AND ROLLED BEAMS

4.1 THE INFLUENCE OF FLAWS ON THE FATIGUE STRENGTH

4.1.1 Internal Weld Defects

Cracks initiating from pores in the fillet weld similar to those shown in Fig. 2 accounted for most of the failures in plain-welded beams. A large variety of conditions can affect the welding process⁽³⁸⁾ and cause porosity in the weld. Careful fabrication techniques can reduce the number and size of pores, but entrapped gas cannot be eliminated in commercial fabrication of structures.

Fatigue test data from beams failing at porosity in the longitudinal weld are shown in Fig. 14. Distinction is made between the three grades of steel tested (A36, A441 and A514). It is visually apparent that the beams where crack initiation from porosity was verified by fractographic inspection (solid symbols) represent the total sample of the beams well. Since each beam often contained a number of larger and smaller cracks, those examined in detail were assumed to be characteristic for the porosity that existed in all the beams tested. This sample of pores was also assumed to be stress range independent because of randomization of the beams.

Also shown in Fig. 14 is the mean line of the linear

model using the logarithmic transformation of stress range and number of cycles to failure. The equation of the mean line resulting from the least-squares fit to the data from all three grades of steel combined is given at the upper right-hand corner of the figure. Also shown is the standard error of estimate. (43,61)

Excluded from the least-squares fit were data at the 18 ksi stress range level because of the significant influence a single datum point would have on the slope of the curve. Also, this level of stress range seems to be near the run-out level.

Not shown in the figure and also excluded from the least-squares fit were the beams that failed from defects other than porosity. These include weld repairs, stop-start positions, other weld defects, and severe notches in the flame-cut flange-tips. These latter defects generally resulted in a more severe condition than porosity in the fillet-weld.

The two lines in Fig. 14 parallel to the mean line contain the scatter of the data. This scatter-band theoretically predicts with 95% confidence that 95% of all beams tested should fall within its limits. A lognormal distribution of the data was assumed. The distribution of the data has been found to be very close to the theoretical lognormal distribution. (11)

All the beams failing from porosity were replotted as solid symbols in Fig. 15. Available test results from a current

study on welded beams with stiffeners and short attachments were also used to provide a larger data base. These supplemental tests employ the same type of plain-welded beams with stiffeners or attachments added in the shear span. A number of these beams failed in the constant moment region from pores in the longitudinal fillet weld. There was good agreement between the data from the basic experiment and these tests.

The open symbols in Fig. 15 indicate plain-welded beams that failed from defects other than porosity. Also plotted by the same symbol are beams with stiffeners or attachments that failed in the welded beam mode. This includes beams failing from weld repairs, stop-start positions, other weld defects, and severe notches in the flame-cut flange-tips. Generally, these beams yielded shorter lives than beams failing from porosity.

When weld repairs were absent in the fillet weld, failure sometimes occurred at the stiffener or attachment only after a large number of cycles without visible cracking in the flange-web fillet welds. Some of these beams yielded longer lives than predicted by the mean line for porosity extended into lower stress range regions. The test points are identified by an open symbol and an attached arrow.

An indication of a run-out level is seen at the 18 ksi stress range level. Only three data points from beams failing from porosity were obtained. One beam sustained 10 million

applied load cycles without visible cracking. Hence, the mean line in Fig. 15 is representative of test data at stress ranges above 18 ksi for beams that failed from porosity (solid symbols). The open data points for beams failing from defects other than porosity indicate a run-out level in the vicinity of 18 ksi stress range.

4.1.2 External Weld Defects

Beams with manually deposited fillet welds have been observed by Gurney⁽¹⁹⁾ to yield shorter fatigue lives than automatically welded beams because of cracks starting from surface ripples or stop-start positions of the weld. A similar condition exists in continuously welded beams at locations of accidentally introduced stop-start positions or at weld repairs. Weld repairs become necessary when a part of the weld has to be replaced because of excessive porosity or other undesirable factors.

A number of the test beams contained weld repairs at locations or undercut or insufficient profile. These beams generally failed from a single crack which initiated at the start of a repair as illustrated in Fig. 7. The fatigue test data from beams having large cracks at weld repairs are shown in Fig. 16 and indicate a decrease in life. The mean line for these data points is parallel to the mean line for beams failing from porosity.

The start of a weld repair constitutes a local stress raiser very similar to the reinforcement at a butt-welded joint. The severity of the weld repair seemed to decrease when a smaller deposit was placed at the start of the weld repair and a smoother weld profile resulted. This observation is reflected by two beams that had cracks developing simultaneously from porosity and weld repairs (open symbols). Three beams did not reveal any visible cracking at the weld repair and failure occurred from porosity. The weld repairs were less critical than porosity in these latter cases and the life of the beams is described by the mean-life of the beams failing from porosity.

Weld repair defects appear to be also very similar to the defects introduced by stop-start positions in continuously welded beams or irregularities in manually welded beams. Data from the test beams with weld-repair defects are compared with similar data reported by other investigators in Fig. 17. The nominal bending stress on the inside surface of the flange was used as a basis for comparison. The mean line and the 95% confidence limit for 95% survival from this study correlate well with other test data.

Gurney⁽¹⁹⁾ reported failure of two automatically welded beams containing accidental stop-start positions. The possibility of improving the fatigue strength of such stop-start locations was examined by Gurney with five additional test

beams. A special technique for restarting the weld on the mechanically tapered stop of the weld bead was developed. Treatment on four specimens was successful. However, one beam failed from a repaired restart position.

Gurney also reported that three of four manually welded beams failed at stop-start positions with the crack initiating from the surface of the fillet weld. Braithwaite⁽⁶⁾ reported multiple cracks from various locations at stop-start positions in 24 inch deep manually welded plate girders. Multiple locations of crack initiation was also observed in this study when more than one weld repair was made. This was especially true for beams loaded in partial reversal where additional small cracks were observed in both flanges at various weld repairs. Small cracks were also found in the shear span of a few beams that started at weld repairs subjected to reduced bending stresses.

Fisher and Stallmeyer⁽¹²⁾ also reported several failures from weld-craters. These data are also shown in Fig. 17 for comparison. The beams were manually welded using a backstepping procedure. Failure was observed to occur at points where the next deposit began to overlap the previous weld. This location was similar to the start of a weld repair with high local heat input and a larger deposit of material.

It is apparent from Figs. 16 and 17 that weld repairs

and discontinuities in the welding process usually lead to more severe defects than acceptable porosity. The start of a weld repair was ground to the same profile as the continuous fillet-weld in one beam. However, crack initiation still occurred at the original start location of the weld repair and resulted in failure. The improvement of the surface condition probably did not eliminate a small flaw at the start of the weld repair, and had no significant effect on the life of the beam.

4.1.3 Surface Flaws in Welded and Rolled Beams

In plain-welded beams most cracks originated from defects in the longitudinal fillet weld. In this study no cracks originated from the surface of the welded-beam flange unless fretting and the influence of high local stresses were present. A few beams developed cracks from the flame-cut flange-tips. The data from beams containing flange-tip cracks are plotted in Fig. 18 and compared with the mean life for beams failing from porosity.

The welded beams which failed from crack growth at a single edge crack resulted from unusually large notches as illustrated in Fig. 9(b). When simultaneous cracking from the flange-tip and porosity in the weld was observed, the life of the beam was comparable to the mean line for porosity as illustrated in Fig. 18. It was apparent that beams with normal flange-tip

roughness (ASA roughness less than 1000) could not develop critical cracks from the small flange-tip notches before cracks grew from porosity and controlled the fatigue life. Porosity provided the critical condition for these beams.

Three beams were reported to fail from the flame-cut edge by Fisher and Stallmeyer.⁽¹²⁾ These beam data compare well with the results of this study as shown in Fig. 18.

Cracks in the rolled beams originated from either a small flaw in the rolled surface of the flange or from a discontinuity in the flange-tip. The flaws were very small and usually not well defined. Fretting was also observed during the test on plain-rolled beams. This was particularly true for partial reversal of loading.

Most cracks in the A36 and A441 steel rolled beams developed under the applied loads. Only a few cracks initiated on the rolled surface away from the load. Run-out (~ 10 million cycles) was also observed for the A36 steel rolled beams at the 30 ksi stress range level.

The test on the A514 steel rolled beams used improved set-up arrangements which made it possible to eliminate most of the local influences. Lateral braces in the shear span were used in place of the wooden stiffeners. Cracks usually developed from the flange-tip or from the flange surface. These originated from

both the inside and outside corners of the flange-tip. Cracks also started on the inside flange surface as well as from the extreme fibre. Five run-outs were observed for the A514 steel rolled beams at stress ranges of 34 and 36 ksi.

The test data are compared with data from previous investigators^(37,44,56,64) in Fig. 19. Only cracks that originated from the rolled flange surface away from possible load influence are considered. The solid points identify the grades of steel beams tested at Lehigh. Previous studies are also categorized according to the yield strengths reported. Most of these data are for the high strength T-1 steel rolled beams. No failure occurred for a number of beams after 4 to 7 million cycles of loading even with stress ranges as high as 55 ksi. Run-out of the beams was then assumed in these studies. The number of beams surviving a large number of cycles increased with decreasing stress range. All data fall above the mean of the plain welded beams and a small increase in life is found at the lower stress ranges.

Gurney⁽¹⁹⁾ reported that four plain-welded beams failed from the extreme fibre and approached the life of rolled beams. A small reduction in life is apparent in Fig. 19 when these data are compared to the rolled-beam data. This might be due to higher residual tensile stresses at the flange-web junction in the welded beams and difference in beam geometry.

Rolled beams with cracks originating from the flange-tip were distinguished from beams with surface flaws and are plotted with solid symbols in Fig. 20. The scatter is relatively large at each level of stress range. The plain-welded beams with flange-tip cracks are also replotted in Fig. 20 by open symbols. The comparison reveals a further reduction in fatigue life for the flame-cut flange-tip cracks in welded beams. This was expected for the following reasons:

- (1) Only the most severe flange-tip notches in welded beams could become critical because the defects in the longitudinal fillet-weld generally provided the critical flaw-condition and prevented further cycles of loading.
- (2) The notches introduced by flame-cutting that caused failure were more severe and sharper than the notches introduced by the rolling operation.
- (3) The notches in the flame-cut edge were in zones of high residual tensile stresses. The residual stresses at the tips of rolled beams are usually compressive.

A summary of all rolled beam data including the beams failing from locations of possible load influence is shown in Fig. 21. The test data for the three grades of steel combined are classified according to the failure mode. All data from other investigators^(37,44,56,64) are for beams that failed from the rolled surface (Fig. 19). Also indicated in Fig. 21 is the mean line for welded beams failing from porosity, and test data⁽³¹⁾

from machined tension specimens of T-1 steel.

The following conclusions can be drawn from the preceding discussion and Fig. 21:

- (1) The mean fatigue life for porosity in a welded beam constitutes a lower bound to the fatigue life of rolled beams.
- (2) The longest lives observed for rolled beams approach the life of plain plate specimens.
- (3) A run-out level is apparent in the vicinity of 30 ksi stress range.
- (4) A decreasing number of beams sustained a large number of cycles without failure at higher stress ranges.
- (5) Severe notches can initiate cracks in a rolled beam and cause failure at much lower levels of stress range as was illustrated by the failure of an A514 steel beam at the 20.5 ksi stress range level.

4.2 CRACK DISTRIBUTION IN WELDED BEAMS

4.2.1 Crack Distribution in the Tension Flange

An examination of the crack formation in welded beams⁽¹¹⁾ revealed that the cracks in the tension flange generally occurred at random locations. The A36 steel beams usually failed from a single crack in the tension flange. More than one crack formed

in each beam for the other two grades of steel. Multiple cracking was more frequent in the A514 steel beams.

The frequency distribution of cracks in the tension flange that initiated from porosity is plotted in Fig. 22(a). Only cracks from beams loaded in tension were used to eliminate possible load effects. Cracks from the three grades of steel are shown combined for both halves of the span. Cracks originating from weld repairs were not considered since weld repairs were generally necessary in the vicinity of tack welds. Tack welds had been placed in this study in a somewhat common pattern starting from the end of the beams.

It was apparent from Fig. 4(a) that the flaws were randomly distributed along the span. Hence, a uniform distribution of cracks should result in the constant moment region. The distribution of cracks shown in Fig. 22(a) suggests that slightly higher stresses existed a short distance away from the load.

The stresses calculated by beam theory were corrected for the local effect near a load point as suggested in Ref. 59. The correction at the flange-to-web junction was estimated from the solution of a concentrated force at midspan of a beam with rectangular cross-section. The correction was computed based on the web alone and is plotted in Fig. 22(b). The stresses along the span are non-dimensionalized by the nominal bending stress σ_B at midspan. Figure 22(c) shows the stress distribution along

the span for beam theory and corrected for the local effect. A reduction of bending stress at the load point is apparent together with increased stresses in the constant moment region and the shear span.

This stress distribution was experimentally verified on a beam with the loads 24 in. apart. The experimentally observed deviations from beam theory stresses were not as large as predicted. The load influence decreased faster than expected away from the load point. This can be attributed to the shear-lag effect in a welded wide-flange beam as compared to a beam with rectangular cross-section as assumed for the analytical model.

The corrected stress distribution shown in Fig. 22(c) models reasonably well the stress distribution at the flange-to-web junction along the span. This stress distribution also correlates well with the experimentally observed distribution of cracks in the beam flange shown in Fig. 22(a). A concentration of cracks was observed about 7 inches away from the load application. This corresponds to the highest stress in the tension flange.

The shape of the frequency distribution for crack occurrence is similar to the stress distribution if the concentrations at the wooden stiffener edges are ignored. The cracks at these locations had initiated from porosity in the fillet weld

and not from surface defects as was observed in the rolled beam study.

4.2.2 Crack Occurrence in the Compression Flange

When beams were subjected to partial reversal of loading, the compression flange behaved very similarly to the tension flange. Cracks were found in all grades of steel with an increasing number for the higher grades. A few beams failed due to complete fracture of the compression flange. The fatigue life of these beams was found to be comparable with the life of the beams failing in the tension flange.⁽¹¹⁾

When no reversal of loading was applied to the compression flange, the nominal bending stresses remained compressive. No visible cracks were found in the compression flange of the A36 and A441 steel welded beams. A large number of cracks was observed in the compression flanges of welded A514 steel beams in the constant moment region.

The difference in behavior due to grade of steel is believed due to the difference in the residual stress condition as was illustrated in Fig. 10. The lower yield strength of the A36 steel results in a redistribution of residual stresses in the compression flange. This redistribution is caused by yielding of the compressive residual stress zones. The tensile residual stresses are reduced when this occurs. A cyclic load introduces

a stress fluctuation from this reduced residual stress level as indicated in Fig. 10. Only a part of the stress excursion may be in the tension stress state. Hence, the full stress range is not effective.

No redistribution takes place in the compression flange of the A514 steel beams. Hence, the same stress condition exists at the weld for both tension and compression flanges as indicated in Fig. 10.

No beams failed due to fracture of the compression flange when only nominal compressive stresses were applied. In a few beams cracks were visible in the compression flange before the appearance of cracks in the tension flange. However, crack growth decreased when the crack grew out of the tensile residual stress zone and into a compressive residual stress region. This permitted cracks in the tension flange to propagate and cause failure.

Hence, fracture of the compression flange was only possible when a tensile stress component was applied to it. Crack initiation and growth appears dependent on the state of residual stress at the weld. Small cracks may develop in residual tensile zones but they seemed to arrest when they grew out of the tensile residual stress region unless a tensile stress component was applied.

5. EVALUATION OF FATIGUE BEHAVIOR USING FRACTURE MECHANICS CONCEPTS

The fatigue test data and fractographic observations of small fatigue cracks suggested that fracture mechanics of stable crack-growth might be useful in evaluating the observed behavior of the test beams. During most of the fatigue life of welded beams the cracks cannot be observed on the surface. Hence, a crack-growth equation is derived from the statistically evaluated fatigue test data.

5.1 SUMMARY OF FRACTURE MECHANICS CONCEPTS

5.1.1 Crack-Growth Data

Crack-growth data are usually obtained from crack-propagation measurements on specially designed specimens. A large variety of specimens have been tested under various applied load and boundary conditions.^(5,7,27,48,62) Most specimens have polished surfaces and sophisticated techniques are used to obtain the basic relationship between the number of applied load cycles and the crack size a .

A starter notch is introduced by mechanical means or the electrical discharge process. Usually the procedure is to precrack the specimen and advance the crack until it reaches a

convenient size for observation. This has resulted in measurements of crack-growth rates greater than 10^{-6} inches/cycle. This is equivalent to a crack-increment of one inch per one million cycles. Only a few studies have examined very slow growth because of the testing time involved, and the difficulties connected with testing and the accurate observation of crack advancement.

5.1.2 Elastic Stress Analysis

It has become common practice to use the fracture mechanics concepts introduced by Irwin⁽²⁹⁾ to describe the stress field in the vicinity of a crack tip. The linearly elastic stress field is defined by polar coordinates with origin at the crack tip, and the stress intensity factor K , where

$$K = f[\sigma, a, f(a)] \quad (\text{ksi}/\text{in.}) \quad (5.1)$$

The stress intensity factor K describes in convenient form the influence of the stresses, applied sufficiently away from the crack tip, and the crack size a . The relative size is usually expressed in terms of a correction function $f(a)$ where the linear dimensions of the plate, or the distance to a free edge or surface are introduced.

Because of the assumption of linearly elastic material, a change of applied stress causes a proportional change in K , or as commonly expressed

$$\Delta K = \Delta \sigma \sqrt{\pi a} f(a) \quad (\text{ksi}\sqrt{\text{in.}}) \quad (5.2)$$

The elastic solution for the stress field indicates infinite stress at the crack tip and stresses above the yield point over a small distance at the tip. Corrections for the plastic zone at the crack tip have been proposed.⁽⁵³⁾

5.1.3 Crack-Growth Equation

The application of fracture mechanics permits the three parameters stress range, crack size, and boundary conditions to be described by one variable, ΔK . It is also possible to successfully fit semi-empirical models to the crack-growth data. The following model was introduced by Paris⁽⁴⁵⁾ and will be used

$$\frac{da}{dN} = C \Delta K^m \quad (5.3)$$

This model expresses crack growth per cycle ($\frac{da}{dN}$) in terms of the variation of the stress intensity factor ΔK , and two material constants, C and m . The graphical presentation of Eq. 5.3 in the log-log transformation is a linear function of the form

$$\text{Log} \left(\frac{da}{dN} \right) = \text{Log } C + m \text{Log } \Delta K \quad (5.4)$$

Deviations from a straight line are often encountered due to crack initiation and very slow growth at the lower growth

rates. Fracture-mode transition and net-section yielding at higher levels of ΔK also influence the shape. The slope of the curve was also found to be influenced by grade of steel⁽²⁰⁾ and mean stress^(5,14,27) from growth tests on stress relieved tension specimens. These influences will be further discussed in Sections 5.3 and 5.4.

5.1.4 Integration of Crack-Growth Equation

An analytical expression for the theoretical life-interval between two crack sizes a_i and a_j of a structural element can be developed from Eq. 5.3. This yields

$$N_{ij} = \int_i^j dN = \int_{a_i}^{a_j} \frac{da}{C \Delta K^m} \quad (5.5)$$

The stress-intensity-range ΔK can be replaced by Eq. 5.2. For the case of a crack with constant correction factor $f(a)$ over the range of the integral, and subjected to constant amplitude stress, integration yields

$$N_{ij} = \frac{1}{C} \cdot \frac{1}{\alpha f^m(a) \pi^{m/2} \Delta \sigma^m} (a_i^{-\alpha} - a_j^{-\alpha}), \quad (5.6)$$

$$\text{where } \alpha = \frac{m}{2} - 1. \quad (5.7)$$

If $f(a)$ is a variable correction factor, a closed form solution of Eq. 5.5 is usually not possible and numerical

procedures have to be employed.

For specimens with equal initial crack-size a_i , final crack-size a_j , and identical boundary conditions, a theoretical value for the prediction of the life interval N_{ij} can be expressed in terms of a new constant C' times the applied stress range $\Delta\sigma$ as

$$N_{ij} = C' \Delta\sigma^{-m}, \quad (5.8)$$

$$\text{where } C' = \frac{1}{C} \cdot \frac{1}{\alpha f^m(a) \pi^{m/2}} (a_i^{-\alpha} - a_j^{-\alpha}) \quad (5.9)$$

The log-log transformation of Eq. 5.8 yields a straight line of the form

$$\text{Log } N_{ij} = \text{Log } C' - m \text{Log } (\Delta\sigma) \quad (5.10)$$

5.1.5 Compatibility with Welded Joint Test Data

Statistical evaluation of test data in Ref. 11 and Chapter 4 has indicated that stress range is the dominant stress variable. The model using the logarithmic transformations of stress range and cycle life best described the data. In linear form this model can be expressed as

$$\text{Log } N = B_1 + B_2 \text{Log } S_r \quad (5.11)$$

A comparison with Eq. 5.10 suggests the equivalence of

the following terms

$$\text{Log } C' = B_1 \quad (5.12)$$

and
$$m = - B_2 \quad (5.13)$$

The validity of this comparison and the assumptions involved will be further discussed in the following sections.

Mention should be made of the fact that effects of stress concentrations have to be included in the comparison. The stress range $\Delta\sigma$ refers to the stresses removed from the crack. At weldments and changes in geometry a stress concentration exists. The stress $\Delta\sigma$ must reflect this,

hence
$$\Delta\sigma = \lambda S_r \quad (5.14)$$

where S_r is the nominal applied stress range, and λ reflects the stress concentration effects. For the plain welded beam λ was taken as unity.

5.2 APPLICATION TO THE PLAIN-WELDED BEAM

Two basic stages of growth were observed for cracks originating from pores in the longitudinal fillet-weld of welded beams. The first stage of growth was in the flange-to-web junction from the initial crack-size up to the point where the crack reached the extreme fibre of the flange. The crack was observed

to be of nearly circular shape during this mode of growth.

After penetration of the extreme flange-fibre, the crack changed its shape rapidly to become a three-ended crack. Continued growth in this second stage was observed with two crack fronts in the flange and one front in the web.

Fracture mechanics concepts are applied in this section to characterize the two modes of crack growth. A penny-shaped crack is assumed to model the growth until the crack penetrates the extreme fibre of the flange. Crack-growth measurements on a three-ended crack are used when evaluating the second mode of growth. The computed crack-growth rates for the two modes of growth are compared. Comparison with growth rates from other investigations are then made in Section 5.3.

5.2.1 Application of the Penny-Shaped Crack Model

Fractographic examination of small cracks that had originated from pores in the fillet weld showed that many were almost perfectly circular in shape. This circular shape was found at various stages of growth up to the point where the crack had reached the extreme fibre of the flange, as illustrated in Figs. 23 through 25.

One of the smallest cracks was discovered when examining a crack in the fillet weld. Another small crack about

0.07 inch in diameter was found in the opposite weld as shown in Fig. 23. The tiny crack had originated from a very small pore. The extent of the crack is seen from the smooth crack surface surrounding the pore, as compared to the rough appearance caused by static tearing when the cross section was opened for inspection. This small crack was completely inside the flange-to-web junction and could not be detected by inspection of the weld surface.

A small crack discovered by the magnetic particle inspection method is shown in Fig. 24. The crack had initiated from the elongated pore and grown to the surface of the fillet weld. Almost no deviation from a circular shape is visible. This crack is about 0.26 inch diameter and could not be detected on the weld surface with the aid of a magnifying glass even under favorable circumstances and under sustained loading.

A crack which has nearly penetrated the extreme fibre of the tension flange is shown in Fig. 25. Again, no significant disturbance of the circular shape is apparent at either side of the web or at the front approaching the surface of the flange. This crack, although quite sizeable, is not easily detected on a structural element under applied loading. The linear dimension of the crack on the surface of the flange-to-web junction is somewhat less than an inch.

This phenomenon of a circular crack-shape, seemingly

not influenced by the free surfaces, is believed to be a consequence of the compatibility condition of the basically elastic cross-section. Based on this photographic evidence, a circular disc-like crack was assumed to model the actual crack during growth inside the flange-web connection.

Various stages of crack growth were schematically shown in Fig. 13. The cross section at the flange-to-web junction was magnified by a factor of three. The pore constituting the initial defect was random in shape and is indicated by Stage 1. Stage 2 represents a circular crack circumscribing the pore. The crack growing in the fillet-weld eventually reached the near weld-surface (Stage 3) and later the surface of the far weld (Stage 4). The penetration to the extreme fibre (Stage 5) terminated growth as a disc-like crack in the flange-to-web core. This occurred for beam PWB-341 at 435,000 cycles when subjected to a stress range of 36 ksi. The transition to a three-ended crack was observed to occur rapidly.

5.2.2 K-Estimates and Crack Model

Fractographic examinations revealed that a penny-shaped crack describes the crack over a large portion of the fatigue life as the crack grows from its initial size to about 3/4 inches in diameter. However, additional assumptions and estimates are necessary to account for the various shapes of the pores that were illustrated in Figs. 2, 4, 23, 24 and 25. The shape and

size of the original pore that is visible on the fracture surface was assumed to represent the initial crack. The crack is assumed to start growing with the first cycles of loading and no delay due to crack initiation was considered.

The work done by Signes et al.⁽⁵⁷⁾ has shown the morphology of some defects to be comparable to sharp notches. This work lead to the often cited and used "crack growth only" theory for welded details. Porosity constitutes an internal defect and was not considered by Signes. An indication of a similar crack-like condition at the pores in welds was discussed recently by Lundin.⁽⁴⁰⁾

Fracture mechanics provides a means of estimating K-values at distinct points on the perimeter of an arbitrary shaped crack in an infinite body. Equation 5.2 can be expressed as

$$\frac{\Delta K}{\Delta \sigma} = \sqrt{\pi a} f(a) \quad (5.15)$$

This yields a system of parallel lines for various values of $f(a)$ in a log-log presentation of $\Delta K/\Delta \sigma$ versus a , as shown in Fig. 26.

A number of basic K-values (or $\Delta K/\Delta \sigma$ values) are included in this figure.⁽⁴⁷⁾ Values for an elliptical disc-like crack embedded in an infinite body are plotted for various ratios of minor to major half-axes a/b . A tunnel crack ($a/b=0$) and a circular penny-shaped crack ($a/b=1$) represent the two boundary

conditions. Other estimates show a K-value at the convex side of a tunnel-like crack [$f(a)=1.05$], and an estimate of two bounds for a penny-shaped crack with an adjacent pore [$2/\pi \leq f(a) \leq 0.75$].

Figure 27 is an enlarged portion of Fig. 26 for half crack-sizes, a , between 0.01 in. and 0.1 inch. The pore in the photograph of Fig. 2(a) shows a sequential arrangement of three globular voids and was characterized by the idealization shown in Fig. 27. A number of K-values were estimated at various locations on the periphery of this pore and are given by solid dots in Fig. 27.

The stress-intensity factors correspond to the following assumptions:

- (1) At the extreme ends of the pore the estimates for the bounds of the stress-intensity factor for the inscribed circles are indicated by K_1 and K_2 for the radii a_1 and a_2 , respectively.
- (2) K_3 is the estimate for the neck at the transition between the end and center circles.
- (3) The dashed line represents the change in K for an ellipse with variable minor axis $2a$ over the constant major axis $2b$.
- (4) The smallest estimate of K_4 is for an inscribed circle, and the largest for a circumscribed ellipse.
- (5) The circumscribed circle with radius $a=b$ contains the whole pore and gives the largest estimate for the

crack size a . Its corresponding K -value is about equal to the values given at the transition and on the ellipse for this example.

Obviously, a number of K -values can be estimated for the flaw idealized in Fig. 27. The stress intensity K_3 at the neck seems to be the most critical. As a_3 grows and approaches the value of a_4 , the estimate of K for a circumscribed ellipse with axes $2a_4$ and $2b$ is approached. The shadowed path indicates one possible change of the K -value with increasing crack size a . Only a slight influence is apparent due to the increase of the dimension, a , from a_3 to b . It is also possible for the crack to initiate at the center pore instead of at the transition. K_4 would then describe the critical location.

For the idealized defect shown in Fig. 27 a circumscribed ellipse was selected to describe the initial flaw condition. K_4 was estimated for the circumscribed ellipse with minor half-axis $a_4 = 0.032$ in. and $\Delta K/\Delta\sigma = 0.250$.

A more complex flaw is shown in Fig. 2(b) where a circular pore is connected by a neck to a long, narrow ellipse. The largest K -estimate was obtained for this neck and used to describe the initial flaw condition. K is difficult to estimate as the crack grows.

A large number of cracks that originated from porosity in the fillet weld were examined closely so that reasonable

characterizations of their shape could be made. These cracks and defects represented a random sample from the welded beam test series shown in Figure 14. The flaws were photographed and enlarged at least three times as was illustrated in Fig. 2. The dimensions of the defects were measured under 10-power magnification which provided an accuracy of about ± 0.0003 inch.

Cracks were examined in beams fabricated from three different grades of steel. The estimated K-values corresponding to the measured flaw dimensions are summarized in Fig. 28. The estimate for the defect that corresponds to the largest observed crack from each beam is indicated by a solid symbol. The estimates were obtained using a circumscribed ellipse for flaws similar to the shapes illustrated in Fig. 2(a) and 27. For flaws comparable to those shown in Fig. 2(b) the estimate at the transition from the circular void to the elongated pore was generally used.

It was concluded from fractographic inspection of very small fatigue cracks (Figs. 23 and 24) that a penny-shaped crack-model described the shape of these cracks. However, the estimated K-values for the initial flaws shown in Fig. 28 represent a collection of elliptical shapes with various a/b-ratios. Hence each individual defect was transformed into a penny-shaped crack with an "equivalent crack-radius a_e " corresponding to the estimated $\Delta K/\Delta\sigma$ -value. The sample of the resulting equivalent crack-radii is indicated at the bottom of Fig. 28.

An average equivalent crack-radius $a_e = 0.04$ inch was selected to represent the sample of measured pores. The initial crack-radius a_i was assumed equal to this average value.

5.2.3 Derivation of Crack-Growth Constants

The coefficients of the crack growth equation can be established from the equivalence of the coefficients given by Eqs. 5.12 and 5.13. The following assumptions were made to assist with the evaluation of the crack growth constants:

- (1) The crack was assumed to be described by a constant correction factor $f(a)$ over the interval of integration. A circular, disc-like crack satisfies this condition. The correction factor $f(a)$ for a penny-shaped crack is $2/\pi$.
- (2) The estimates of the initial and final crack radii a_i and a_j were available from visual measurements. The average initial crack-radius a_i was assumed to equal the estimate of the equivalent crack radius, $a_e = 0.04$ in. (Fig. 28). This represents a penny-shaped crack of 8/100 inch diameter.

The final crack radius a_j was assumed to be reached when the crack had penetrated the extreme fibre of the flange. Experimental observations indicated this to be reasonable. The life remaining after this occurred was at most 10% of the total fatigue life of

the beam as was illustrated by the measurements given in Fig. 13. The final crack radius was assumed to be equal to the nominal flange thickness.

- (3) It was assumed that all three grades of steel could be represented by the same crack-growth equation. This assumption was based on results of tests on welded beams. It was shown in Ref. 11 that grade of steel did not significantly influence the fatigue life of the beams. The values for B_1 and B_2 from Fig. 14 were representative of all beams that failed from porosity.

Equating the values for B_1 and B_2 from the mean regression curve to the coefficients m and C' , and substituting the crack radii a_i and a_j , and the correction factor $f(a)$ into Eq. 5.9 yields the growth constants

$$m = 2.98 \quad (5.16)$$

$$C = 2.05 \times 10^{-10} \quad (5.17)$$

Substitution of these constants into Eq. 5.3 yields

$$\frac{da}{dN} = 2.05 \times 10^{-10} \Delta K^{2.98} \quad (5.18)^*$$

This equation is shown as a straight line in the log-log transformation of Figs. 29 and 30.

* The dimensions used for crack-growth rates $\frac{da}{dN}$ were in./cycle, and the stress-intensity-factor range ΔK was ksi $\sqrt{\text{in.}}$.

5.2.4 Crack Growth in a Welded Beam

The penny-shaped crack was used to model the first stage of growth from initial crack-size up to the point where the crack reached the extreme fibre of the flange. After penetrating the extreme fibre, the crack changed its shape and became a three-ended crack. The mode of growth changed from plane-strain to plane-stress. Crack-growth measurements for a portion of this transition and for growth as a three-ended crack were discussed earlier. The experimentally obtained relationships between crack size and applied stress cycles were plotted in Figs. 11 and 12. Crack-growth rates were determined from these measurements using a secant method as follows:

- (1) Smooth curves were graphically fitted through the data points obtained from crack-size measurements (Fig. 12). The relationship for the crack length a_c on the inside of the flange was obtained from the two individual measurements at the crack tips at a and c .
- (2) Crack sizes on the inside and outside of the flange were selected from the smooth curves for a_c and e_f at intervals of 1000 cycles, starting at 440,000 cycles of applied loading.
- (3) Crack-growth rates $\frac{da}{dN}$ were determined from the crack size increments per 1000 cycles for the inside and outside cracks.
- (4) Corresponding ΔK values were computed for the mid-

points of the intervals. The geometry correction function $f(a)$ was estimated at each stage as described below. The resulting crack-growth rates are plotted in Fig. 29 and compared with Eq. 5.18 for crack growth before penetration of the extreme fibre.

ΔK -values for the apparent crack size a_c on the inside of the flange were estimated using two assumptions for the correction function $f(a)$.

(a) A penny-shaped crack was assumed with a diameter equal to the total crack size a_c . This constituted a "lower bound" for ΔK . The data points for the transition zone before growth as a three-ended crack are plotted as open dots in Fig. 29. They fall well below Eq. 18.

(b) A through-the-thickness crack in the flange was considered as a second possibility. ΔK values were computed using the secant correction for finite width⁽³⁰⁾ and a plastic zone size correction.⁽⁵³⁾ The radius of the plastic zone was assumed equal to

$$r_y = \frac{1}{2\pi} \left(\frac{\Delta K}{2\sigma_y} \right)^2. \quad (5.19)$$

The value of ΔK was computed for the corrected crack size

$$\bar{a} = a + r_y, \quad (5.20)$$

σ_y was taken equal to the yield strength of the base material.

This resulted in an "upper bound estimate" of ΔK for crack a_c during the transition from a penny-shaped crack to a three-ended crack. The crack length e_f on the extreme fibre was less than crack length a_c during this transition. Hence, the assumption of a through-crack equal to a_c overestimated the value of ΔK on the inside of the flange. The data points corresponding to the upper bound estimate are plotted as solid dots in Fig. 29. They fall above Eq. 18 in the transition zone.

The data points for continued growth as a three-ended crack are parallel to and slightly below Eq. 18 up to nominal net-section yielding. An increase in crack-growth rate is apparent after nominal net-section yielding.

(c) The apparent crack-size e_f on the extreme fibre was also used to estimate ΔK -values for a through-the-thickness crack. The same corrections as stated in (b) were used. This estimate was not very satisfactory during the transition from a penny-shaped to a three-ended crack. The crack inside the flange was larger than the apparent crack size e_f on the extreme fibre. The data points are shown as triangles in Fig. 29 and fall below the straight line estimate in the transition region.

It was visually observed that the crack on the bottom surface of the flange tried to match the size of the crack on the inside surface of the flange during the transition from a penny-shaped to a three-ended crack. The observed growth rates reflect this behavior. Growth rates computed from the estimates of the

inside and outside crack lengths, a_c and e_f , correlate well in the region of growth as a three-ended crack. Good correlation is also apparent in Fig. 29 with the extrapolated straight line estimate provided by Eq. 18 for a penny-shaped crack. This is particularly true for stable growth as a three-ended crack.

The various stages of crack growth in the test beam are summarized in Fig. 30. The straight line estimate (Eq. 18) for crack growth as a penny-shaped crack from initiation until penetration of the extreme fibre is shown. Also replotted are the data points from Fig. 29 for crack-growth rates on the inside and outside surfaces of the flange. The various stages are labelled and the crack radius, a , for a circular crack, and the length, $2a$, for a through-the-flange crack are indicated. The corresponding number of cycles are also shown.

It is apparent from Fig. 30 and the schematic shown in Fig. 13 that most of the life is spent growing the crack from its initial equivalent flaw-radius, $a_e = 0.04$ inch, to its penetration of the extreme fibre of the flange, $a_f = 0.375$ inch. The corresponding range of ΔK for the test beam was between 8 ksi $\sqrt{\text{in.}}$ and 25 ksi $\sqrt{\text{in.}}$ under a constant amplitude stress range of 36 ksi while 435, 000 cycles elapsed. The transition from the penny-shaped crack to a three-ended crack required about 16,000 cycles. An additional 10,000 cycles were required to grow the crack large enough to cause nominal net-section yielding. Rapid crack growth and failure of the beam occurred at 467,000 cycles.

It is also apparent from Fig. 30 that most of the life was spent while growth occurred in a region of small ΔK . This is particularly true for lower applied stress ranges as illustrated in Fig. 31. The ΔK regions applicable to growth as a penny-shaped crack are indicated for the test beams subjected to the stress ranges used in this study. Crack initiation took place at ΔK -values below 10 ksi $\sqrt{\text{in.}}$ in all test beams. Most of the life was spent at growth rates smaller than 10^{-6} in./cycles.

5.3 COMPARISON OF CRACK GROWTH IN BEAMS WITH CRACK PROPAGATION STUDIES

5.3.1 Stable Crack Growth

The theoretical crack-growth equation (Eq. 18) shown in Fig. 31 was derived from the stress-life relationship of a large number of welded beams failing from pores in the longitudinal fillet-weld. It was based on the penny-shaped crack-model and is extrapolated for comparison with data from crack-growth specimens. The extrapolated curve falls within the scatterband reported by Crooker and Lange.⁽⁸⁾ This scatterband contains data from tests on carbon and low-alloy steels with yield strengths between 34 ksi and 127 ksi. This was comparable to the yield strengths of the steel beams.

A conservative upper bound for growth rates on ferrite-pearlite steels was proposed by Barsom.⁽⁴⁾ This proposed

equation is virtually parallel to the derived equation (Eq. 18) as shown in Fig. 31.

Since much of the growth in the plain welded beams took place in the weld metal and heat affected zone, a comparison of the theoretical curve with Maddox's data⁽⁴¹⁾ is relevant. An approximate envelope for Maddox's data on four different weld metals is shown. Three had about equal yield strength (67 ksi), the fourth had a higher yield point equal to 90 ksi. Also included in the scatterband are test data for a simulated heat affected zone in mild steel material with the same yield strength. The correlation of the theoretical curve (Eq. 18) with these crack-growth data is good.

Hertzberg and Nordberg⁽²⁴⁾ reported crack-growth rates in the weld metal an order of magnitude less than in the base material. This effect disappeared when the welded specimen was heat-treated and stress relieved. Maddox⁽⁴¹⁾ did not find a significantly different crack-growth rate in weld material as compared to the plain material reported by Gurney.⁽²⁰⁾ A close examination of the beam-crack fracture surfaces shown in Figs. 23 through 25 revealed a quite pronounced texture in the vicinity of the pores. This indicates that the crack had not grown in a perfect plane probably resulting in somewhat slower growth.

It is apparent from Fig. 31 that the Crooker-Lange scatterband does not cover the critical region of interest for

plain-welded beams. Most studies of crack growth rates have been limited to larger ΔK -values and higher crack-growth rates because of the difficulties encountered in the slow growth region. However, the theoretical curve (Eq. 18) extrapolated into the higher ΔK -regions shows the same general trend reported by others on basic crack-growth specimens (Fig. 31). The theoretical curve is just above the crack-growth data and underestimates their growth rate. This is surprising since the penny-shaped crack assumes the best condition for the crack in the welded beams and neglects the influence of free surfaces. This underestimate in growth rate may be due to crack initiation or an overestimate of the stress intensity.

5.3.2 Slope of Crack-Growth Rate Curve

The exponent m of the predicted crack-growth equation was equal to 2.98 (Eq. 18). It represents the slope of the fatigue test data on plain-welded beams fabricated from three grades of steel shown in Fig. 14. Crooker and Lange⁽⁸⁾ observed from a review of the literature that the value of the slope m fell between 2 and 4 for a large range of steels.

Gurney⁽²⁰⁾ reported on growth rates in steels with yield strengths varying between 27 ksi and 63 ksi. The mean lines from five steels are shown in Fig. 32 together with the extreme scatterbands for all data. A change in slope m is indicated for increasing yield strength. The theoretically

derived curve (Eq. 18) when extended into the higher ΔK -regions shows, however, good overall agreement with Gurney's test data.

Gurney⁽²⁰⁾ reported the slope of the curve to be a linear function of yield stress of the material. This straight line approximation for the slope m is shown in Fig. 33 as a heavy line over the range of test results. A smaller exponent m results with increasing yield strength. Maddox's data⁽⁴¹⁾ on weld material and heat affected zone are plotted as crosses and Barsom's data⁽⁴⁾ from ferrite-pearlite steels as triangles. An averaged value for martensitic steels with yield above 90 ksi is indicated by an arrow to the right of 100 ksi.⁽⁴⁾ Also included for comparison are the values for the regression curves for plain-welded beams (Fig. 14) derived from the three individual steels used in this study.

A general trend observed in crack-growth studies is for the value of the exponent m to decrease with increasing yield strength of the material. This trend was not as pronounced in the welded-beam study. The exponent m did not appear to vary greatly from 3.

The effect of a decrease in m on crack-growth rates as reported by Gurney can be seen from Fig. 32. A decreasing slope m (steeper curve in this graphical representation) was indicated for increasing yield strengths. These lines intersected at about 5×10^{-6} in./cycle. This leads to larger

values of the constant C for smaller m values. Hence, a larger constant C does not necessarily mean faster crack-growth rate since the rate is also dependent on the level of ΔK and the exponent m . The higher strength steels with smaller m showed faster growth in the region below 5×10^{-6} in./cycle, and slower growth in the higher growth-rate regions, as compared to the growth rates for lower strength steels (Fig. 32).

Careful evaluation of the coefficients m and C is needed for a wider range of rates of growth. Most of the data used to fit the straight line approximation only extend over a small range of ΔK . In other cases, data points at the extremes cause rotation of the line. Substantial over- or underestimates of the fatigue life of a structural component might result if these relationships are used to extrapolate beyond the range of the test data.

5.3.3 Transition Zones

Most crack-growth rate data on aluminum and steel show deviations from the straight line model proposed by Paris (Eq. 5.3).⁽⁴⁵⁾ Growth-rates smaller than predicted by the model have been experienced in the slow growth region. Increases in growth rate have been observed at higher ΔK -values. Empirical crack-growth equations were proposed by Forman et al.,⁽¹³⁾ and by Broek and Schijve⁽⁵⁾ to include transitional behavior.

No comprehensive understanding of the causes for these deviations has been acquired, although a number of authors have offered explanations based on the fracture-mode appearance. Wilhelm⁽⁶³⁾ and Maddox⁽⁴¹⁾ observed a change of fracture mode in the slow growth region when the slow growth behavior started to follow the straight line approximation. This transition, termed first knee by Maddox,⁽⁴¹⁾ corresponded to a change from tensile to shear fracture mode. The slope of the crack-growth curve before the knee and the location of the knee itself were observed to be stress dependent.⁽⁴¹⁾ The knee was found to occur at higher ΔK -values under higher applied stresses. Hudson and Scardina⁽²⁷⁾ observed the change of fracture mode to fall within a reasonably narrow range of crack-growth rates.

A second knee is sometimes observed at high ΔK -values. The crack-growth rates are much higher and growth approaches the unstable regime. Wessel⁽⁶²⁾ has attributed this knee to a change of mode from normal incremental crack-growth to the dual mode of fracture. Hertzberg and Paris⁽²³⁾ found the transition from plane-strain to plane-stress to be completed at a constant ratio of plastic zone size r_y to sheet thickness t equal to 0.5. Klingerman⁽³⁴⁾ observed a short transition to faster growth rates when approaching net-section yielding. The growth rate curve was almost parallel after the transition to the original curve until the stress on the net-section approached the ultimate strength and growth rate increased rapidly.

Barsom⁽⁴⁾ has related the onset of the transition at high ΔK -values to the crack-opening-displacement range, $\Delta\delta$ which is a measure of the strain range at the crack tip. Since crack-opening-displacement is indirectly proportional to yield-strength of the material, the transition should occur at higher ΔK -values for higher strength materials.

Most information on the transitional behavior relates to fracture-mode changes and hence plastic zone size. Varying the grade of steel or the thickness of the material can be expected to influence the occurrence of the transitions. In performing crack-growth studies one may observe one or more transitional zones depending on the material, specimen shape, and thickness.

The transition regions can significantly change the slope m of the straight line approximation. Since transitions occur at the extreme ends of the growth-rate vs. ΔK relationship they can easily cause rotation of the curve. For example, when testing various grades of steels accelerated crack-growth will occur at relatively lower ΔK -values for lower grade steels as compared to higher grade steels. Hence, a larger value for the slope m for lower grade steels is estimated from the test data.

5.3.4 Effect of Stress Ratio

A number of investigators^(5,27,28) have attempted to

establish the influence of mean stress or stress ratio in aluminum alloys. Hudson and Scardina⁽²⁷⁾ found that the compressive part of the stress cycle (negative R-values) did not influence crack-growth rates. Higher stress ratios ($R > 0$) were observed to increase crack growth.

Hertzberg and Nordberg⁽²⁴⁾ observed a moderate influence of the $K_{\max}/\Delta K$ ratio on the crack-growth behavior of A514 steel. No statistically significant influence of minimum stress was found in Ref. 34 for A36 steel. Crack-growth rates exceeded 10^{-6} in./cycle for all these studies.

Tests on plain-welded beams⁽¹¹⁾ indicated no statistically significant influence due to minimum stress. This was true even when the stress cycle was partly compressive. Fig. 10 shows the region of the longitudinal fillet-weld to be subjected to residual tensile stresses about equal to the yield strength of the weld-metal. Hence, the initial flaw was always subjected to a tensile state of stress.

Since both the tension and compression flange fillet-welds were subjected to basically the same cyclic stress condition, cracks would be expected to occur in both the tension and compression flange. A large number of cracks were observed also in the compression flange of the beams even under no reversal of applied loading. These observations confirm the fracture mechanics principle of ΔK being the controlling factor for crack

growth. The maximum stress has a negligible influence in welded beams because the elevated tensile residual stresses are about equal to the yield strength of the material.

5.3.5 Very Slow Growth

Johnson and Paris⁽³²⁾ have suggested that a threshold exists for crack growth. In other words, ΔK at the crack tip may cause a much smaller crack-growth rate than predicted by the straight line approximation describing crack-growth-rate vs. ΔK relationship.

A recent investigation by Paris⁽⁴⁸⁾ on ASTM 9310 steel has provided more information on this phenomenon of very slow growth. The test specimens were precracked and growth data for small ΔK -values obtained. The value of ΔK was then reduced stepwise and observations made on the relative crack-growth rates until a "threshold value" was reached. When ΔK was increased in steps, the rate of growth was comparable to the rates obtained by previous overloading. An approximate mean line fit to Paris' data is compared in Fig. 34 with the predicted crack growth (Eq. 18) from this study. A drastically reduced growth rate for $\Delta K \cong 5.2 \text{ ksi } \sqrt{\text{in.}}$ is observed.

Harrison⁽²¹⁾ has reviewed the literature for run-out data on a variety of specimens. He concluded that "for all materials with the exception of pure aluminum, cracks will not

propagate if $\frac{\Delta K}{E} < 1 \times 10^{-4} \sqrt{\text{in.}}$ " He also found for a number of materials that the limit for non-propagating cracks fell between $\frac{\Delta K}{E} = 1.5 \times 10^{-4} \sqrt{\text{in.}}$ and $1.8 \times 10^{-4} \sqrt{\text{in.}}$ Harrison's levels for four types of steel are also shown in Fig. 34. They correspond to ΔK -values of about 3.3 ksi $\sqrt{\text{in.}}$ for mild steel and 5.3 ksi $\sqrt{\text{in.}}$ for austenitic steel.

5.4 INFLUENCE OF GEOMETRICAL AND MATERIAL FACTORS ON CRACK GROWTH IN WELDED BEAMS

5.4.1 Influence of Plastic Zone Size

The crack radius, a , for the penny-shaped crack did not include a correction for the contribution of the plastic zone at the crack tip. An estimate of the plastic zone radius has been given in Ref. 53 as

$$r_y = \frac{1}{2\pi} \left(\frac{\Delta K}{2\sigma_y} \right)^2. \quad (5.19)$$

When correcting the crack radius a to account for the plastic zone radius r_y , a new geometry correction factor $f'(a)$ results for the penny-shaped crack:

$$f'(a) = f(a) \left[1 / \sqrt{1 - \frac{2}{\pi^2} \left(\frac{\Delta \sigma}{2\sigma_y} \right)^2} \right]. \quad (5.21)$$

This geometry correction is only dependent on the yield strength of the material for a given stress range. Equation 5.21 can be approximated by

$$f'(a) \approx f(a) \left[1 + \frac{1}{2} \frac{2}{\pi^2} \left(\frac{\Delta\sigma}{2\sigma_y} \right)^2 \right]. \quad (5.22)$$

This approximation allows a quick evaluation of the influence of the plastic zone on the life estimate. For steels with nominal yield strengths of 36 ksi, 50 ksi and 100 ksi and subjected to the highest stress range of 42 ksi, a change in $f(a)$ of 3.5, 1.8 and 0.45 percent, respectively, results.

The fracture appearance suggested that a plane strain condition prevailed at the crack tip of the penny-shaped crack in the welded beams. Hence, the percentage change in $f(a)$ would be even reduced by two-thirds.⁽⁵³⁾ It was concluded that the influence of plastic zone size could be neglected for the penny-shaped crack.

5.4.2 Influence of Flange Thickness

Observation of crack growth during fatigue testing (Figs. 11 through 13) revealed that most of the fatigue life of a welded beam had been consumed when the crack penetrated to the extreme fibre of the flange. An estimate of the fatigue life of beams with thicker flanges can be made with the penny-shaped

crack-model. A thicker flange can be reflected by an appropriate final crack-size a_f .

Figure 35 shows the mean life for the test beams with nominal flange thickness of 0.375 inches. Various other flange thicknesses are indicated. Only a slight increase in fatigue life occurs for beams with larger flange thickness. The increase is not significant and would not justify an increase of allowable stresses for thicker flanges. This has been confirmed from the comparison with data from other studies on plain-welded beams with thicker flanges.⁽²⁶⁾ Also, the comparison of data from flange-spliced beams with 3/4 inch flange-thickness that failed from pores in the longitudinal fillet-weld yielded good agreement with the data from plain-welded beams with 3/8 in. flanges.⁽¹¹⁾

It should also be noted that an increase in flange thickness generally results in a decrease in fracture toughness which can lead to brittle failure. This becomes even more critical with the use of high strength steels.⁽⁸⁾

An additional conclusion can be drawn from the study of the mechanism of crack growth in the flange-to-web junction. The photographic evidence did not indicate a significant influence of the weld size and geometry on the mode of growth as a penny-shaped crack. Most of the life of a welded beam is spent as the crack grows from the initial defect to a visible crack. The initial crack-size is the dominant factor and is independent

of the exact geometry of the cross-section. Hence, if the size of the fillet weld is increased, no increase in fatigue life can be expected for the same size pore.

5.4.3 Influence of Defect Size

The life interval between the initial and final crack-sizes a_i and a_j can be determined from Eq. 5.6. For a given final crack-size, the computed number of cycles can be expressed as a function of the initial crack-size for a given stress range, as shown in Fig. 36.

The final crack-radius for the penny-shaped crack-model was assumed equal to the flange-thickness of the welded test beams. This becomes less important for larger differences between initial crack-radius a_i and final radius a_j (Eq. 5.6). For very small initial cracks a_i , the curves become linear with a slope of $\alpha = \frac{m}{2} - 1$ in the log-log representation. For a given equivalent pore-radius $a_e = a_i$, Fig. 36 yields the theoretically computed number of cycles for the penny-shaped crack to reach the extreme fibre of the flange.

Alternately the observed fatigue life of a tested beam can be used with the appropriate stress-range line to estimate the equivalent initial pore-radius that caused failure, as illustrated in Fig. 36. The fatigue data from Fig. 14 are replotted in this manner in Fig. 37. Figure 37 is the enlarged portion

indicated in Fig. 36. The scatter of the equivalent pore-radii derived from the fatigue test data is shown on the right ordinate.

The equivalent pore-radii determined from measured flaws are shown on the left ordinate of Fig. 37. The scatter of the porosity as derived from the fatigue test data (right ordinate) is seen to correspond to the scatter from the measured equivalent pore-sizes (left ordinate). The two scatterbands were found independently.

If no variation is assumed in the crack-growth characteristics, this comparison suggests that the scatter in the fatigue test data is caused by the variation in the initial crack-size. This is essentially the same conclusion reached by Harrison⁽²²⁾ for the analysis of test results from butt welds with lack of penetration defects. He concluded that the width of the scatterband probably resulted from variations in initial radii at the defect tips.

5.5 APPLICABILITY OF CRACK MODEL AND PREDICTIONS OF FATIGUE LIFE

5.5.1 Comparison with Other Crack-Models

The computations based on the penny-shaped crack-model employed an equivalent initial crack-radius. This equivalent crack-radius was derived from estimates of the critical K-value for the pore. The scatter in the equivalent crack-radius derived

from the fatigue test data was found to be about the same as the scatter of the measured crack-radii (Fig. 37). No variability was considered due to the influence of the pore-shape on the estimate of the equivalent crack-radius.

Additional crack-models were used to assess their influence on the prediction of the fatigue life. Figure 38 summarizes the results for the various models used. Six A441 steel beams were selected for the comparison. The observed fatigue lives of these six beams are shown by solid dots together with the mean and the 95% confidence interval for all test beams failing from porosity.

The defects that caused crack growth and failure of the six beams were examined. They were assumed to be characterized by a circumscribed ellipse with half-axes a and b . The following models were used to estimate the fatigue life of each individual beam using the known dimensions of the circumscribed ellipse and crack-growth equation 5.18:

Model (a) The open circles in Fig. 38 correspond to the life estimates for the penny-shaped crack with equivalent crack-radius. The equivalent crack-radius was computed from the equivalence of the K -value with the circumscribed elliptical-crack (Section 5.2).

Model (b) Penny-shaped cracks were assumed to inscribe and circumscribe the ellipse. The shortest life estimates

resulted from the circumscribed crack and the longest from the inscribed crack. These two estimates constitute "upper and lower bounds", and are indicated by the T-symbols in Fig. 38.

Model (c) Additional life estimates were made based on the elliptical crack-model. Growth was assumed in the direction of the minor axis $2a$ with constant major axis $2b$ until the size of the circumscribed crack was reached. The computation of the increment of life from an elliptical to a circular crack was done using an available computer program.⁽¹⁶⁾ Numerical integration was employed because of the variable correction factor $f(a)$. This increment of life was added to the estimate for the circumscribed penny-shaped crack. The total life estimate is indicated by open triangles in Fig. 38.

The comparison between the estimates for each individual beam provided by the different models and the observed fatigue life permitted the following observations to be made:

- (1) The life estimates employing the equivalent penny-shaped crack-radius [model (a)] resulted in slightly shorter lives than the estimates that assumed the elliptical crack first to grow to a circular shape [model (c)].
- (2) Both of these estimates were bounded by the estimates provided by the inscribed and circumscribed initial cracks [model (b)].
- (3) The observed fatigue data was also contained within

the bounds from the estimates of the circumscribed and inscribed circles in all but one case.

- (4) Long flaws with a small a/b-ratio [as illustrated in Fig. 2(b)] provided the greatest deviation between the computed "lower and upper bound".
- (5) All three defects of the type shown in Fig. 2(a) had their life underestimated when the equivalent initial crack-radius was used [model (a)]. The estimate improved for the elliptical model [model (c)].
- (6) Most of the estimates from models (a) and (c) fell within the two limits of dispersion representing the 95% confidence interval of all the beam test data.

5.5.2 Prediction of Fatigue Life

Maddox,⁽⁴²⁾ and Harrison⁽²²⁾ have demonstrated that good predictions of the fatigue life can be obtained from crack growth data. Barsom's⁽⁴⁾ conservative estimate of crack-growth rate (Fig. 31) for ferrite-pearlite steels has been used here to predict a lower bound to the fatigue life of the beams failing from porosity. The result is shown in Fig. 39 together with the mean line and the 95% confidence interval for the original data from Fig. 14. The mean-line and confidence limits were extended to the 18 ksi stress range level and the long-life data from Fig. 15 added.

Also shown in Fig. 39 is the prediction based on Paris'

data,⁽⁴⁸⁾ indicating a threshold level for run-out at about 23 ksi stress range. This prediction was obtained using the straight line segments shown in Fig. 34 which approximate the data from the study on very slow growth. The threshold values by Harrison⁽²¹⁾ shown in Fig. 34 were also used to estimate run-out. Run-out tests are predicted to occur at levels as high as 20 ksi stress range for low-alloy steel.

The predictions based on the crack-growth data underestimate the mean fatigue life of the test beams at the higher stress range levels. This was expected from the comparison of the crack-growth data. Since any assumption other than a penny-shaped crack-model for the welded beams would further reduce the life prediction, a crack-initiation period may be responsible for the slight underestimate. Other factors that could be responsible for the underestimate are an overestimate of the initial crack-size, an overestimate of the stress intensity, or a slower growth rate under plane-strain conditions.⁽⁷⁾

Using the straight-line segment approximation to Paris' slow growth data, the fatigue life was also computed as a function of the initial crack-radius a_i as shown in Fig. 40 for various stress range levels. Also shown on the left is the sample of estimated equivalent crack-radii and the representative flaw-size $a_e = 0.04$ in. from Fig. 28. The observed beam data are plotted on the appropriate stress range lines together with the

mean and the 95% confidence interval. Two observations can be made from Fig. 40.

The test data for the 42 ksi, 36 ksi and 30 ksi stress range levels indicate a slightly smaller average defect size of about 0.03 in. This estimate of 0.03 in. compares with an average value for the estimated flaw size in Fig. 28 when the shape corrections are disregarded. A change of the estimate for the initial crack-radius from $a_i = 0.04$ in. to $a_i = 0.03$ in. increases the computed value of the constant C in the crack-growth equation from $C = 2.05 \times 10^{-10}$ (Equation 5.17) to 2.51×10^{-10} . This only increases the theoretical crack-growth rate slightly if m is kept constant.

It appears reasonable to assume that the flaw sizes at the various stress range levels are about the same. The mean line for the observed fatigue data should then remain horizontal in Fig. 40. The upward slope of the mean line indicates that the threshold level of 5.2 ksi $\sqrt{\text{in.}}$ suggested by Paris⁽⁴⁸⁾ is too high for the steels used in this study. Figure 39 showed a number of beams that sustained longer lives than predicted by the mean line at the 18 ksi stress range level. One beam yielded a life of 10 million cycles without visible cracking. Hence, run-out data for the observed porosity seem to fall at or slightly below the 18 ksi stress range.

If this arbitrary run-out level for plain welded beams

is correlated with the two ΔK -threshold values suggested for low-alloy steel and mild steel in Fig. 34 (4.6 ksi $\sqrt{\text{in.}}$ and 3.3 ksi $\sqrt{\text{in.}}$) a "threshold" defect radius a_{TH} can be estimated. Equation 5.2 yields $a_{\text{TH}} = 0.051$ in. for low-alloy steel and 0.026 in. for mild steel. This compares with the range of measured equivalent pore-radii shown on the left ordinate in Fig. 40.

The same computation was used to estimate the flaw size in the rolled beams. Run-out data were observed in Figs. 19 and 20 at the 30 ksi stress range level for A36 and at 34 ksi for A514 steel rolled beams. These run-out levels were confirmed by comparison with other rolled beam data. The run-out levels were correlated to the ΔK -threshold values of 3.3 ksi $\sqrt{\text{in.}}$ and 4.6 ksi $\sqrt{\text{in.}}$ for mild steel and low-alloy steel, respectively.

Two crack models were used to estimate the flaw size in the rolled beams. A corner crack⁽⁴⁷⁾ was assumed to model the cracks originating from the flange-tip corners. A defect radius of 0.010 in. and 0.014 in. resulted for the two grades of steel. An elliptical surface crack (a/b very small) was used (with a correction factor $f(a)$ equal to 1.0) to describe the surface flaws in the rolled beams. The depth of the flaws was found to be between 0.004 in. and 0.006 in.

5.5.3 Scatter in Crack-Growth Rates

The scatter in the test data shown in Fig. 39 was

attributed in part to the variation in shape, size and severity of the porosity. Other factors contribute to the variation in test data. Beams with equal defects would still experience scatter in the fatigue test data because of variation in the crack-growth rates and other variables.

The scatter represented by the 95% confidence interval in Fig. 39 can also be assumed to result from variation in crack-growth rates. This is illustrated in Fig. 41 for an initial crack radius of 0.04 in. The scatterband is shown for growth-rates below 10^{-5} in./cycle over the range of ΔK -values corresponding to the penny-shaped crack used in this study. Since three grades of steel were used to fabricate the test beams, the scatterband also includes the effect of grade of steel. In addition, two different electrodes were used for the fillet welds causing different weld material and heat affected zone for each grade of steel.

The scatter in growth-rate data for a single grade of steel taken from Gurney's study⁽²⁰⁾ is also shown for comparison in Fig. 41. This data was obtained from center notched specimens of BS968 grade steel which is comparable in yield stress to the A441 steel used in this study. All but two of the nine specimens⁽²⁰⁾ were tested at different stress ranges under zero to tension loading. The band is shown over the region of stable crack-growth⁽²⁰⁾ or growth rates larger than 5×10^{-6} in./cycle.

The width of the scatterband of growth rates from specimens (measured horizontally for a given ΔK -value) is about half the width of the band based on the beam data.

The average width of the envelope for Maddox's data⁽⁴¹⁾ for weld metal and heat affected zone that was summarized in Fig. 31 compares with the variation observed in the beam tests. Hence, the scatter observed in crack growth studies appears in part responsible for the scatter in the test data.

The derived growth-rate scatterband is also compared with the data obtained by Maddox⁽⁴²⁾ on the propagation of a part-through-thickness crack. Maddox's data points are replotted in Fig. 41 and show comparable scatter. Maddox computed the averaged growth rate from measurements of markings on the fracture surface caused by stepwise increased loads.

The comparison of the growth-rate curve from this study with Maddox data for ΔK -values below 10 ksi $\sqrt{\text{in}}$. indicates growth-rates of almost an order of magnitude smaller. As before, the question remains whether this can be attributed to a crack initiation period, an overestimate of the stress intensity, smaller growth rates in the plane strain condition as suggested by Clark and Trout,⁽⁷⁾ or other influences. Further work is needed to clarify these questions.

6. INITIAL FLAWS AND FABRICATION OF ROLLED AND WELDED BEAMS WITHOUT ATTACHMENTS

6.1 PLAIN-WELDED BEAMS

Welded beams without attachments that are fabricated according to current practice can be expected to exhibit crack growth from flaws in the continuously welded web-flange connection. Except for blow holes extending to the surface of the fillet weld, flaws such as gas pores cannot be detected by visual inspection and only with great difficulty using modern inspection techniques. Non-destructive testing methods cannot define the exact size and shape of these defects in the weld.

The comparison of the welded beam test data with data from other investigations in Refs. 11 and 26 had indicated that good correlation of the data existed. The 95% confidence limit for 95% survivals was found to provide a lower bound to the data. A study on welded girders⁽¹⁰⁾ recently reported significantly reduced fatigue lives for girders with large porosity in the weld. Insufficient information is given to allow a comparison with the porosity observed in this study. It appears desirable to evaluate the porosity that can be expected to be found in commercially fabricated structures.

It was concluded from the experimental and theoretical

studies that the size of porosity should not exceed the magnitude observed in this study. Appropriate welding and fabrication techniques should be used to reduce the possibility of premature failure from larger pores.

This dissertation used fracture mechanics models to evaluate the effect of pore geometry and size on the fatigue life of plain-welded beams. Similar methods can be used to analyze the effect of continuous welds in the direction of the applied stresses. The continuous welds at longitudinal stiffeners or the flange-web connection of box-girders provide one upper bound condition for the fatigue strength of the structure. Generally, attachments, transverse stiffeners, or the ends of the continuous weld at the longitudinal stiffeners provide more critical conditions.

Other defects in the longitudinal weld are introduced by incomplete fusion, undercut, slag inclusions, or cold lap at tack welds, and generally result in a shorter fatigue life for the beam than porosity causes. It is common practice to repair undercut which frequently occurs in the vicinity of tack welds. Also, insufficient weld profile is usually filled to the required weld size by a local weld repair.

It was found in this study that the start of a weld repair constitutes a defect slightly more severe than the usual porosity. This can further reduce the fatigue life of the beams.

The same effect was observed at accidentally introduced restarts in the continuous weld. Since such defects cannot be eliminated during fabrication, design must account for their existence. This concept was used in Ref. 11 to develop design stresses that were adopted as AASHTO Interims Specifications.⁽¹⁾ The specifications provide for defects that are comparable to those observed in this study.

Flange-tip cracks may occur from sharp notches that are more severe than the regular flange-tip roughness introduced by flame-cutting the plates to size. These notches should be removed by grinding. It is possible that handling beams with chains and hooks during the fabrication and erection of structures will introduce undesirable defects. Additional studies are necessary to evaluate these effects on the fatigue strength of beams.

6.2 PLAIN-ROLLED BEAMS

Flaw size estimates for rolled beams were derived from fatigue test data with fracture mechanics concepts. A defect depth between 0.004 and 0.006 inch was determined from the run-out data. This crack size is an order of magnitude smaller than the equivalent penny-shaped crack ($a_e = 0.04$ inch) in welded beams. The defects in the rolled beams are believed to be introduced during the rolling operation or result from mill scale which adhered locally to the flange surface.

Flange-tip flaws in the rolled beams were found to be somewhat larger than the surface flaws. The radius of the quarter-circular crack with origin at the flange-corner was of the order of 0.010 in. to 0.014 inch. This larger defect was reflected by the fatigue data which indicated shorter lives for rolled beams failing from flange-tip flaws.

Rolled beams provided the least severe flaw condition for a structural element and can yield extremely long lives. However, a large flaw in the surface or at the flange-tip can reduce the fatigue life of the beam substantially. This was observed in a few beams in the high stress range region, and in one beam failing in the shear span from a large notch in the flange-tip. These beams yielded fatigue lives equivalent to the mean life for welded beams. Large or sharp notches at the flange-tip should be repaired by grinding to avoid a reduction in the fatigue life of the beam.

7. CONCLUSIONS

The main findings of this study are summarized hereafter. They are based on a detailed examination of the test data, fracture surfaces, initial flaw conditions provided by the experimental work, and on the theoretical studies of stable crack growth.

- (1) The characterization of the initial flaw condition revealed porosity to be the most common defect in plain-welded beams. The welded beam fatigue data fell within a narrow scatter-band when plotted as the logarithmic transformation of stress range and cycles to failure.
- (2) Undercut, incomplete fusion, restart of the weld, weld-repair starts, and other discontinuities were found to reduce the fatigue life of welded beams.
- (3) Design specifications should account for the existence of such defects in welded beams.
- (4) The distribution of the size and location of the pores in the longitudinal web-to-flange fillet-weld was random. The distribution of the cracks along the span was compatible with the theoretical bending stress distribution in the tension flange corrected for the local load influences.
- (5) Cracks were observed in the nominal compression flange for all three grades of steel when partial reversal of stresses

was applied. Only A514 steel beams revealed cracks in the compression flange when the applied nominal stresses remained compressive.

- (6) The compression flange cracks were related to the initial residual stress distribution and the differences in redistribution of the residual stresses under applied loading for the three grades of steel beams.
- (7) Compression flange cracks were not critical unless a tension stress component was applied with the stress range. This permitted crack growth outside the residual tensile stress core.
- (8) Rolled beams yielded longer lives than the welded beams and exhibited a large scatter in the data.
- (9) The examination of the initial flaw conditions revealed that cracks in rolled beams originate from small defects in the rolled surface or from the flange tip.
- (10) Fracture mechanics concepts provided a rational way to analyze and characterize the behavior of welded and rolled beams. These concepts were applied to describe numerically the initial flaw conditions in rolled and welded beams, and to derive a crack-growth rate vs. range of stress-intensity relationship from welded-beam fatigue data.
- (11) A penny-shaped crack was found to model crack growth from porosity in welded beams. An equivalent crack with a 0.04

inch radius described the average pores observed in the welded beams.

- (12) The depth of the flaws in the surface of the rolled beams was estimated to be at least an order of magnitude smaller than the welded beam pore radius. Flange-tip defects in rolled beams formed a slightly more severe defect than the surface flaws.
- (13) Coefficients for a linear log-log transformation of crack-growth rate vs. ΔK relationship were derived from the stress-life relationship of welded beams using the initial and final crack-size.
- (14) The derived relationship correlated well with measured crack-growth data from a welded beam.
- (15) The derived crack-growth equation exhibited the same trend as measured data from crack-growth specimens. It provided a lower estimate of the growth rate. Among other factors, this difference was attributed to crack initiation, a possible overestimate of the stress intensity, and slower growth in the plane-strain condition for the welded beams.
- (16) Available crack-growth data were shown to only cover a small region of growth-rates. Extrapolation into regions outside the data could be misleading, particularly when used for fatigue life estimates.
- (17) It was also apparent that factors influencing the deviations from the straight line approximation of the crack-

growth equation are not well understood. No experiments have been conducted to evaluate statistically the influence of the major factors that influence the transitional behaviors.

- (18) Very little information is available for growth rates below 10^{-6} in./cycles. This was found to be the region most critical for the fatigue behavior of welded and rolled beams. More than 75% of the life was spent in this region growing a crack from its initial size to a visible crack.
- (19) It was shown that an increase in flange-thickness and larger weld-sizes should not permit an increase in allowable defect-size. The initial crack-size was the controlling factor for the fatigue life of welded beams.
- (20) The plastic zone size correction was shown to have no significant influence on the fatigue behavior of welded beams containing the assumed penny-shaped crack. Since most of the life was consumed growing a penny-shaped crack there was little effect on beam behavior.
- (21) A transition from plane-strain to plane-stress behavior was observed when the crack reached the extreme fibre of the flange. The mode of growth also changed to a three-ended crack. The plastic zone size correction was significant for the three-ended crack.
- (22) The scatter of the fatigue data was found to be related

in part to the variation in the initial pore-condition and fatigue crack-growth rates.

- (23) Fracture mechanics concepts were found to be applicable in the analysis of welded and rolled beams. More information is needed outside the regions of available growth-rate data, and on the statistical variation of the individual parameters that influence crack-growth rates.

NOMENCLATURESYMBOLS

- B_1 = constant; intercept of log-log transformation of regression curve
- B_2 = constant; slope of log-log transformation of regression curve
- C = a material related constant in crack-growth equation
- C' = $\frac{1}{C} \cdot \frac{1}{\alpha f^m(a) \pi^{m/2}} (a_i^{-\alpha} - a_j^{-\alpha})$ (Eq. 5.9)
- K = elastic stress-intensity factor for a crack; (ksi $\sqrt{\text{in.}}$) (Eq. 5.1)
- N = number of applied stress cycles
- N_{ij} = number of cycles required for a crack to grow from size a_i to size a_j (Eq. 5.6)
- S = nominal applied stress in the extreme fibre of the tension flange
- S_{max} = maximum stress
- S_{min} = minimum stress
- S_r = stress range

- a = crack size;
 crack-radius for penny-shaped crack, half crack-width for tunnel crack or through-the-thickness crack, crack-depth for surface crack, crack-radius for corner crack, minor half-axis for elliptical crack
- \bar{a} = crack size corrected for plastic zone at crack-tip
 (Eq. 5.20)
- a_c = total crack size on the inside surface of the flange; computed from the measurements a and c on both sides of the web
- a_e = equivalent radius of a penny-shaped crack that provides the same K-factor estimated for the arbitrarily shaped crack
- a_f = final crack-size
- a_i = initial crack-size (for integration interval)
- a_j = final crack-size (for integration interval)
- b = major half-axis for an elliptical crack
- e_f = crack size on extreme fibre of the flange
- $f(a)$ = nondimensional geometry correction factor for stress-intensity factor K
- $f'(a)$ = geometry correction factor including correction for plastic zone-size at the crack-tip
 (Eqs. 5.21 and 5.22)
- m = exponent of crack-growth equation; slope of equation in log-log transformation

- r_y = plastic zone-size radius at the crack-tip (Eq. 5.19)
- s = standard error of estimate
- α = $\frac{m}{2} - 1$ (Eq. 5.7)
- ΔK = stress-intensity-factor range (Eq. 5.2)
- $\Delta\sigma$ = stress range relevant for the determination of the stress-intensity-factor range
- λ = stress concentration factor (Eq. 5.14)
- σ = stress applied sufficiently away from the crack-tip
- σ_y = yield strength (or 0.2% offset) of material

GLOSSARY

Blow hole = tunnel-like pore extending to the surface of the weld

Cell of factorial = a particular testing condition within the factorial experiment

Compression flange = flange subjected to only or predominantly compression stresses in the stress cycle

Confidence interval = statistical interval that is expected to contain with a given confidence a given percentage of the test data

Confidence limit = statistical limit that describes with a given confidence the expected survival of a given percentage of the test beams

Defect = imperfection or discontinuity that is judged damaging to the function of the material

Factorial experiment = experiment plan where observations are taken at all possible combinations that can be formed for the different levels of the factors

Failure = generally defined in this study as an increase in mid-span deflection of 0.020 inch due to fatigue cracking of the test beam

Fatigue behavior = description of crack initiation and propagation under given stress conditions

Fatigue life = number of load cycles to failure

Fatigue strength = derived relationship between fatigue life and applied stress

Flaw = any imperfection or discontinuity in the base material, in the weldment, or introduced by the weld. A flaw may become a defect under certain stress conditions

Fractographic examination = examination of the surface of the fatigue crack to evaluate the location of crack initiation and direction of crack propagation

Fretting = microscopic slip between two metallic surfaces under the action of oscillating forces

Gas pore = small cavity in the weld metal caused by entrapped gas

Initial flaw condition = defect that exists in a welded or rolled beam before application of cyclic loading

Life interval = number of cycles required to grow a crack from size a_i to size a_j

Lognormal distribution = normal distribution of a dependent variable in the logarithmic transformation

Notch = local discontinuity in the geometry of the specimen

Penny-shaped crack = disc-like crack in an infinite body

Pipe hole = blow hole

Plastic zone size = size of the plastic zone at the tip of a crack

Pore = small cavity in the weldment caused by entrapped gas

Porosity = describes the presence of cavities in the weld metal that are generally completely inside the weld

Stable crack growth = region of growth that can be described by an analytical model relating crack-growth rate to stress-intensity-factor range

Stress range = algebraic difference between maximum and minimum stress

Stress ratio = algebraic ratio of minimum stress to maximum stress

Tack weld = small length (about 3 in.) of manually placed weld to preliminarily assemble the components of a structure

Three-ended crack = crack in the web-flange junction of beams with two crack fronts in the flange and one in the web

Threshold crack growth = level of ΔK -value where diminishingly small crack growth occurs

Tunnel crack = long crack with two parallel crack fronts

Worm hole = gas pore consisting of a series of small cavities

Weld repair = generally local repair of weld because of undercut,
insufficient weld, or other weld deficiencies

FIGURES

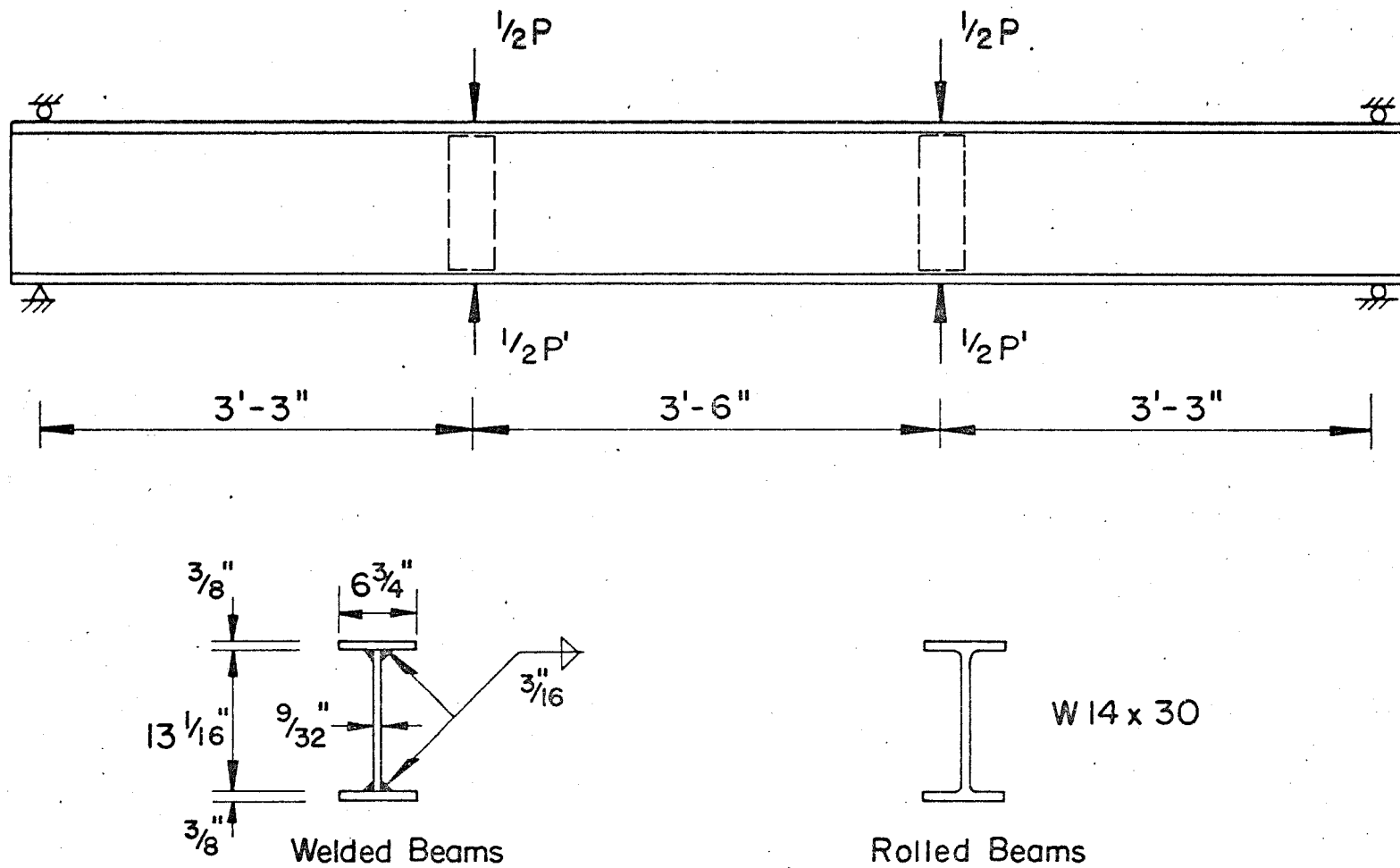
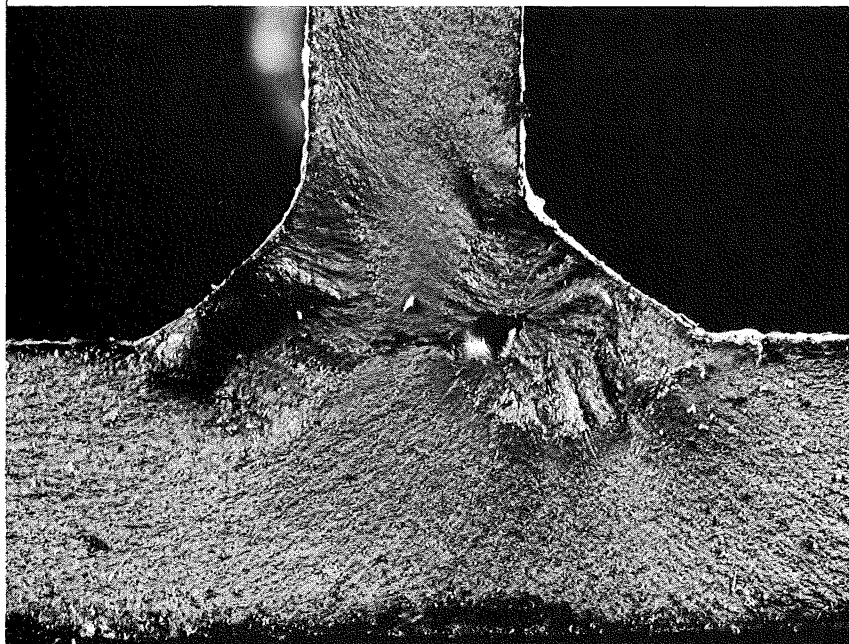
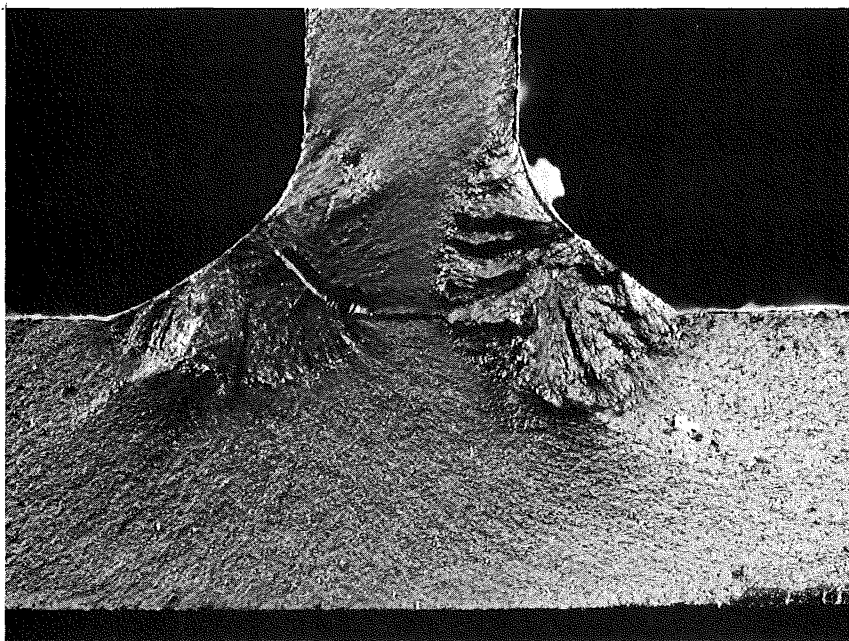


Fig. 1 Loading geometry and cross-sections of plain-welded and plain-rolled beams



(a) Typical gas pore (x4)



(b) Pore elongated and perpendicular to the weld surface (x4)

Fig. 2 Examples of porosity from the root of the longitudinal fillet-weld

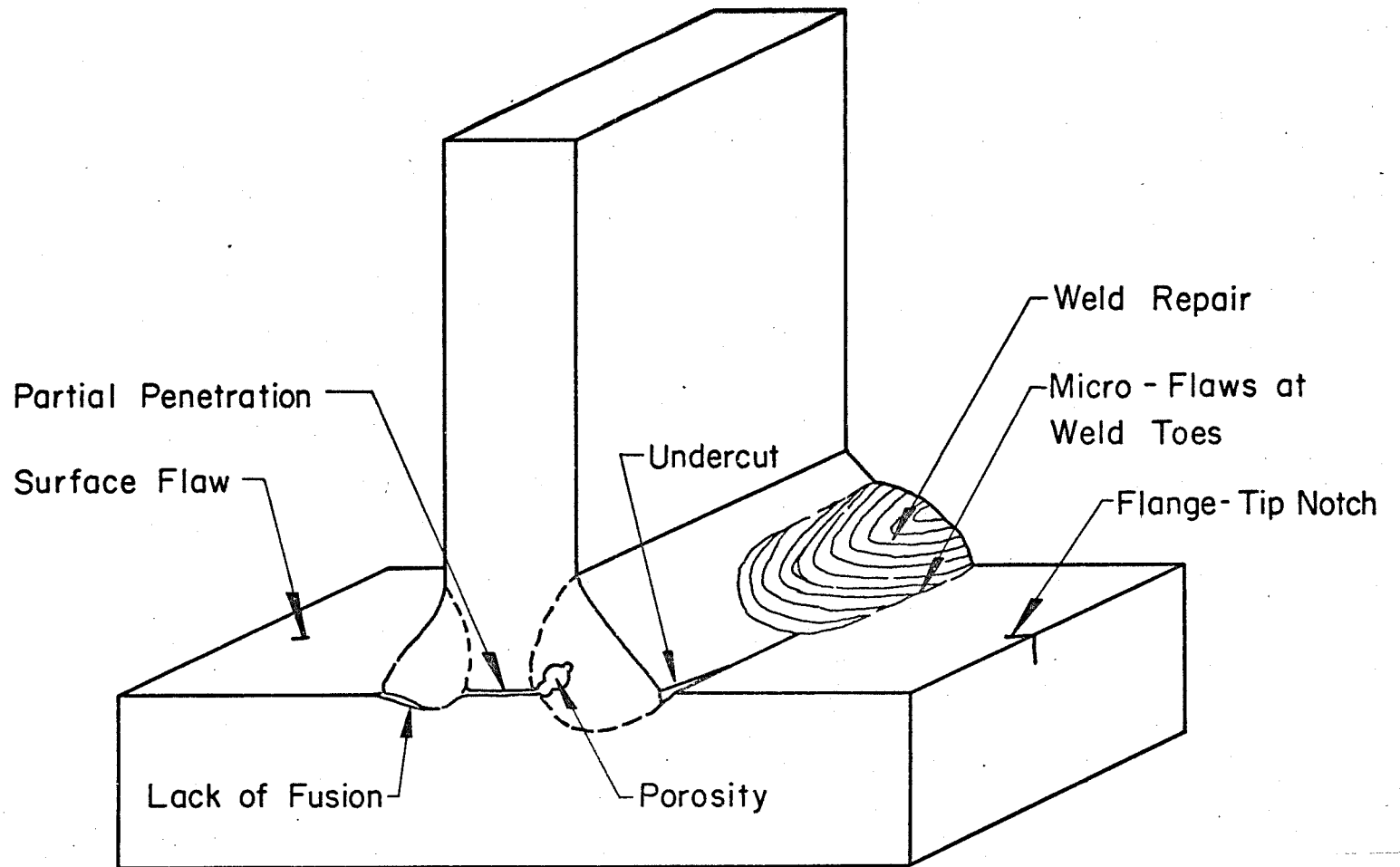
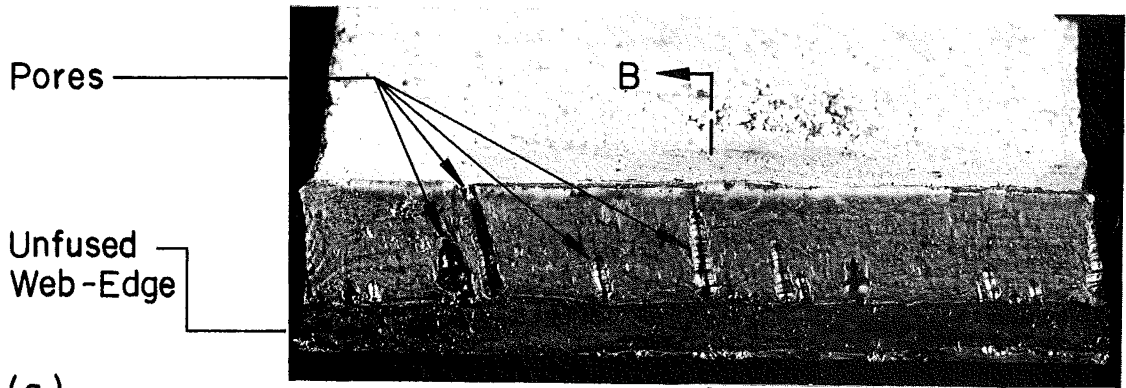
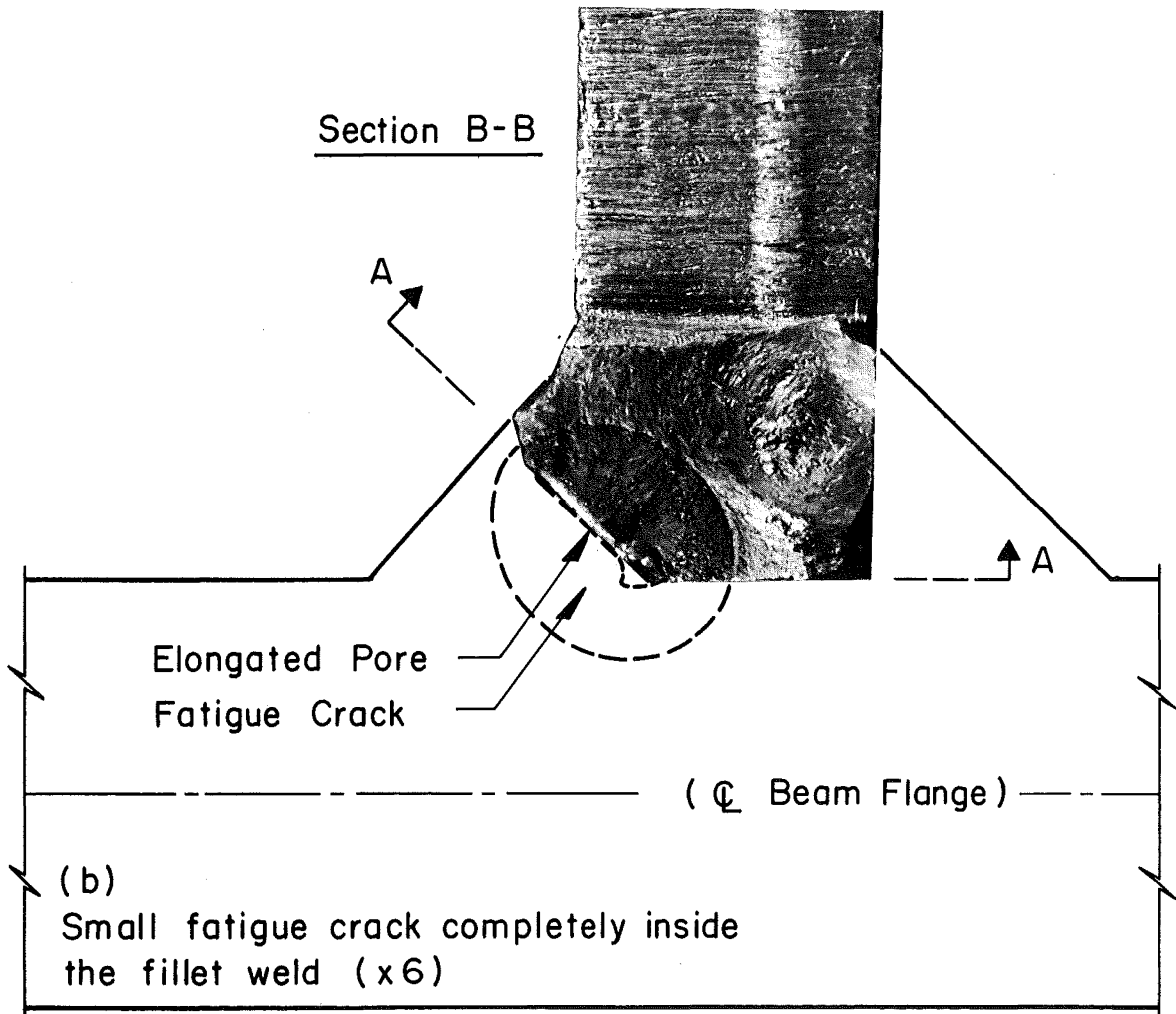


Fig. 3 Schematic of possible locations for crack initiation in welded beams



(a)
Location and distribution of shapes
and sizes of pores in the longitudinal
fillet weld (x3)

Section A-A



(b)
Small fatigue crack completely inside
the fillet weld (x6)

Fig. 4 Small fatigue cracks originating from porosity in the flange-to-web fillet weld, and growing perpendicular to the axis of the weld

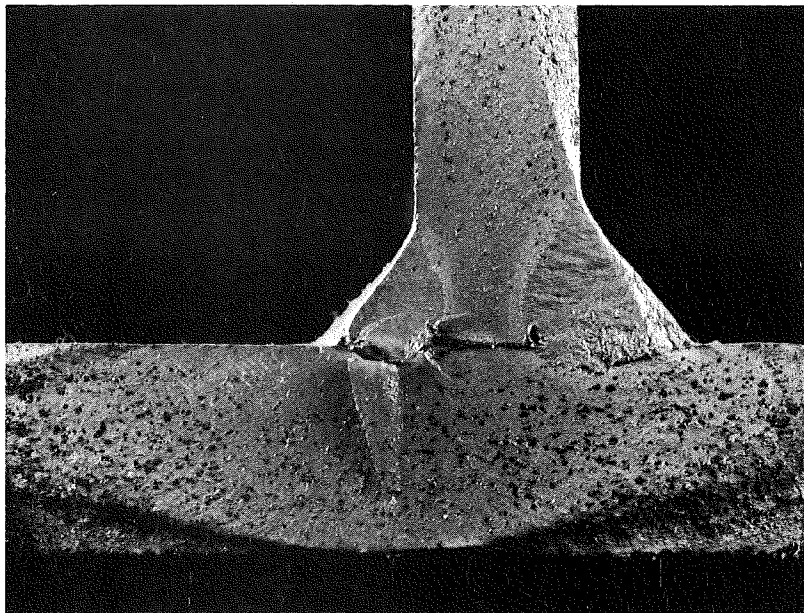


Fig. 5 Crack initiation from lack of fusion of the fillet weld in the flange (x3)

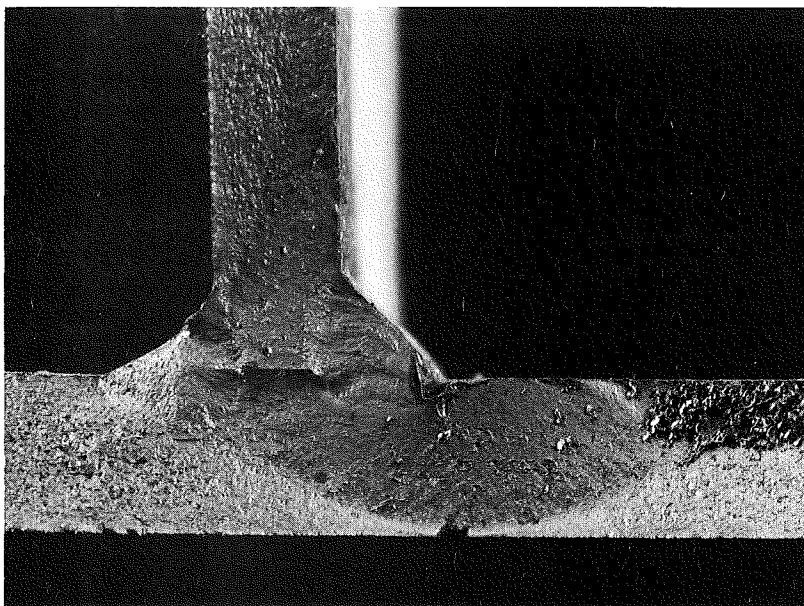


Fig. 6 Local undercut in the flange at the location of the continuous weld passing over a tack weld (x2.2)

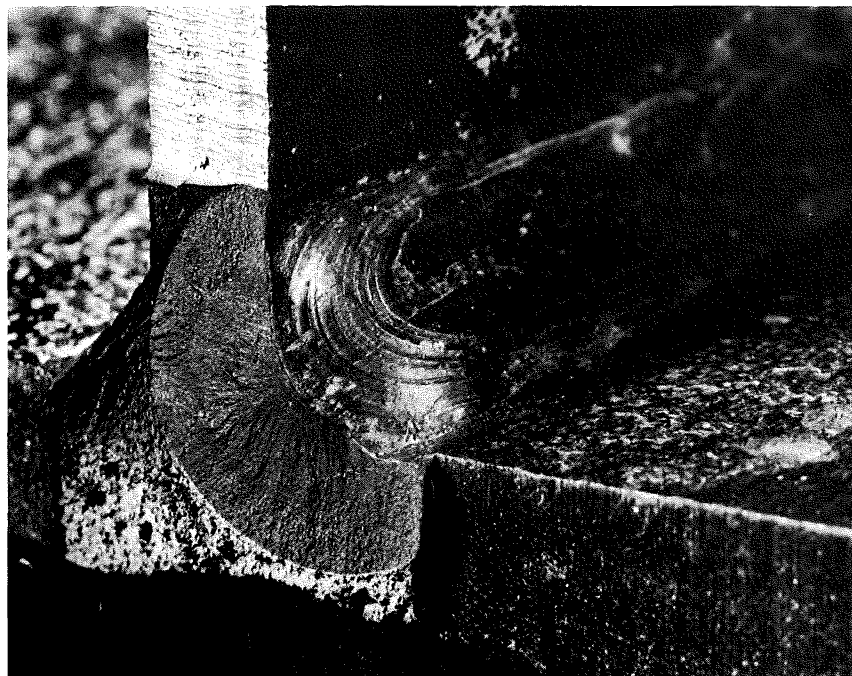


Fig. 7 Initiation of a crack at the start of a weld repair placed to fill insufficient weld profile ($\sim x2.5$)

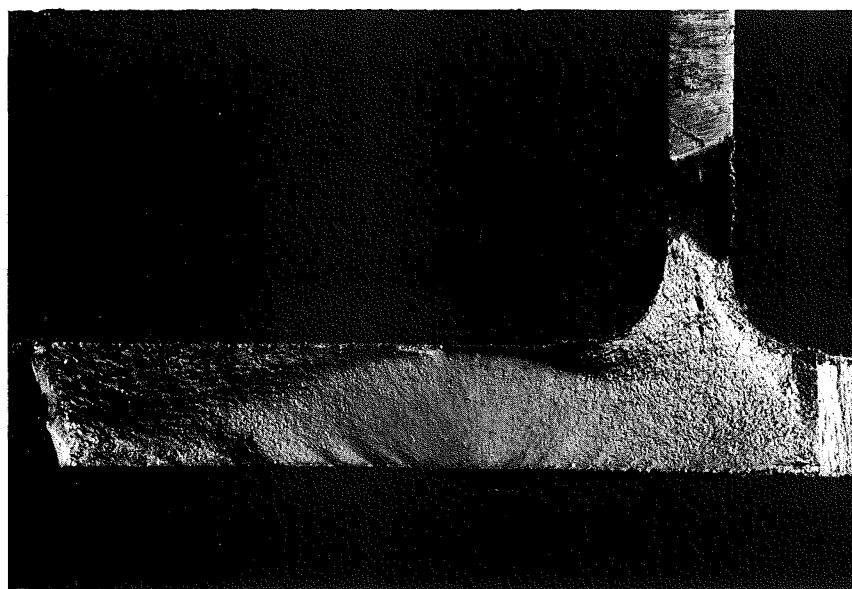
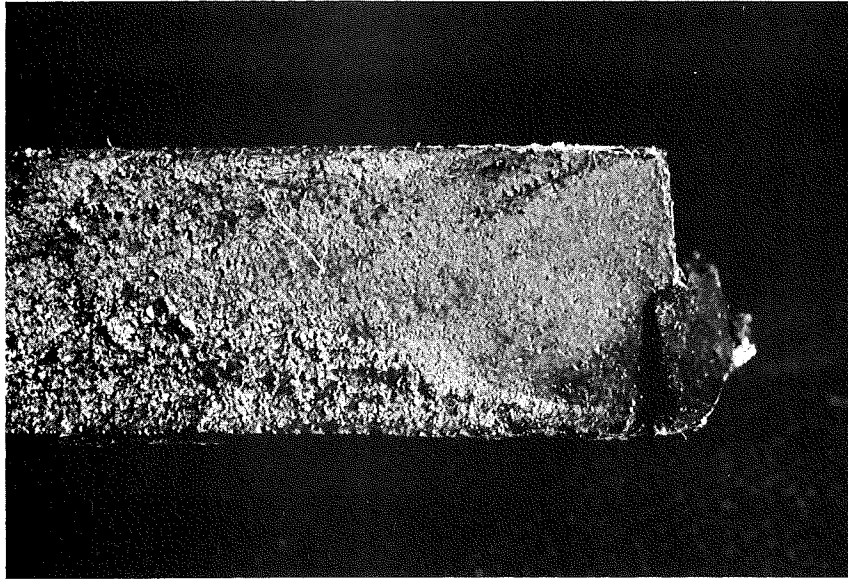
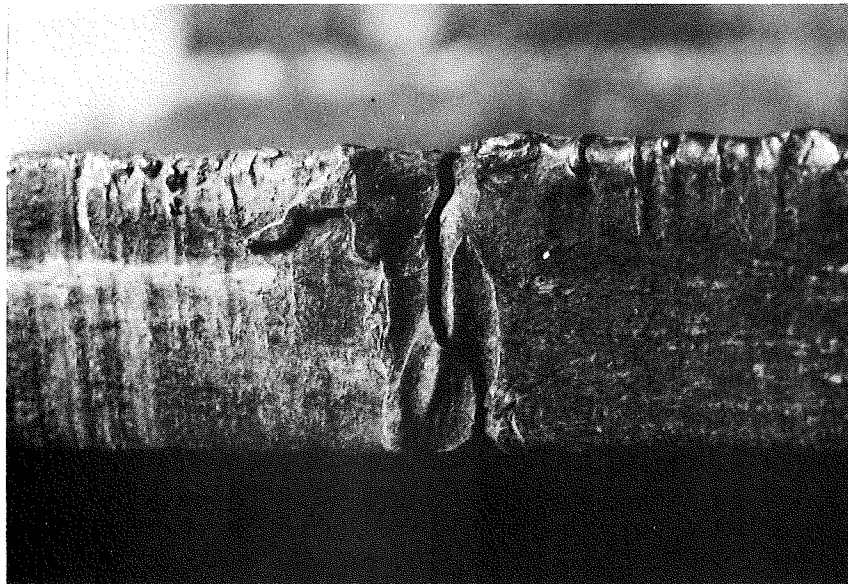


Fig. 8 Crack initiation from a flaw in the rolled surface of a plain-rolled beam ($x1.7$)



(a) Lamination at the flange-tip of a rolled beam (x4)



(b) Severe notch at the flame-cut flange-tip of a welded beam (x4)

Fig. 9 Examples for crack-initiation from the flange-tip

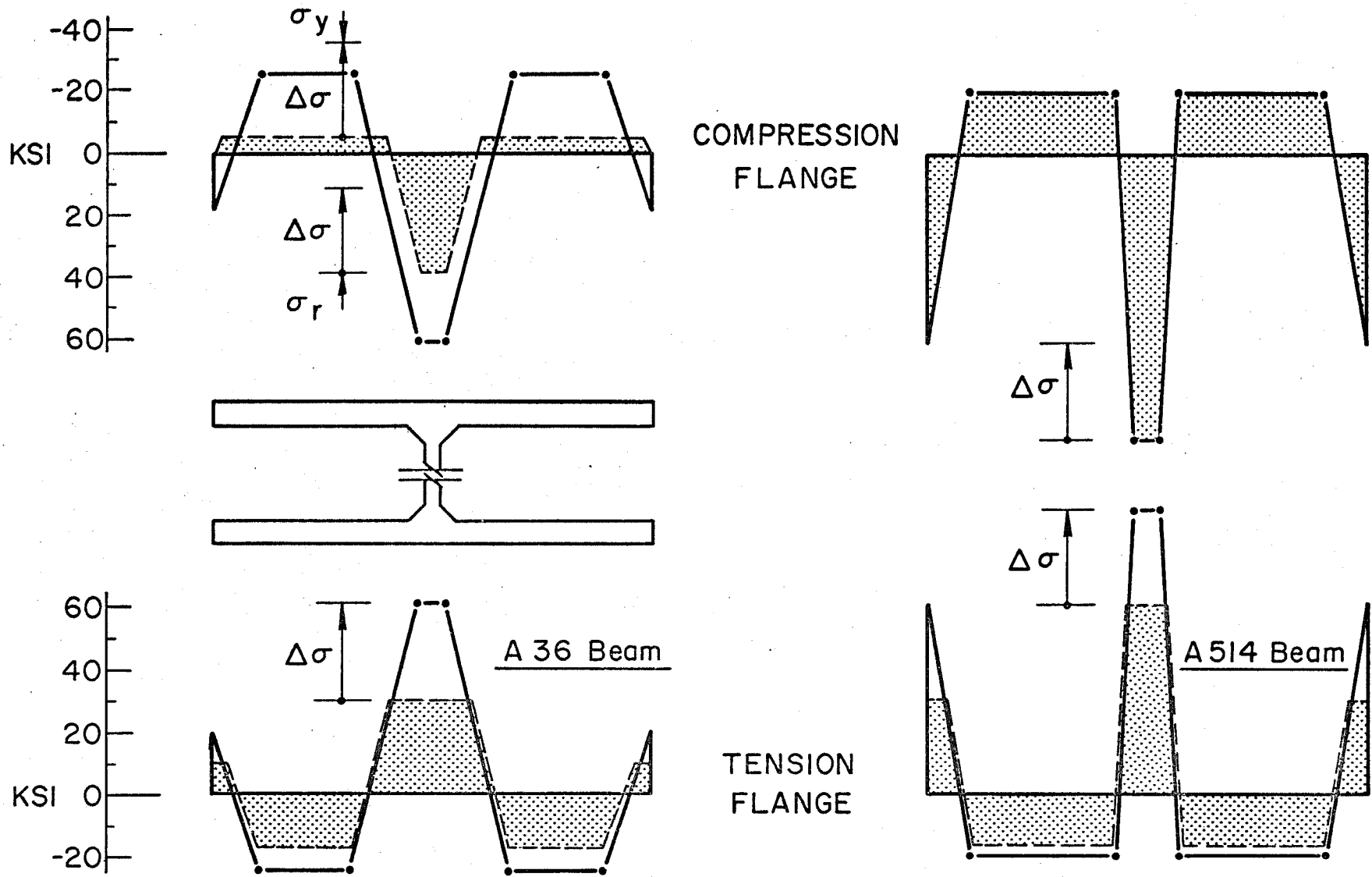


Fig. 10 Schematic of distribution and redistribution of residual stresses in welded beams

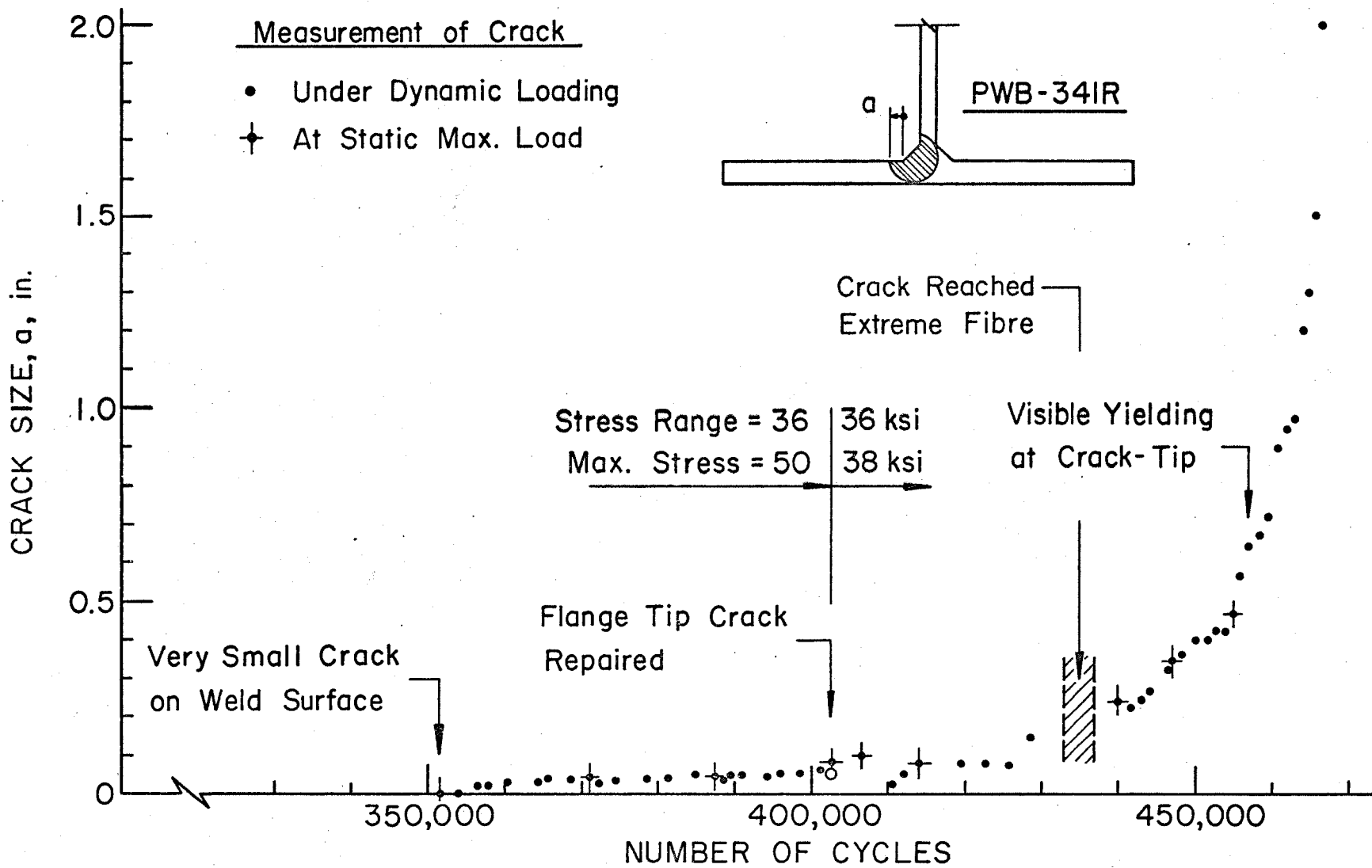


Fig. 11 Summary of crack-growth study on a plain-welded beam

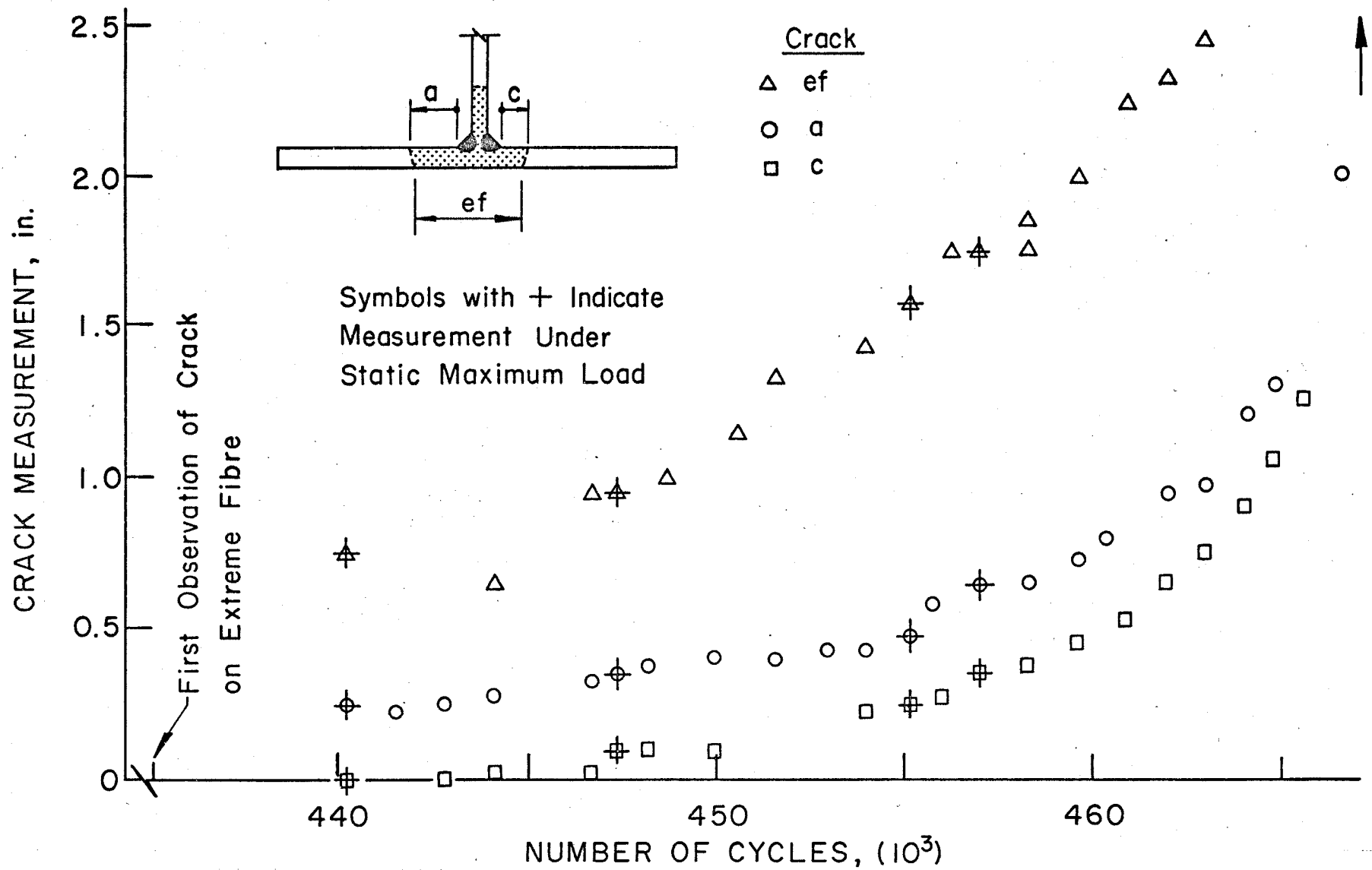


Fig. 12 Measurements of crack sizes of a three-ended crack in the test beam

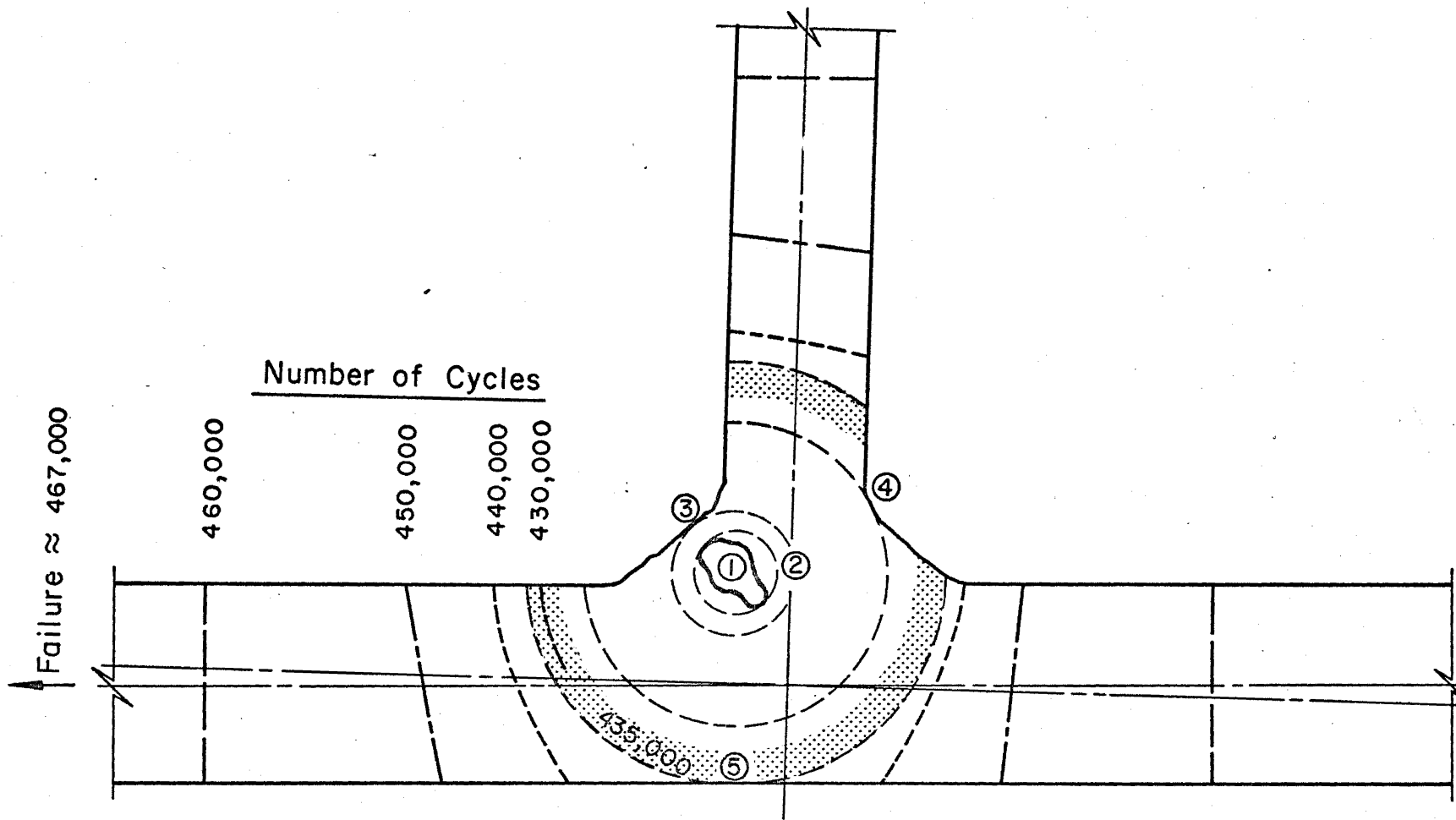


Fig. 13 Schematic of the stages of crack growth from a pore in the fillet weld

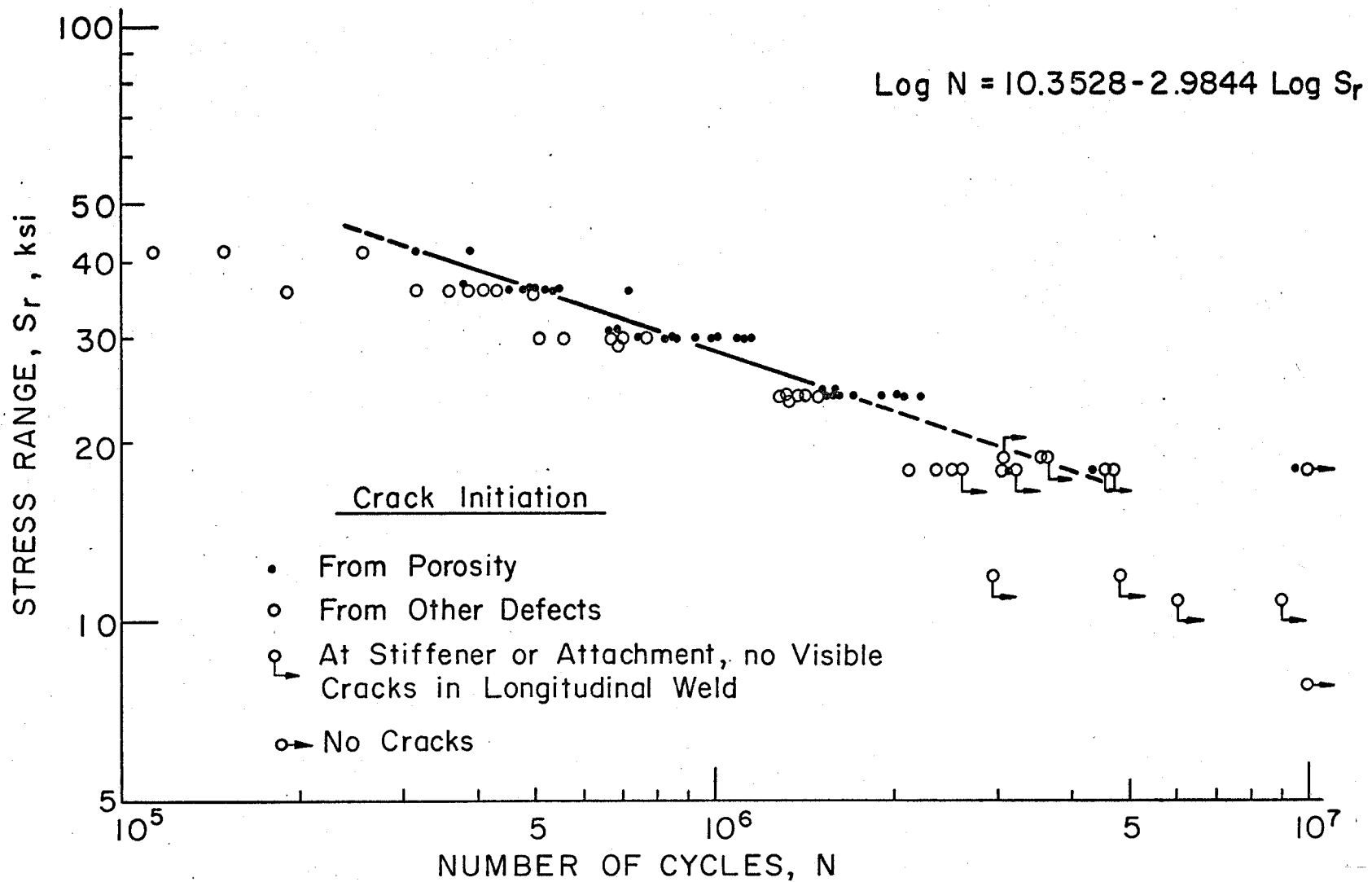


Fig. 15 Comparison of all welded beams failing from porosity in the fillet weld with beams failing from other defects

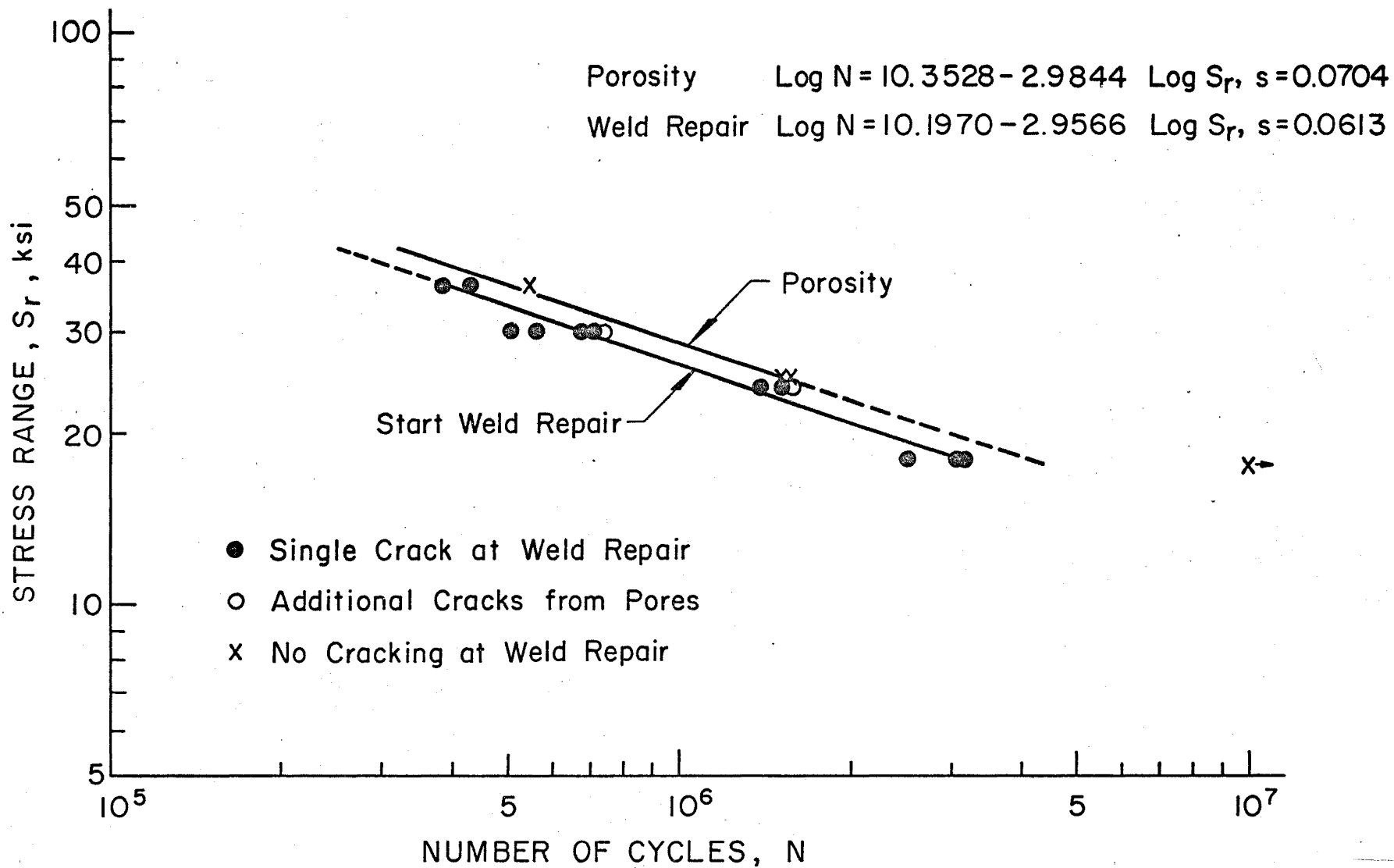


Fig. 16 Comparison of beams failing from weld-repair defects with the mean for porosity

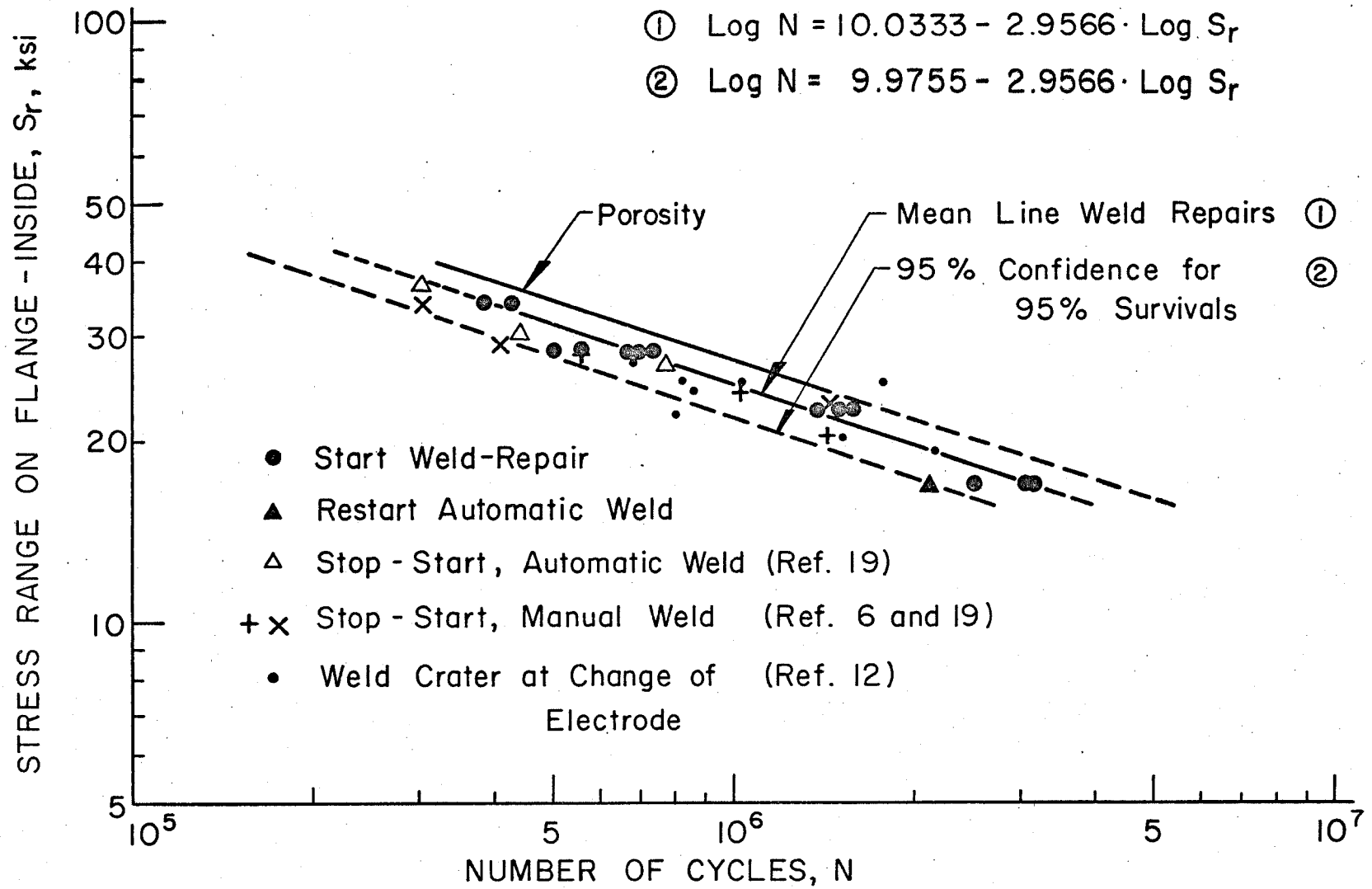


Fig. 17 Comparison of weld-repair failures with failures from stop-start positions or weld craters

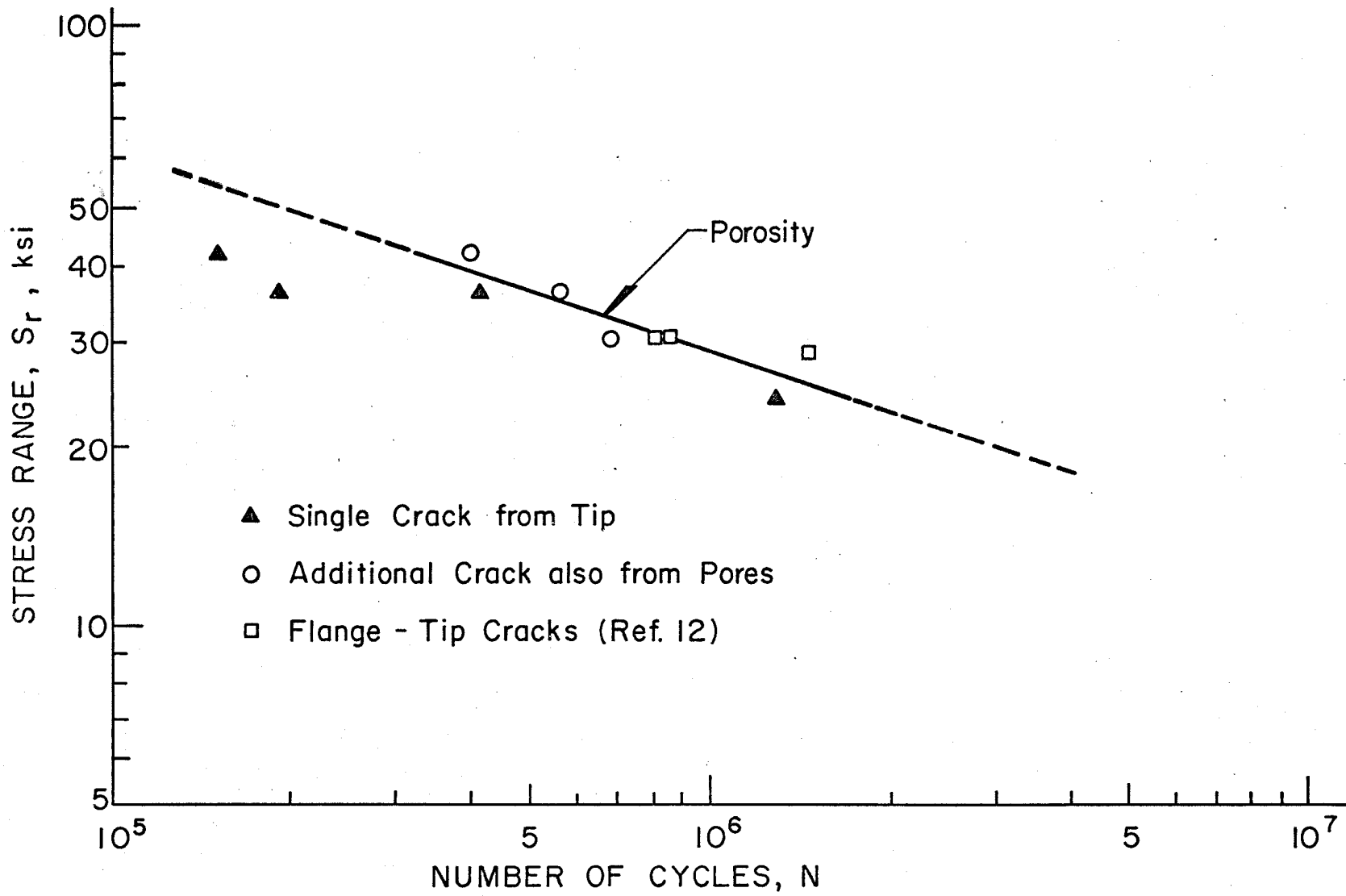


Fig. 18 Fatigue test data from welded beams with cracks originating from the flame-cut flange-tip

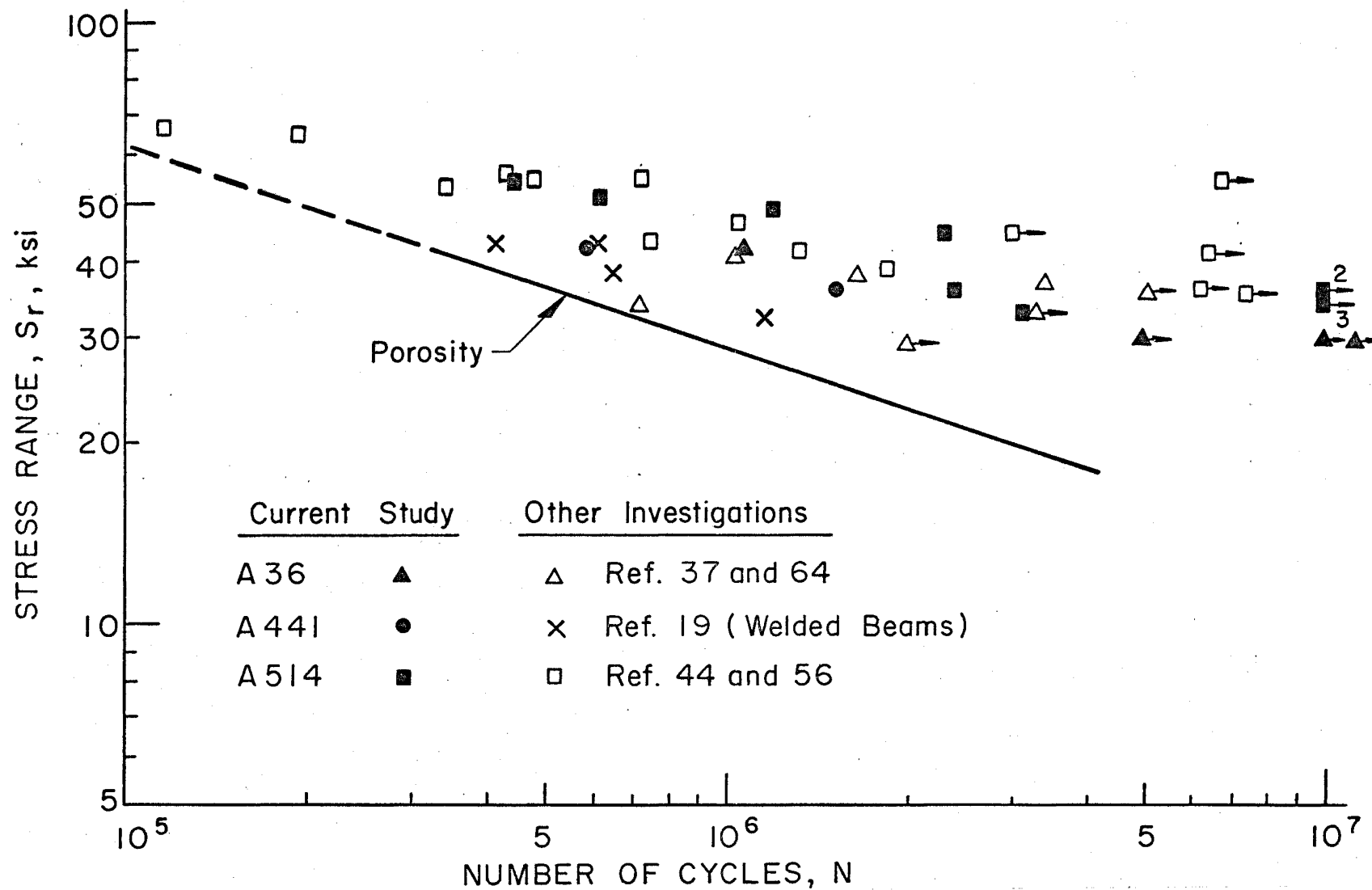


Fig. 19 Comparison of rolled-beam test data with previous results of beams that developed cracks from the rolled surface

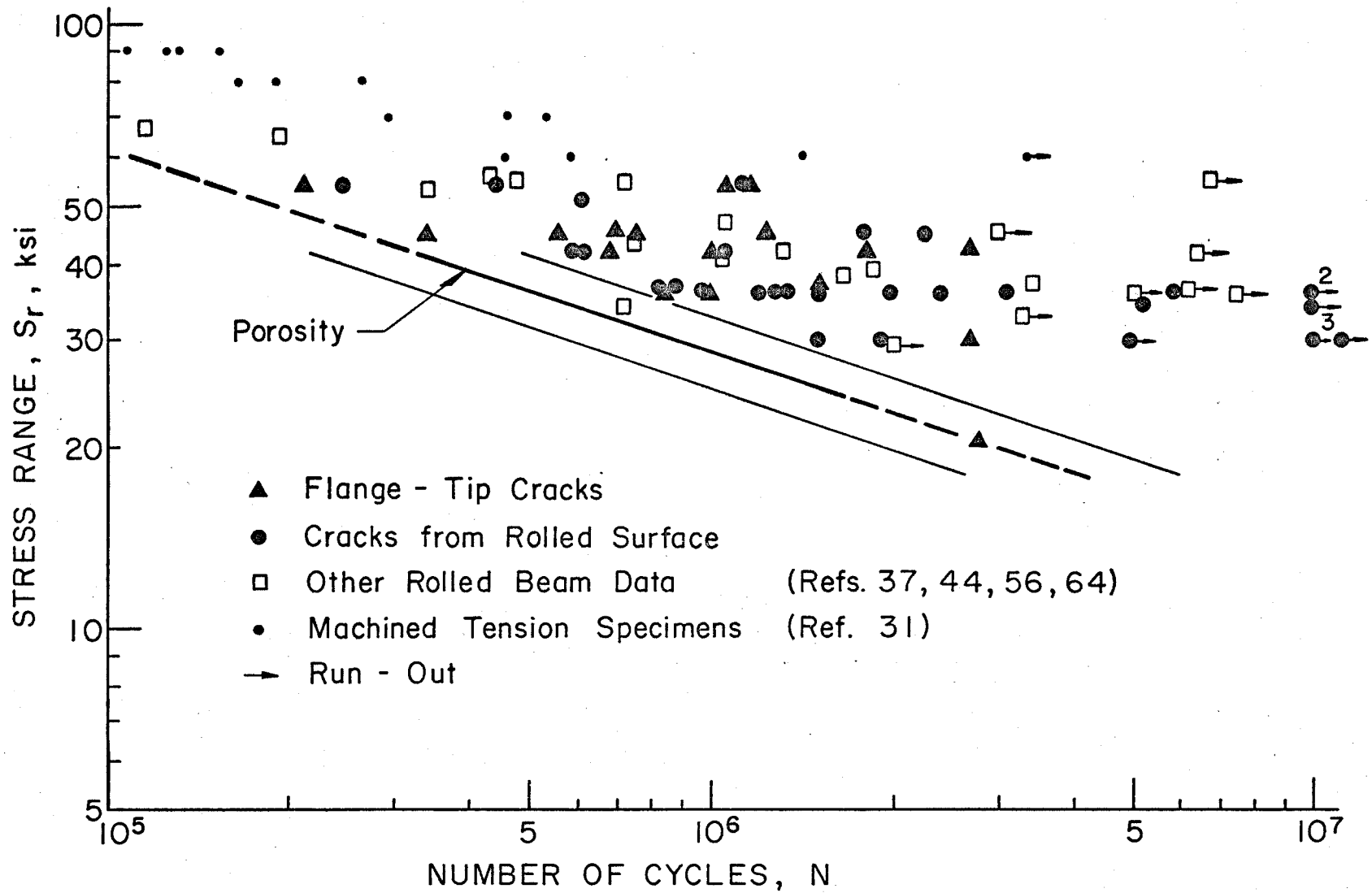
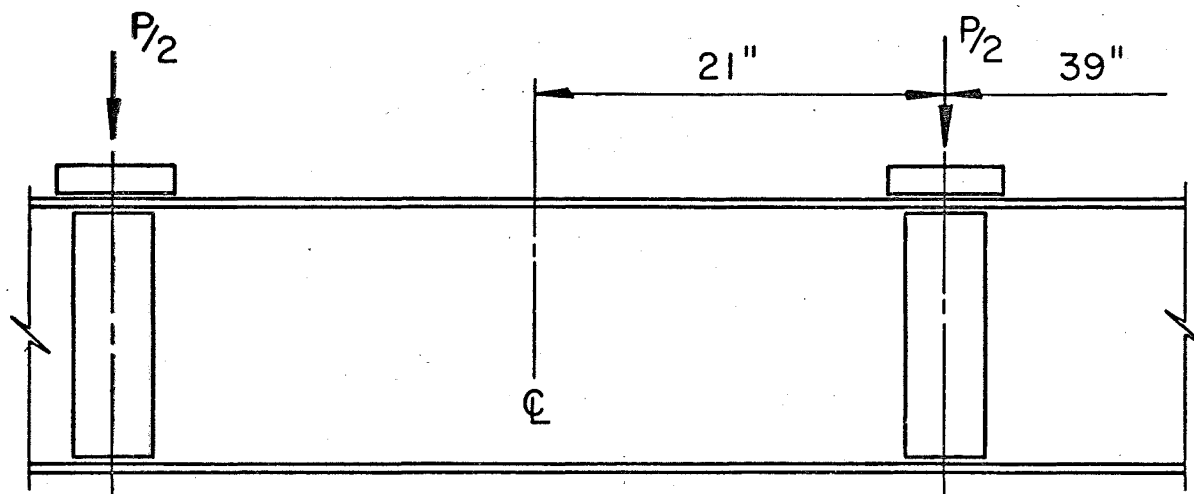
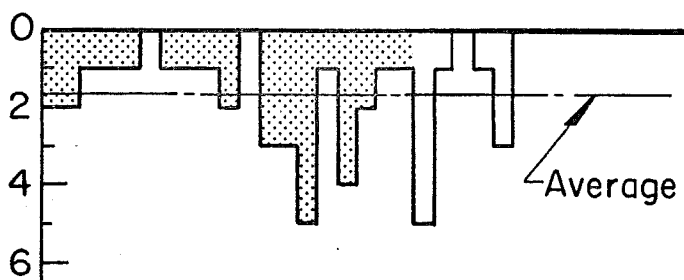


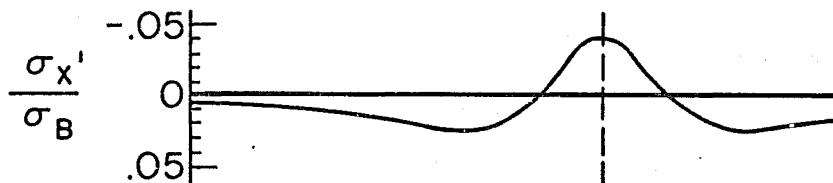
Fig. 21 Summary of rolled-beam data from this study and other investigations



(a) Frequency Distribution (Cracks Per Inch)



(b) Correction for Load Influence



(c) Total Bending Stress at Flange - Web Junction

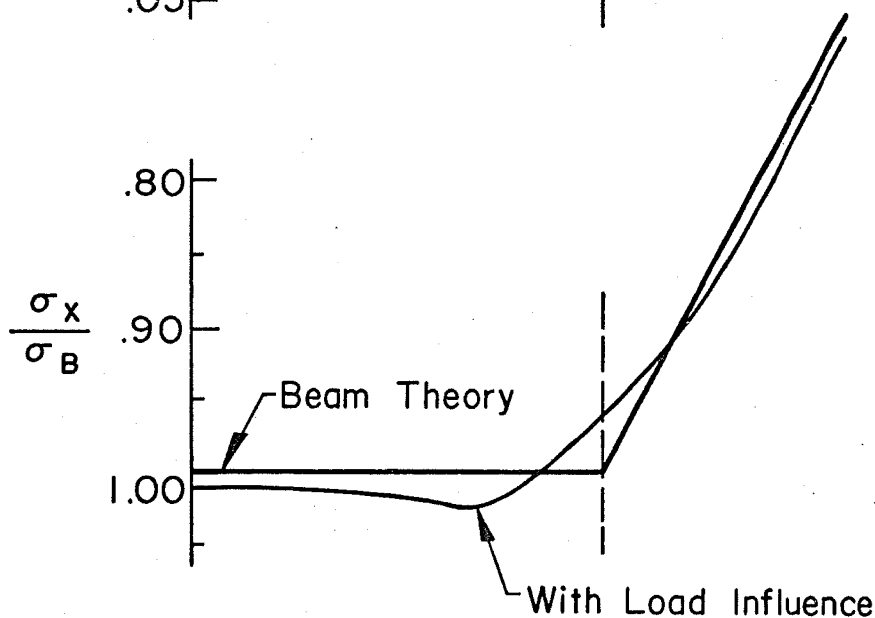


Fig. 22 Comparison of the frequency distribution of cracks with the stress distribution in the tension flange of plain-welded beams

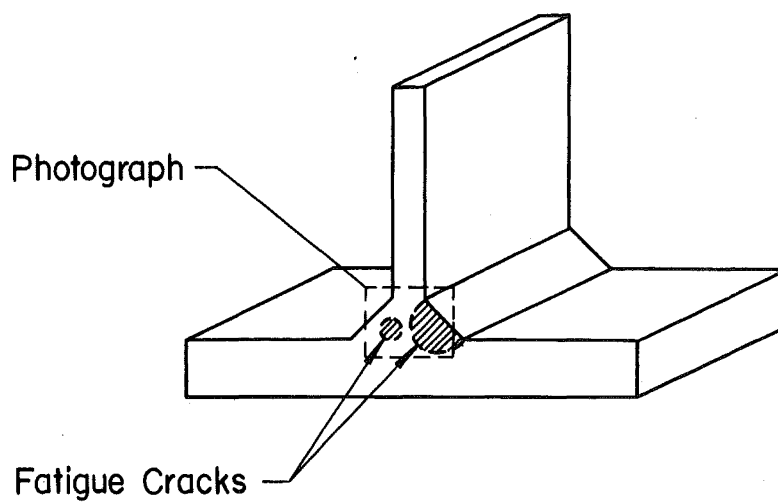


Fig. 23 Two small fatigue cracks that initiated from pores in the longitudinal fillet-weld and grew perpendicular to the axis of the weld ($\sim x8.5$)



Fig. 24 Small crack with penetration to the fillet-weld surface ($\sim x11$)

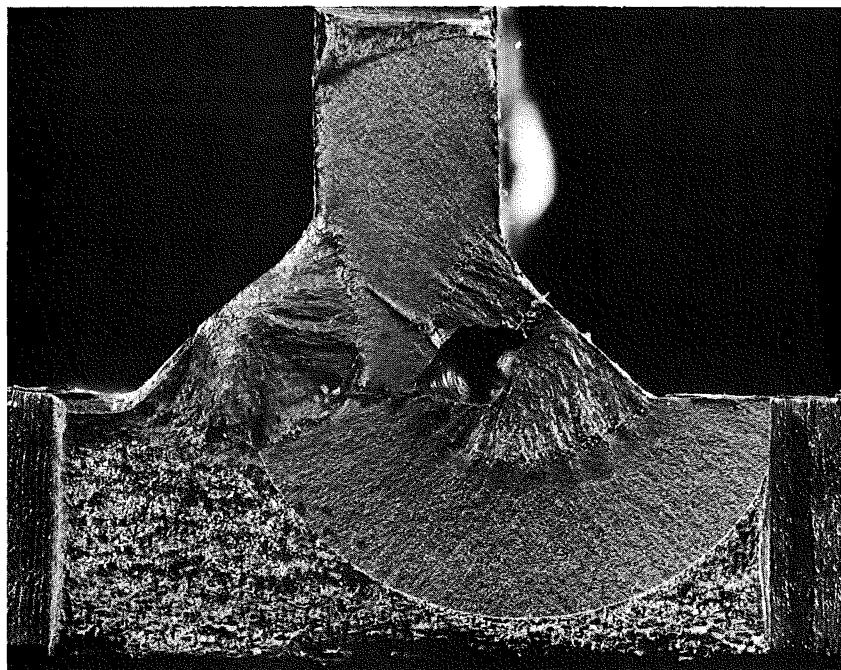


Fig. 25 Crack in flange-to-web junction approaching the extreme fibre of the tension flange ($x3.6$)

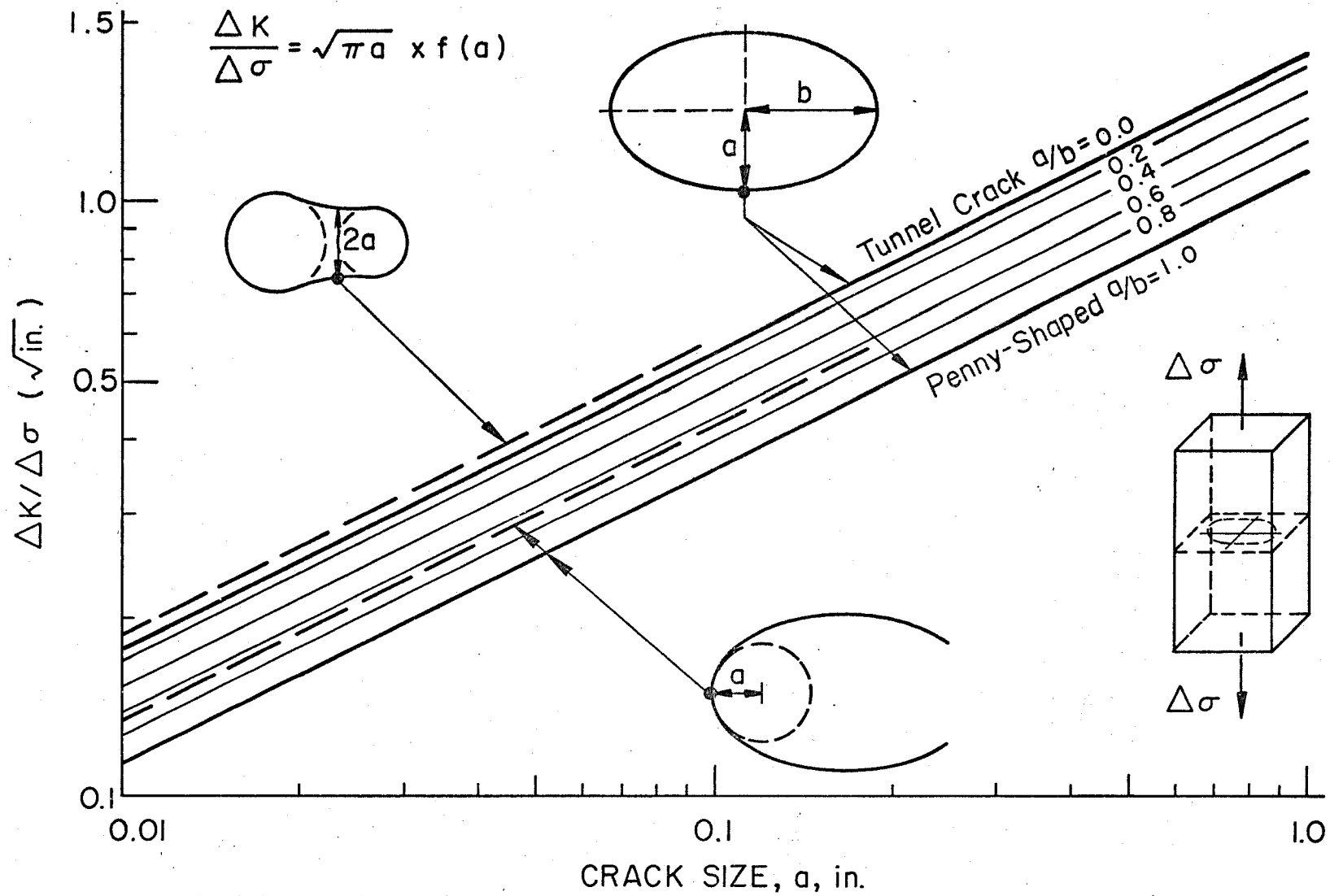


Fig. 26 Estimates of K-values for disc-like cracks in an infinite body

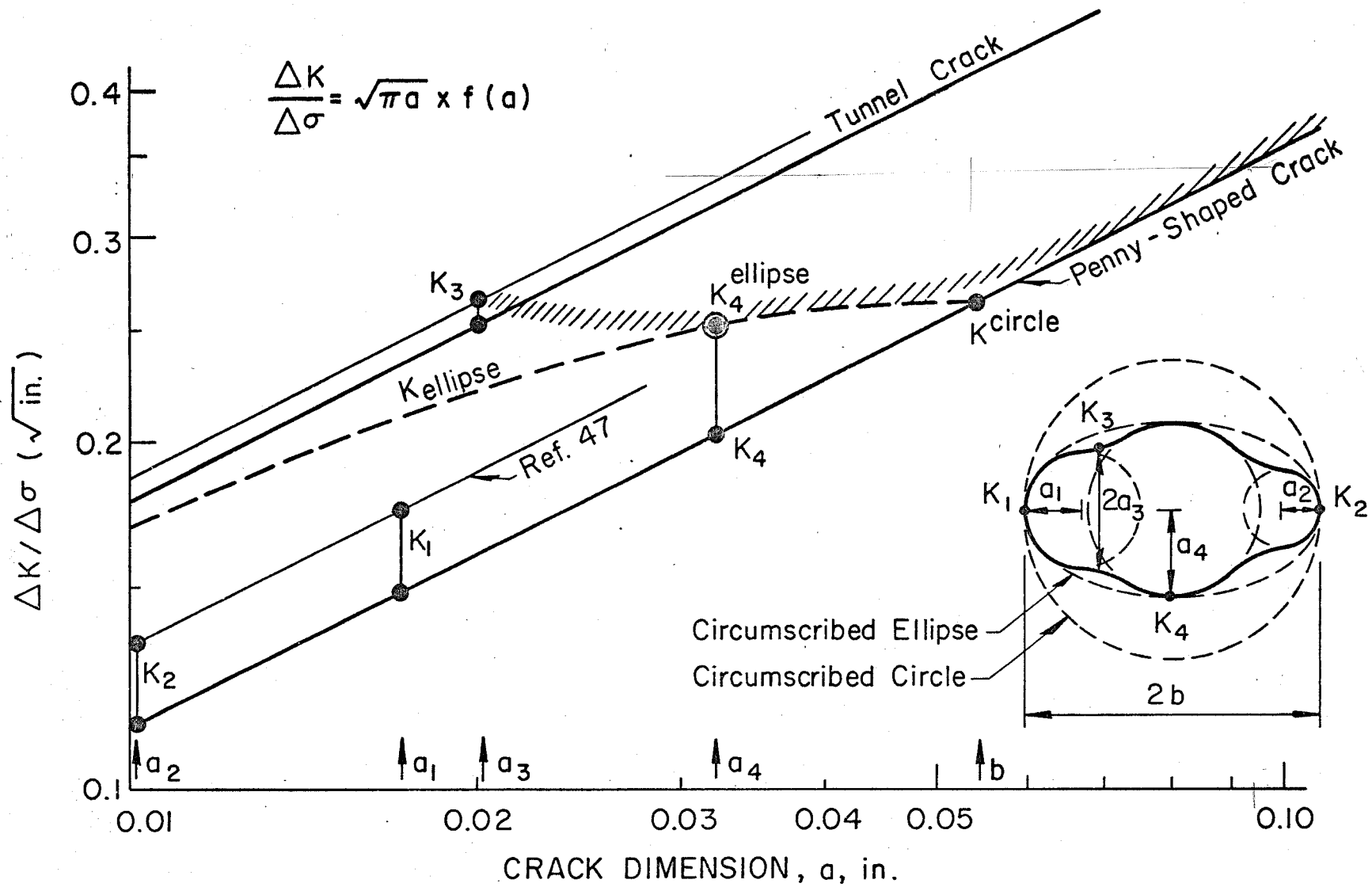


Fig. 27 Example for the estimates of K-values of an arbitrarily shaped pore

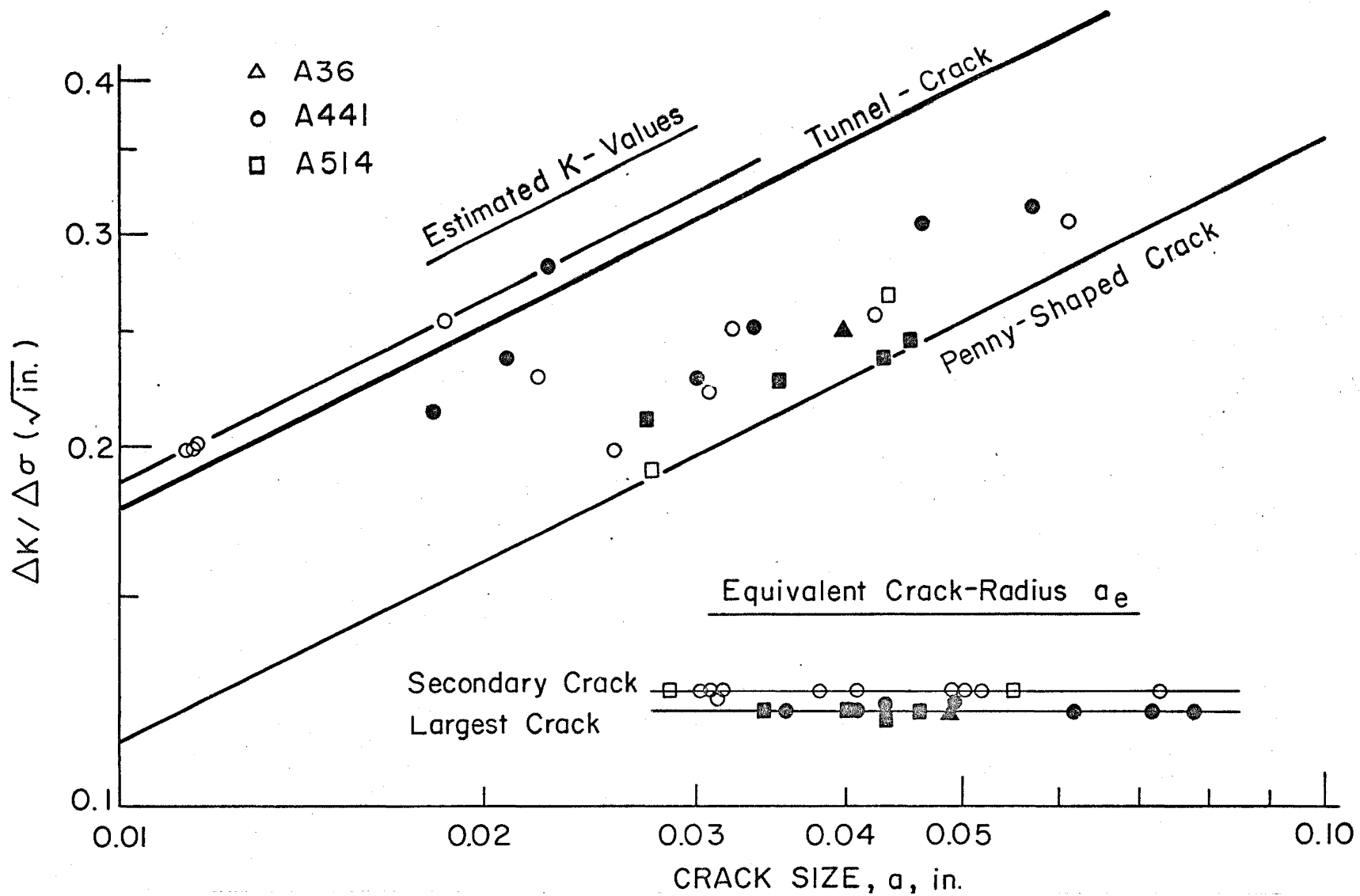


Fig. 28 Distribution of estimated K-values and equivalent crack-radii

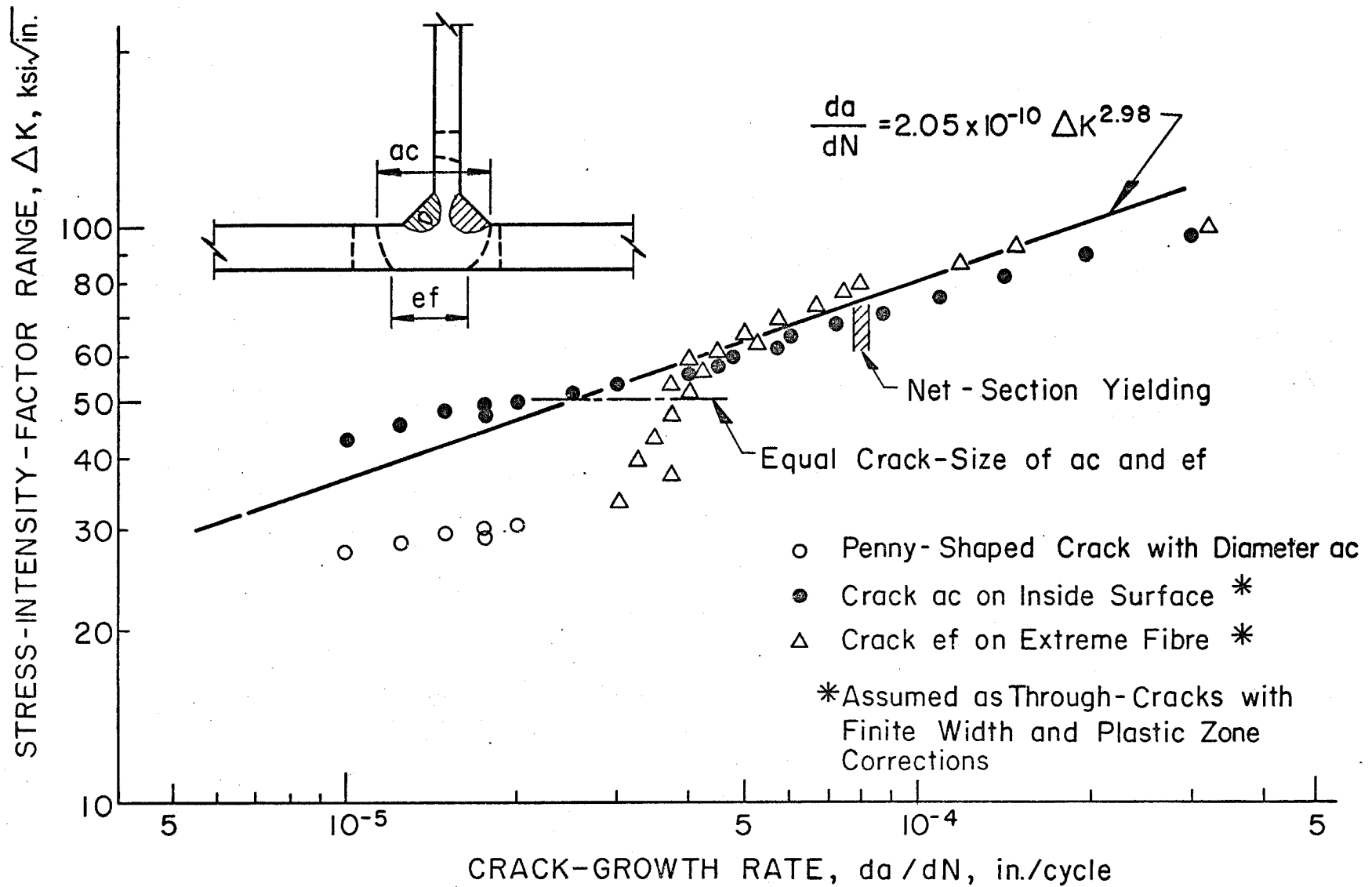


Fig. 29 Crack-growth rates computed from measurements on a plain-welded beam

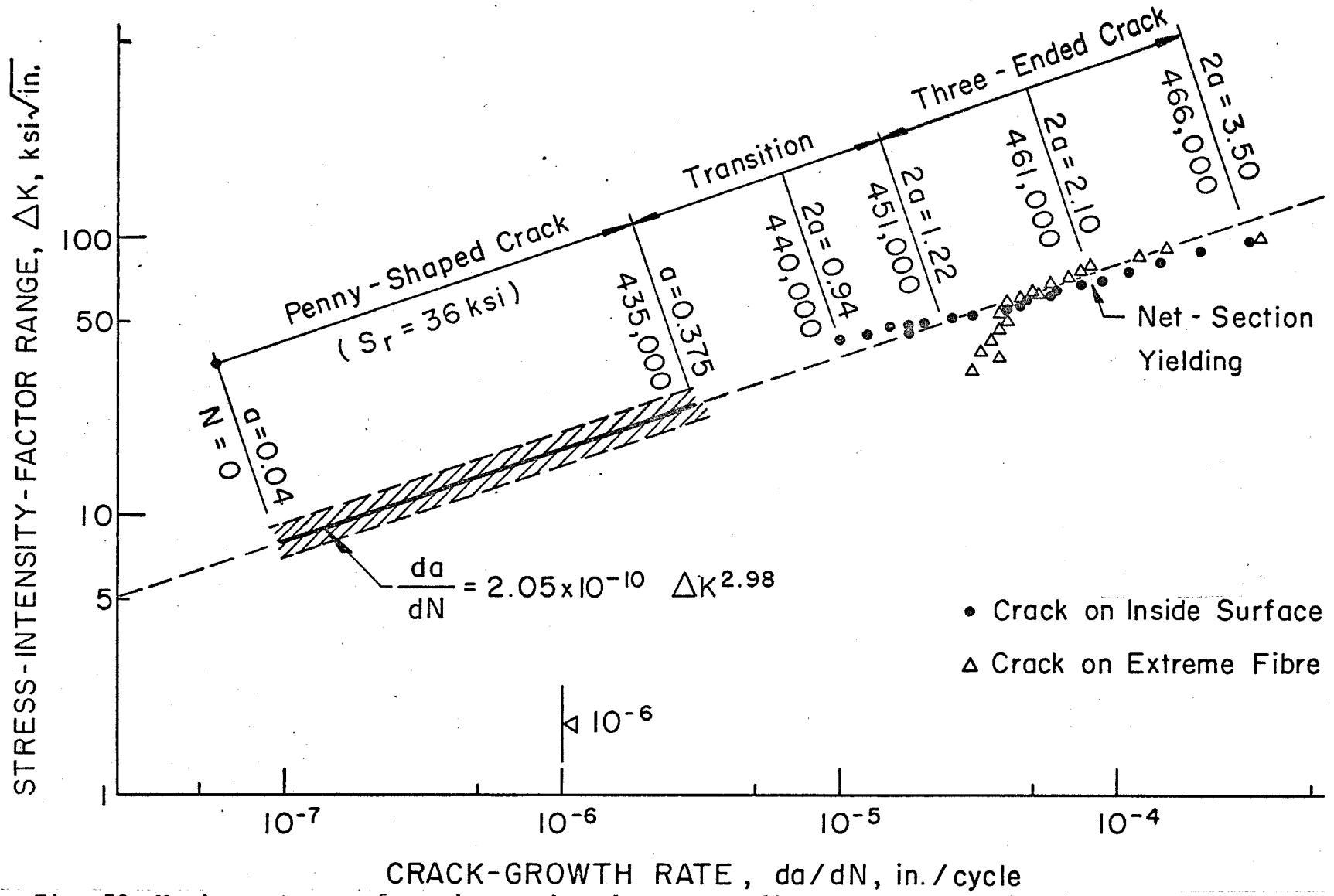


Fig. 30 Various stages of crack growth and corresponding growth rates for a crack in a plain-welded beam starting from a pore in the fillet weld

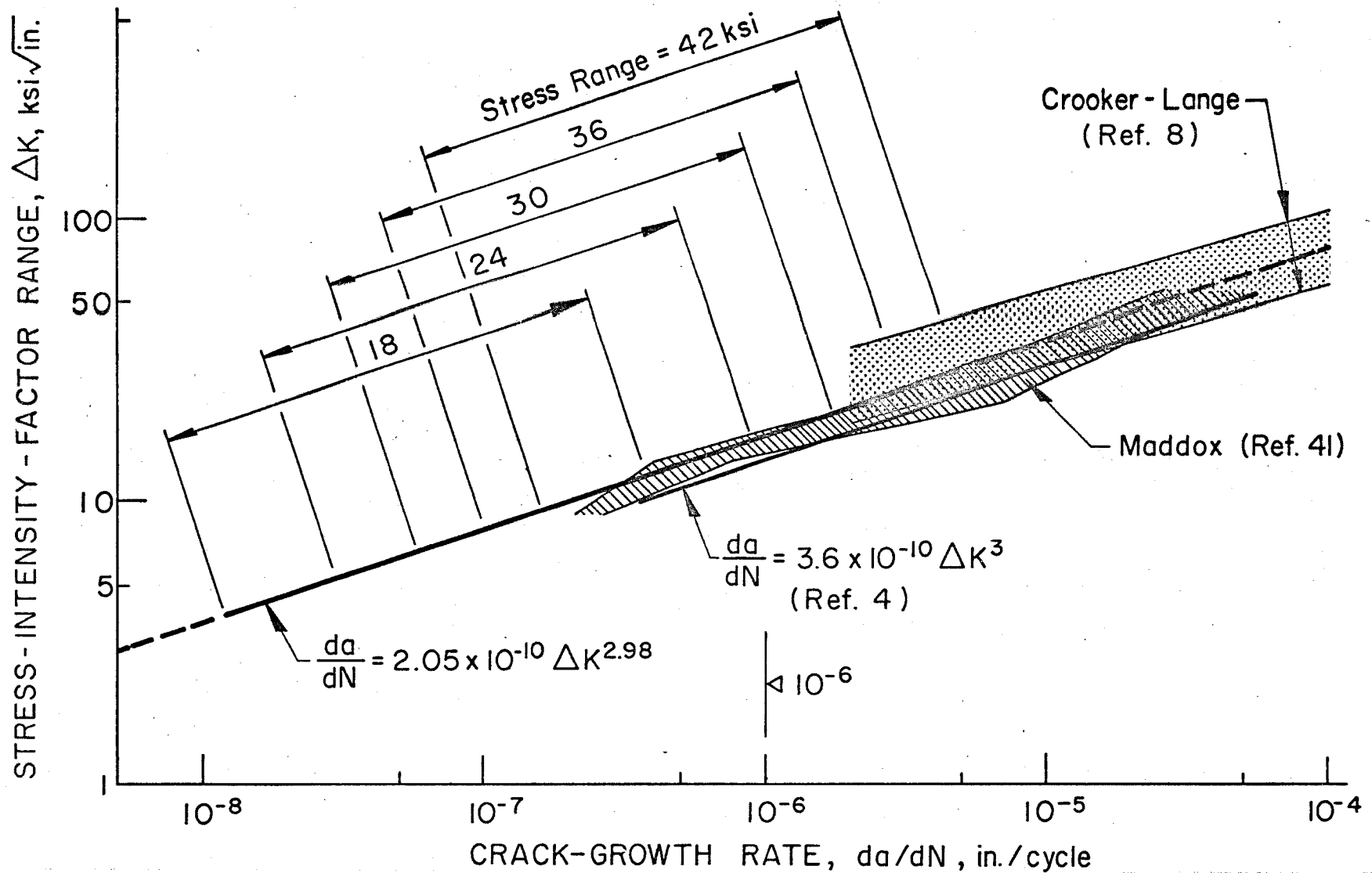


Fig. 31 Ranges for crack growth as a penny-shaped crack. Scatterbands and an upper bound estimate from other crack growth studies.

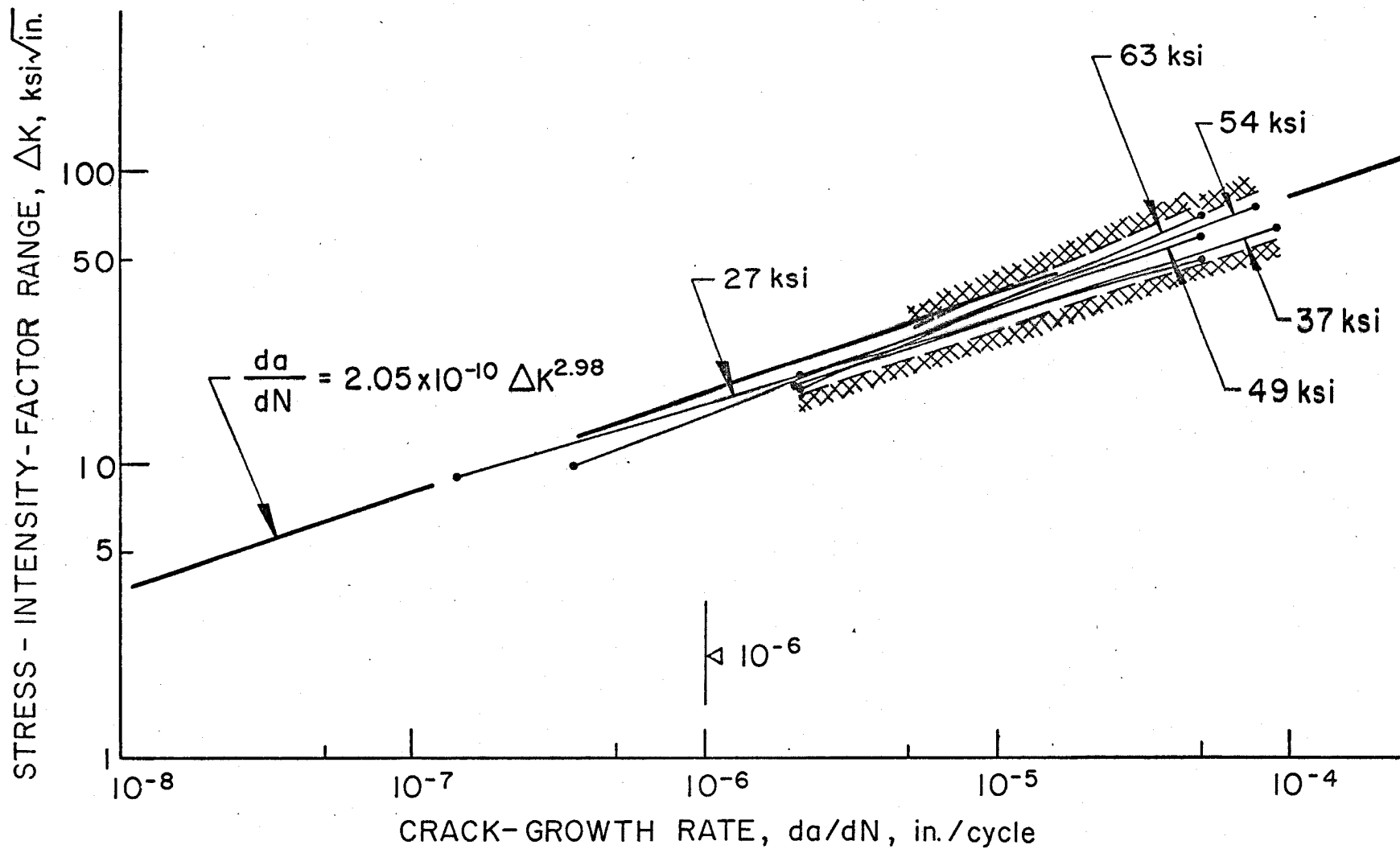


Fig. 32 Comparison of theoretical crack-growth curve with Gurney's test data on a range of steel

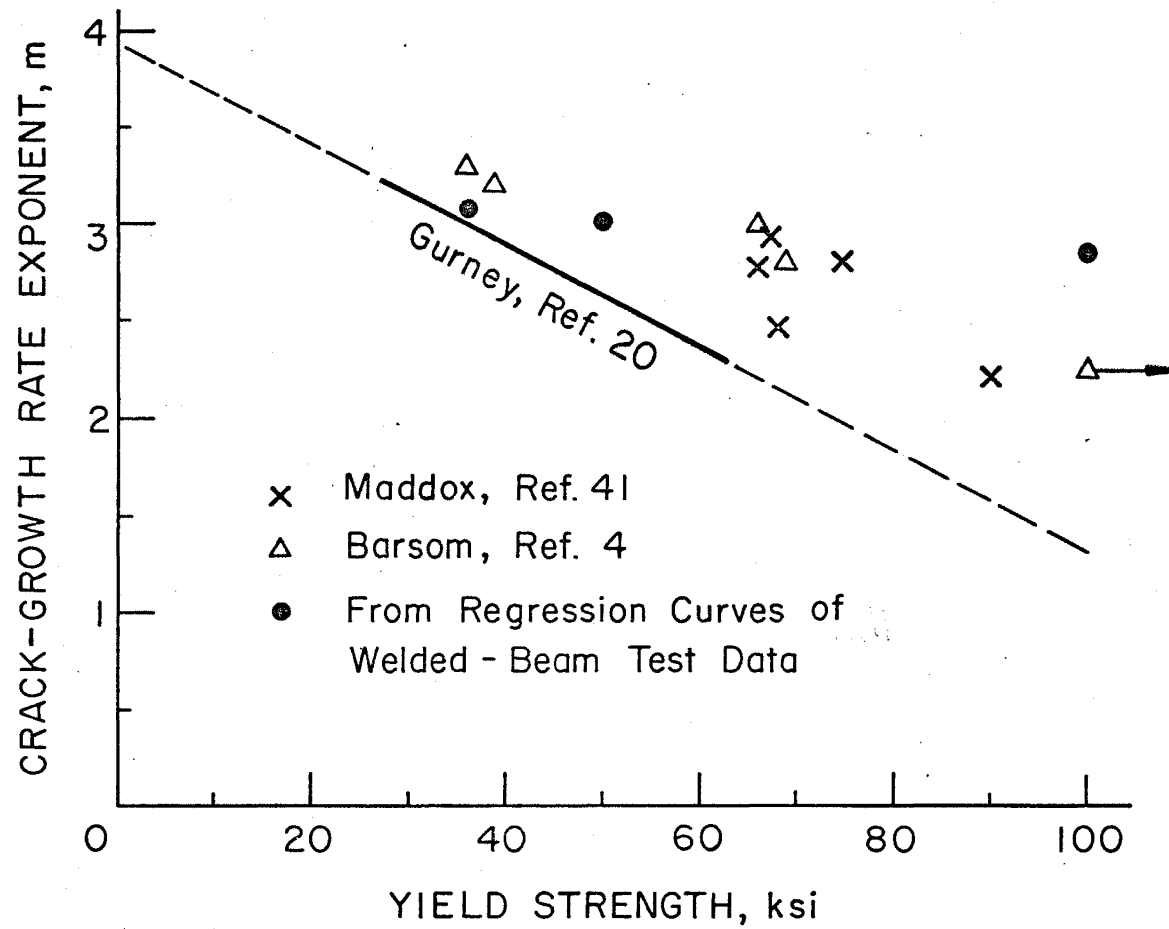


Fig. 33 Variation of exponent m with yield strength

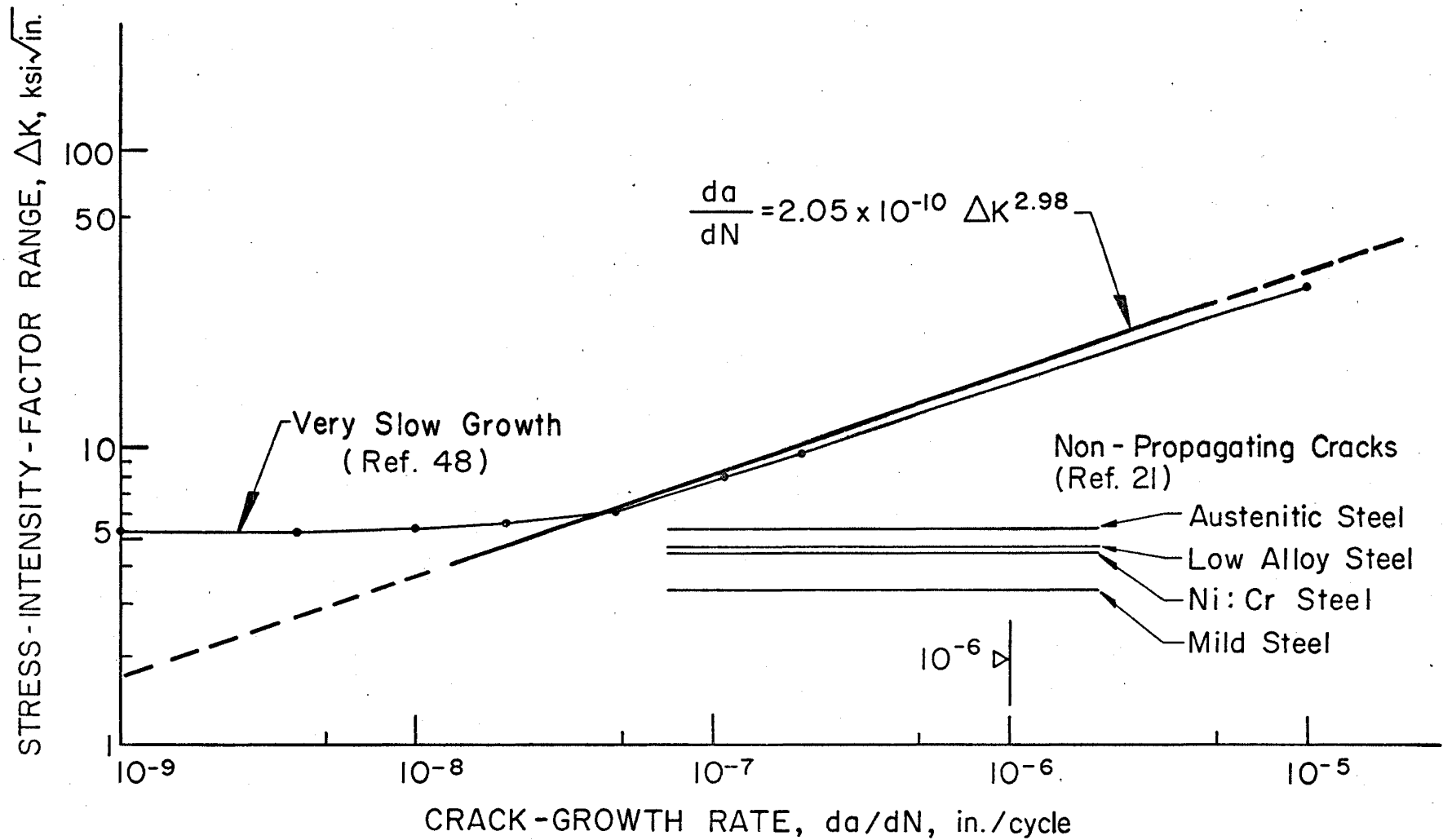


Fig. 34 Approximate mean line of Paris' data for very slow growth, and Harrison's limiting ΔK -values for non-propagating cracks

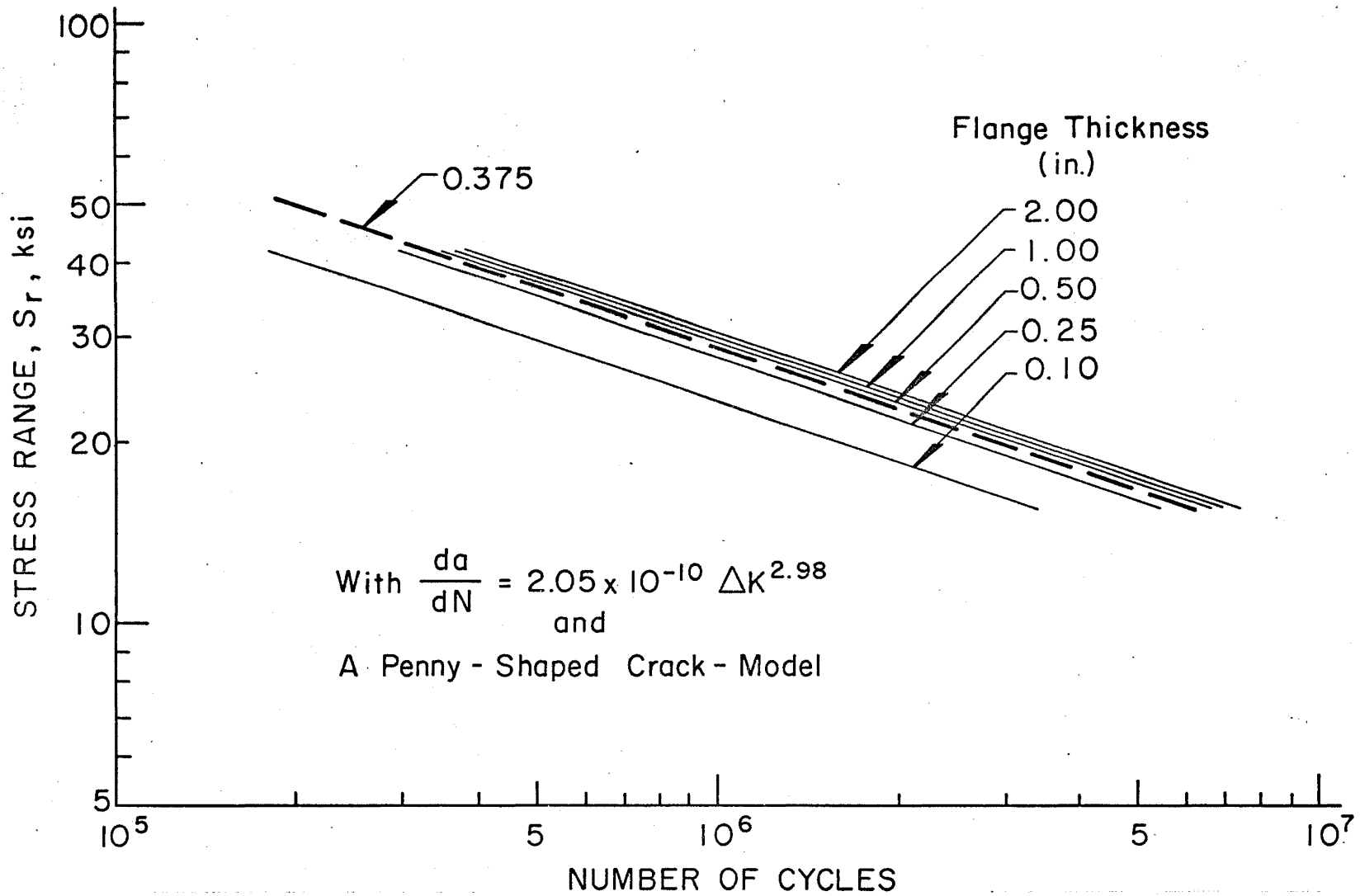


Fig. 35 Effect of flange thickness on the fatigue life of plain-welded beams

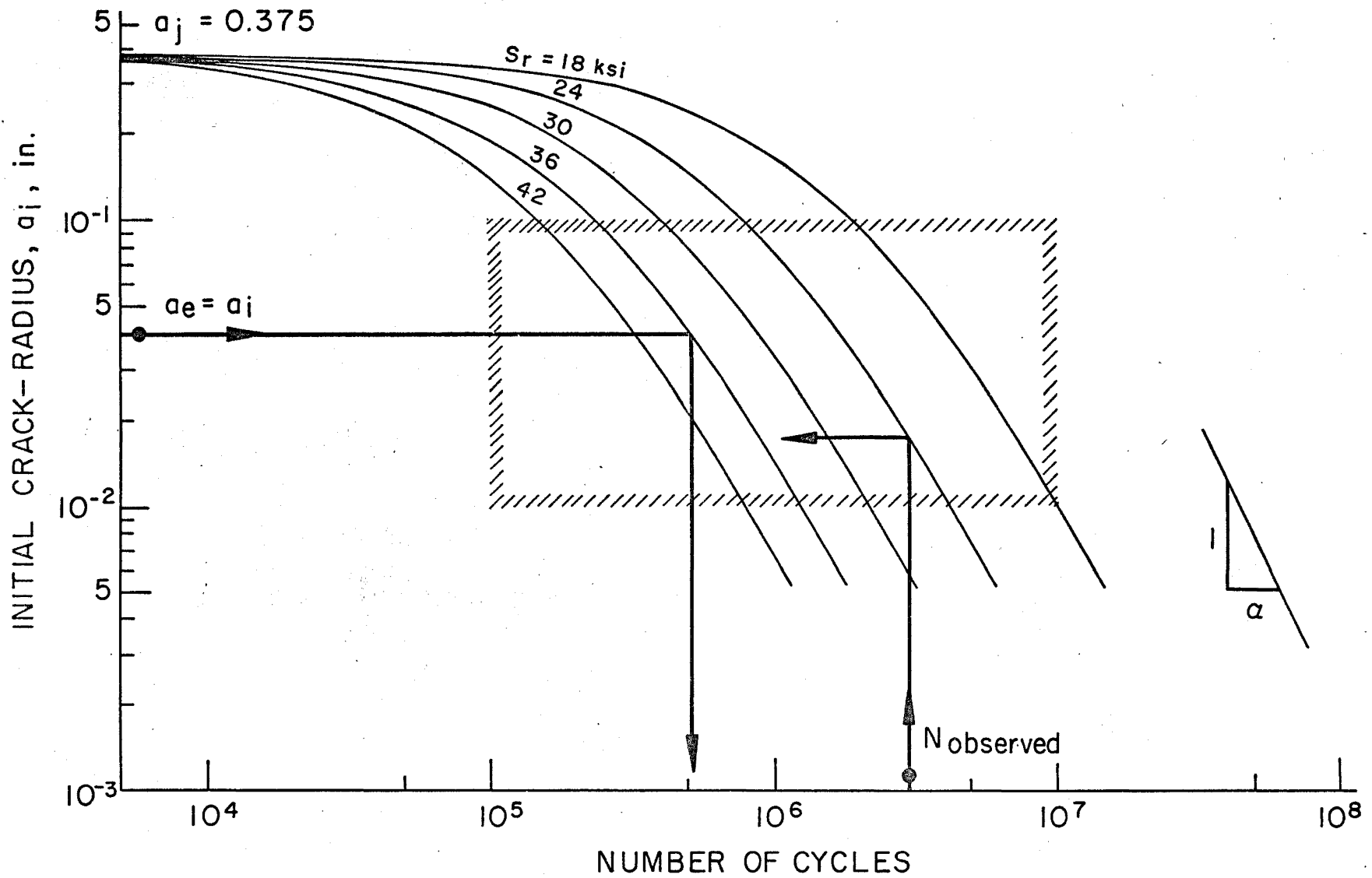


Fig. 36 Number of cycles required to grow a penny-shaped crack from the size a_i to size a_j

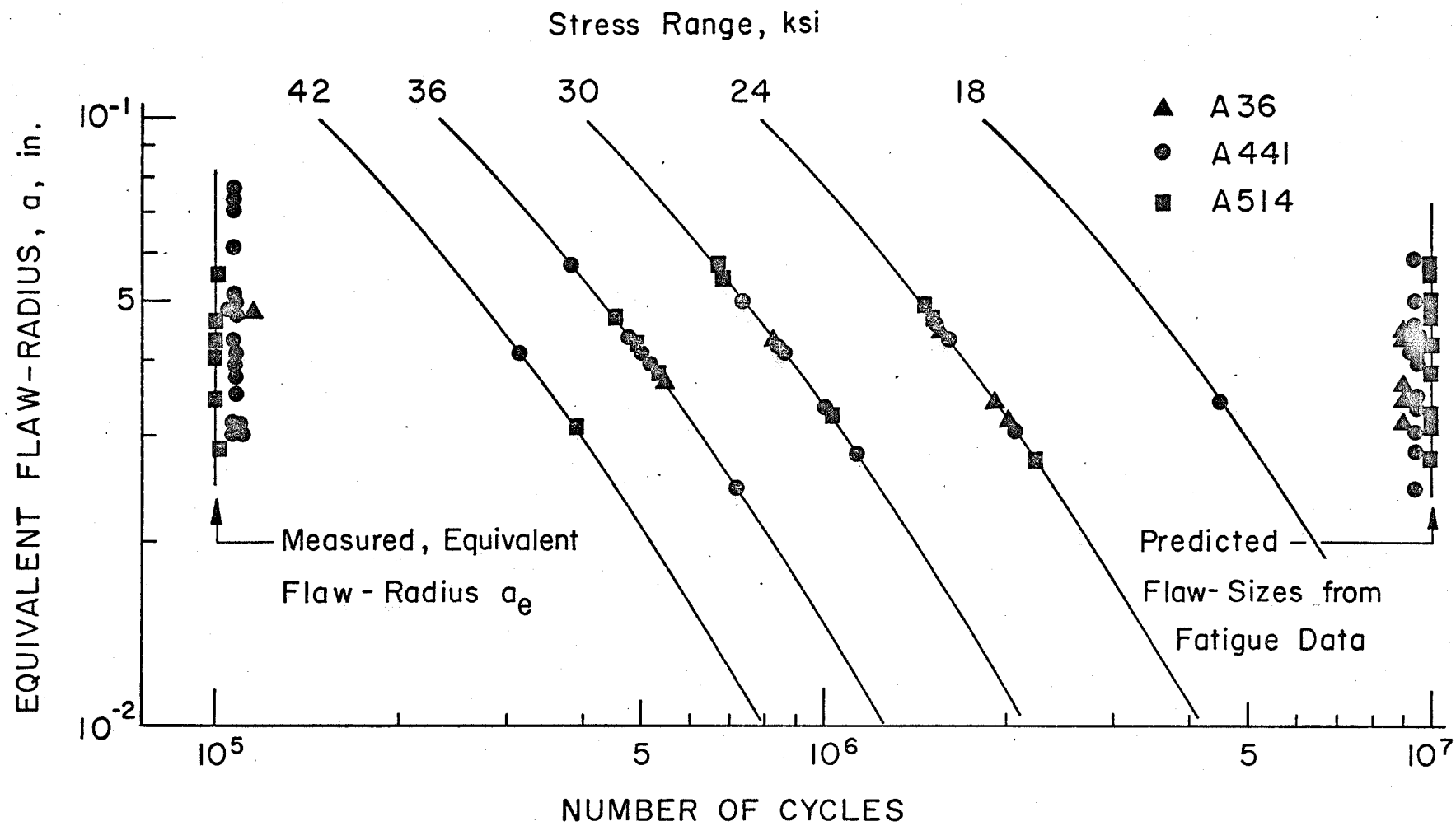


Fig. 37 Comparison of the scatter of measured equivalent flaw-sizes with the scatter of flaw-sizes derived from fatigue data

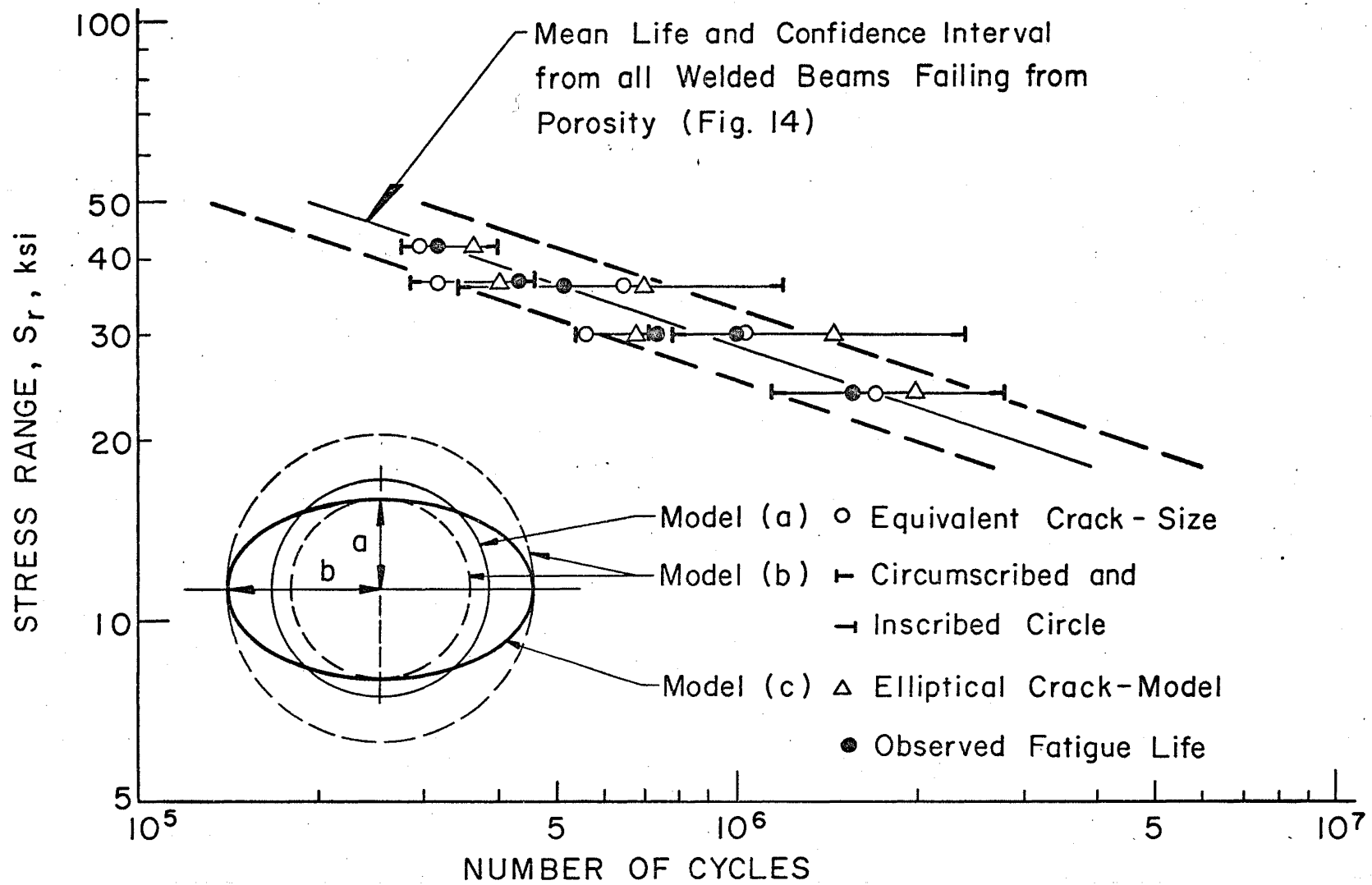


Fig. 38 Prediction of fatigue life using various crack-models

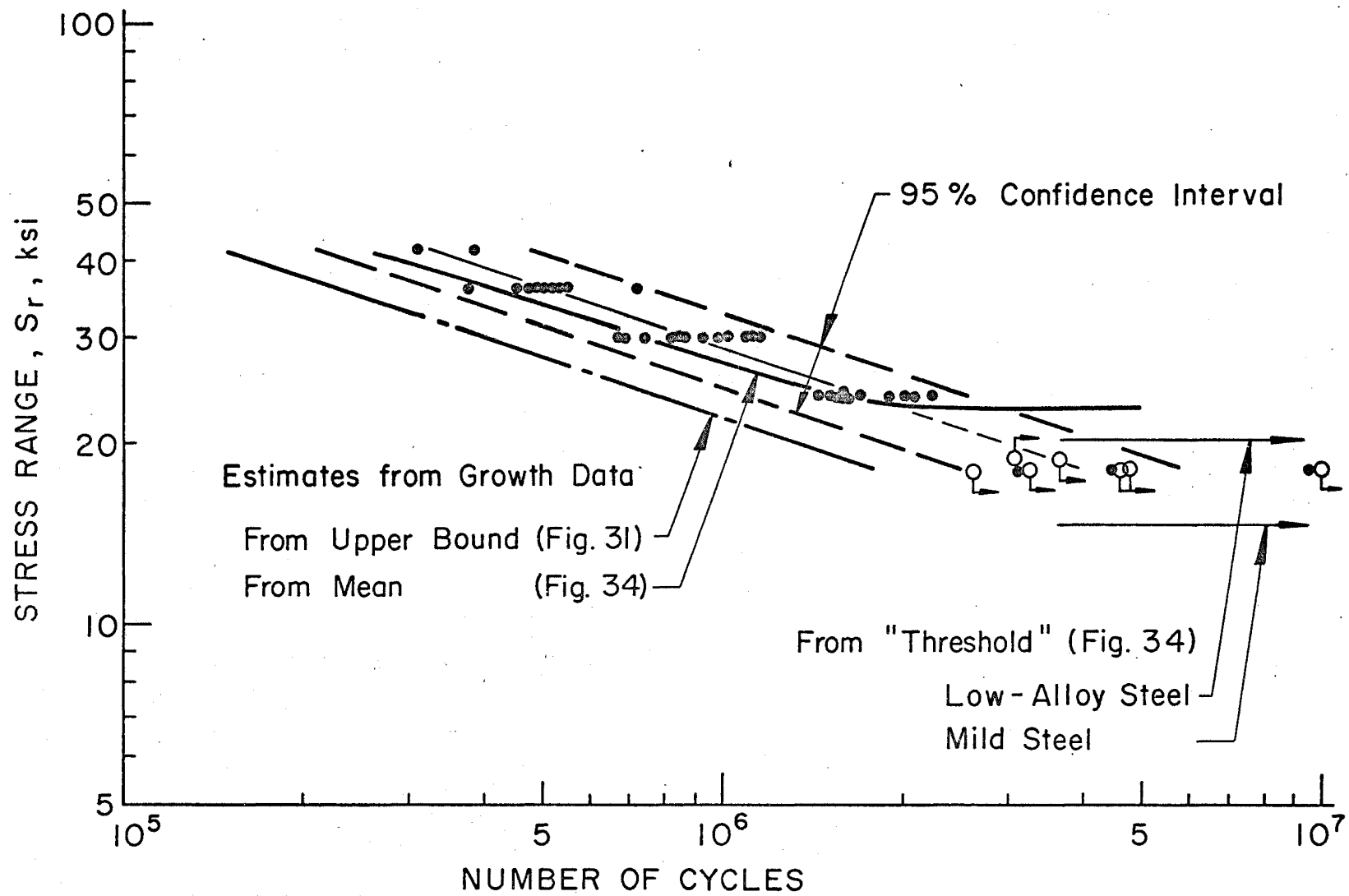


Fig. 39 Comparison of a predicted lower bound and a mean line with mean life and scatterband from test data

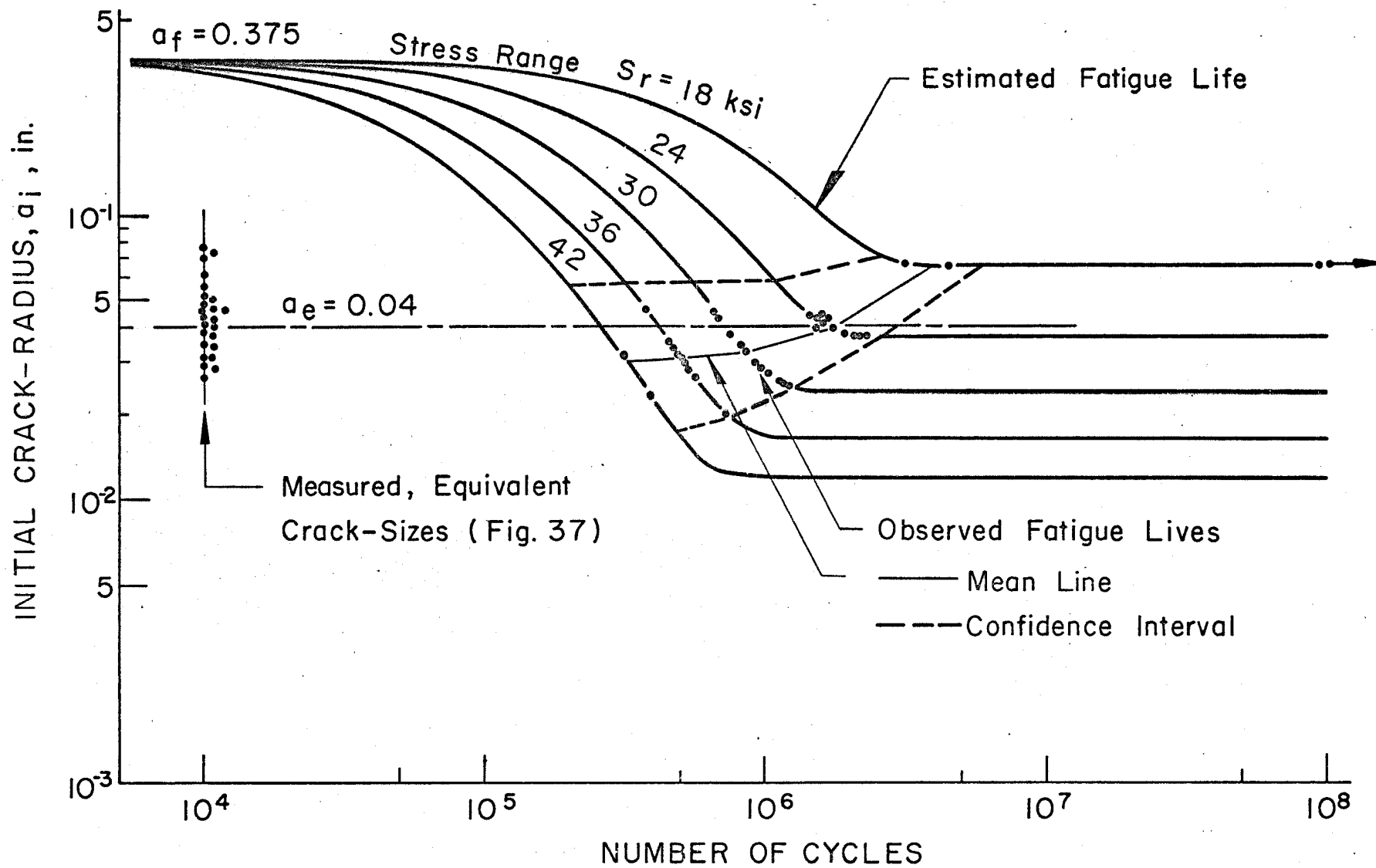


Fig. 40 Prediction of fatigue life based on Paris' data, and comparison with observed fatigue data

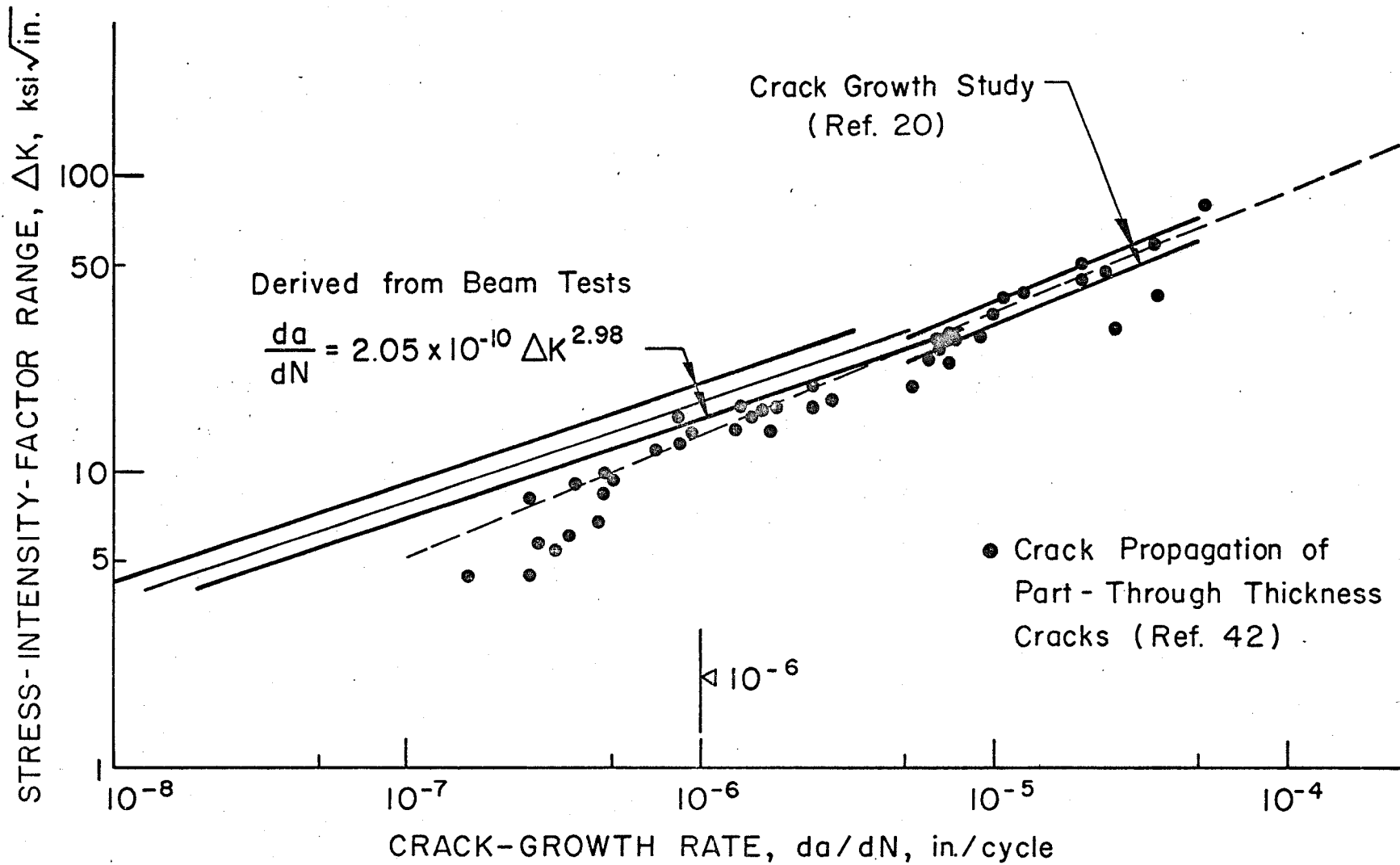


Fig. 41 Comparison of scatterband derived from beam tests with scatter of measurements from crack-growth studies on notched specimens

REFERENCES

1. AASHO
INTERIM SPECIFICATIONS, American Association of State Highway Officials, Washington, D. C., 1971.
2. ASTM
A GUIDE FOR FATIGUE TESTING AND THE STATISTICAL ANALYSIS OF FATIGUE DATA, Special Technical Publication No. 91-A, ASTM, Philadelphia, 1963.
3. AWS
FUNDAMENTALS OF WELDING, Welding Handbook, American Welding Society, Vol. 1, New York, 1968.
4. Barson, J. M.
FATIGUE-CRACK PROPAGATION IN STEELS OF VARIOUS YIELD STRENGTHS, U. S. Steel Corp., Applied Research Laboratory, Monroeville, Pa., 1971.
5. Broek, D. and Schijve, J.
THE INFLUENCE OF THE MEAN STRESS ON THE PROPAGATION OF FATIGUE CRACKS IN ALUMINUM ALLOY SHEET, NLR Tech. Report No. M.2111, National Aerospace Lab., Amsterdam, January, 1963.
6. Braithwaite, A. B. M.
FATIGUE TESTS ON LARGE WELDED PLATE GIRDERS, Report No. D7/36A/65, B. W. R. A., Abington, England, May, 1965.
7. Clark, W. G., Jr., and Trout, H. E. Jr.
INFLUENCE OF TEMPERATURE AND SECTION SIZE ON FATIGUE CRACK GROWTH BEHAVIOR IN Ni-Mo-V ALLOY STEEL, Engineering Fracture Mechanics, Vol. 2, No. 2, November, 1970, pp. 107-123.
8. Crooker, T. W., and Lange, E. A.
HOW YIELD STRENGTH AND FRACTURE TOUGHNESS CONSIDERATIONS CAN INFLUENCE FATIGUE DESIGN PROCEDURES FOR STRUCTURAL STEELS, Welding Research Supplement, Vol. 49, No. 10, October, 1970, pp. 488-496.
9. Davis, O. L.
DESIGN AND ANALYSIS OF INDUSTRIAL EXPERIMENTS, Oliver and Boyd, London, 1954.

10. Fielding, D. J.
FATIGUE TESTS OF SLENDER-WEB HYBRID PLATE GIRDERS UNDER COMBINED MOMENT AND SHEAR, M. S. Thesis, University of Texas, Austin, Tex., June, 1968.
11. Fisher, J. W., Frank, K. H., Hirt, M. A., and McNamee, B. M.
EFFECT OF WELDMENTS ON THE FATIGUE STRENGTH OF STEEL BEAMS, NCHRP Report No. 102, Highway Research Board, National Academy of Sciences - National Research Council, Washington, D. C., 1970.
12. Fisher, W. E., and Stallmeyer, J. E.
BEHAVIOR OF WELDED BUILD-UP BEAMS UNDER REPEATED LOADS, Structural Research Series No. 147, University of Illinois, Department of Civil Engineering, Urbana, Ill., March, 1958.
13. Forman, R. G., Kearney, V. E., and Engle, R. M.
NUMERICAL ANALYSIS OF CRACK PROPAGATION IN CYCLIC-LOADED STRUCTURES, Transactions, ASME, Series D, Vol. 89, No. 3, September, 1967, pp. 459-464.
14. Frost, N. E.
EFFECT OF MEAN STRESS ON THE RATE OF GROWTH OF FATIGUE CRACKS IN SHEET MATERIALS, Journal Mech. Eng. Sci., Vol. 4, No. 1, 1962, pp. 22-35.
15. Frank, K. H.
THE FATIGUE STRENGTH OF FILLET WELDED CONNECTIONS, Ph.D. Thesis, Lehigh University, Department of Civil Engineering, October, 1971.
16. Frank, K. H. and Fisher, J. W.
ANALYSIS OF ERROR IN DETERMINING FATIGUE CRACK GROWTH RATES, Report No. 358.10, Lehigh University, Fritz Engineering Laboratory, March, 1971.
17. Graf, O.
VERSUCHE UEBER DAS VERHALTEN VON GENIETETEN UND GESCHWEISSTEN STOESSEN IN TRAEGERN 130 AUS ST37 BEI OPTIMALS WIEDERHOLTER BELASTUNG, Der Stahlbau, Berlin-Wilmersdorf, January 15, 1937, pp. 9-16.
18. Graf, O.
TESTS OF WELDED BRIDGE GIRDERS, Welding Journal, Vol. 20, 1941, pp. 138-148.

19. Gurney, T. R.
INVESTIGATION INTO THE FATIGUE STRENGTH OF WELDED BEAMS, PART II: HIGH TENSILE BEAMS WITHOUT STIFFENERS, British Welding Journal, Vol. 9, No. 7, July, 1962, pp. 446-454.
20. Gurney, T. R.
AN INVESTIGATION OF THE RATE OF PROPAGATION OF FATIGUE CRACKS IN A RANGE OF STEELS, Members' Report No. E18/12/68, The Welding Institute, December, 1968.
21. Harrison, J. D.
AN ANALYSIS OF DATA ON NON-PROPAGATING FATIGUE CRACKS ON A FRACTURE MECHANICS BASIS, Metal Construction and British Welding Journal, Vol. 2, No. 3, March, 1970, pp. 93-98.
22. Harrison, J. D.
THE ANALYSIS OF FATIGUE TEST RESULTS FOR BUTT WELDS WITH LACK OF PENETRATION DEFECTS USING A FRACTURE MECHANICS APPROACH, Welding in the World, Vol. 8, No. 3, 1970, pp. 168-181.
23. Hertzberg, R. W., and Paris, P. C.
APPLICATION OF ELECTRON FRACTOGRAPHY AND FRACTURE MECHANICS TO FATIGUE CRACK PROPAGATION, Proceedings, First International Conference on Fracture, Vol. 1, 1966, p. 459.
24. Hertzberg, R., and Nordberg, H.
FATIGUE CRACK PROPAGATION IN A514 STEEL, Report No. 358.7, Lehigh University, Fritz Engineering Laboratory, November, 1969.
25. Highway Research Board
AN ANALYSIS OF INSPECTION FACTORS, HRB Special Report, No. 114, Highway Research Board, National Academy of Sciences - National Research Council, Washington, D. C., 1970.
26. Hirt, M. A., Yen, B. T., and Fisher, J. W.
FATIGUE STRENGTH OF ROLLED AND WELDED STEEL BEAMS, Journal of the Structural Division, ASCE, Vol. 97, No. ST7, July, 1971, pp. 1897-1911.
27. Hudson, C. M., and Scardina, J. T.
EFFECT OF STRESS RATIO ON FATIGUE-CRACK GROWTH IN 7075-T6 ALUMINUM-ALLOY SHEET, Engineering Fracture Mechanics, Vol. 1, No. 3, April, 1969, pp. 429-446.

28. Illg, W. and McEvily, A. J. Jr.
THE RATE OF FATIGUE-CRACK PROPAGATION FOR TWO ALUMINUM ALLOYS UNDER COMPLETELY REVERSED LOADING, Technical Note No. D-52, NASA, Washington, D. C., October, 1959.
29. Irwin, G. R.
ANALYSIS OF STRESSES AND STRAINS NEAR THE END OF A CRACK TRAVERSING A PLATE, Transactions, ASME, Series E, Vol. 24, No. 3, September, 1957, pp. 361-364.
30. Irwin, G. R., Liebowitz, H., and Paris, P. C.
A MYSTERY OF FRACTURE MECHANICS, Engineering Fracture Mechanics, Vol. 1, No. 1, June, 1968, pp. 235-236.
31. Jaccard, R. and Fisher, J. W.
FATIGUE STRENGTH OF T-1 MACHINED PLAIN TENSION SPECIMENS, Lehigh University, Fritz Engineering Laboratory, (Report in preparation).
32. Johnson, H. H., and Paris, P. C.
SUB-CRITICAL FLAW GROWTH, Engineering Fracture Mechanics, Vol. 1, No. 1, June, 1968, pp. 3-45.
33. Johnson, K. L. and O'Connor, J. J.
MECHANICS OF FRETTING, Proceedings, The Institution of Mechanical Engineers, Vol. 178, Part 3J, 1963-64, pp. 7-21.
34. Klingerman, D. J., Frank, K. H., and Fisher, J. W.
FATIGUE CRACK GROWTH IN A36 STEEL, Report No. 358.31, Lehigh University, Fritz Engineering Laboratory, May, 1971.
35. Kouba, N. G., and Stallmeyer, J. E.
THE BEHAVIOR OF STIFFENED BEAMS UNDER REPEATED LOADS, Structural Research Series No. 173, University of Illinois, Department of Civil Engineering, Urbana, Ill., April, 1959.
36. Lawrence, F. V., and Radzinski, J. B.
FATIGUE CRACK INITIATION AND PROPAGATION IN HIGH-YIELD-STRENGTH STEEL WELD METAL, Welding Research Supplement, Vol. 49, No. 10, October, 1970, pp. 445-452.
37. Lea, F. C., and Whitman, J. G.
THE FAILURE OF GIRDERS UNDER REPEATED STRESSES, Welding Research Supplement, Vol. 18, No. 1, January, 1939, pp. 28-32.

38. Linnert, G. E.
WELDING METALLURGY, American Welding Society, New York, 1965.
39. Lozano, S., Marek, P., and Yen, B. T.
RESIDUAL STRESS REDISTRIBUTION IN WELDED BEAMS
SUBJECTED TO CYCLIC BENDING, Report No. 358.17,
Lehigh University, Fritz Engineering Laboratory,
June, 1970.
40. Lundin, C. D.
ORIGIN AND NATURE OF WELD DISCONTINUITIES, presented
at the National Meeting of the American Welding
Society, San Francisco, Calif., April 28, 1971.
41. Maddox, S. J.
FATIGUE CRACK PROPAGATION IN WELD METAL AND HEAT
AFFECTED ZONE MATERIAL, Members' Report No. E/29/69,
The Welding Institute, December, 1969.
42. Maddox, S. J.
THE PROPAGATION OF PART-THROUGH-THICKNESS FATIGUE
CRACKS ANALYSED BY MEANS OF FRACTURE MECHANICS,
Members' Report No. E/30/69, The Welding Institute,
December, 1969.
43. Natrella, M. G.
EXPERIMENTAL STATISTICS, Handbook 91, National
Bureau of Standards, August, 1963.
44. Nee, J. D.
FATIGUE STRENGTH OF USS "T-1" CONSTRUCTIONAL ALLOY
STEEL BEAMS WITH AND WITHOUT STIFFENERS, Technical
Report for Project No. 57.019-903(9), U. S. Steel
Corp., Applied Research Laboratory, Monroeville, Pa.
February, 1966.
45. Paris, P. C., and Erdogan, F.
A CRITICAL ANALYSIS OF CRACK PROPAGATION LAWS,
Transactions, ASME, Series D., Vol. 85, No. 4,
December, 1963, pp. 528-534.
46. Paris, P. C.
THE FRACTURE MECHANICS APPROACH TO FATIGUE, Fatigue -
An Interdisciplinary Approach, Proceedings, Tenth
Sagamore Army Materials Research Conference, Syracuse
University Press, Syracuse, N. Y., 1964, p. 107.

47. Paris, P. C., and Sih, G. C.
STRESS ANALYSIS OF CRACKS, Fracture Toughness Testing
and its Applications, Special Technical Publication
No. 381, ASTM, May, 1965, pp. 30-82.
48. Paris, P. C.
TESTING FOR VERY SLOW GROWTH OF FATIGUE CRACKS,
Closed Loop, MTS Systems Corp., Vol. 2, No. 5, 1970,
pp. 11-14.
49. Radziminski, J. B., and Lawrence, F. V. Jr.
FATIGUE OF HIGH-YIELD-STRENGTH STEEL WELDMENTS,
Welding Research Supplement, Vol. 49, No. 8, August,
1970, pp. 365-375.
50. Reemsnyder, H. S.
FATIGUE STRENGTH OF LONGITUDINAL FILLET WELDMENTS IN
USS "T-1" CONSTRUCTIONAL ALLOY STEEL, Report No. 284.6,
Lehigh University, Fritz Engineering Laboratory,
December, 1963.
51. Reemsnyder, H. S.
FATIGUE STRENGTH OF LONGITUDINAL FILLET WELDMENTS IN
CONSTRUCTIONAL ALLOY STEEL, Welding Research Supple-
ment, Vol. 44, No. 10, October, 1965, pp. 458-465.
52. Reemsnyder, H. S.
PROCUREMENT AND ANALYSIS OF STRUCTURAL FATIGUE DATA,
Journal of the Structural Division, ASCE, Vol. 95,
No. ST7, July, 1969, pp. 1533-1551.
53. Rice, J. R.
MECHANICS OF CRACK TIP DEFORMATION AND EXTENSION BY
FATIGUE, Fatigue Crack Propagation, Special Technical
Publication No. 415, ASTM, 1967, pp. 247-309.
54. Schijve, J.
SIGNIFICANCE OF FATIGUE CRACKS IN MICRO-RANGE AND
MACRO-RANGE, Fatigue Crack Propagation, Special
Technical Publication No. 415, ASTM, 1967, pp. 415-457.
55. Sherman, D. R., Hall, L. R., and Stallmeyer, J. E.
FLEXURAL FATIGUE TEST OF WELDED A441 STEEL BEAMS,
Status Report to the Fatigue Committee - Welding
Research Council, University of Illinois, Department
of Civil Engineering, Urbana, Ill., April, 1962.
56. Sherman, D. R., and Stallmeyer, J. E.
FATIGUE OF "T-1" BEAMS, Status Report of the Fatigue
Committee - Welding Research Council, University of
Illinois, Department of Civil Engineering, Urbana,
Ill., May, 1963.

57. Signes, E. G., Baker, R. G., Harrison, J. D., and Burdekin, F. M.
FACTORS AFFECTING THE FATIGUE STRENGTH OF WELDED HIGH STRENGTH STEELS, British Welding Journal, Vol. 14, No. 3, March, 1967, pp. 108-116.
58. Tebedge, N., Alpsten, G. A., and Tall, L.
MEASUREMENT OF RESIDUAL STRESSES - A STUDY OF METHODS, Report No. 337.8, Lehigh University, Fritz Engineering Laboratory, February, 1971.
59. Timoshenko, S., and Goodier, J. N.
THEORY OF ELASTICITY, McGraw-Hill, 1951, pp. 99-107.
60. Watkinson, F., Bodger, P. H., and Harrison, J. D.
THE FATIGUE STRENGTH OF WELDED JOINTS IN HIGH STRENGTH STEELS AND METHODS FOR ITS IMPROVEMENT, Proceedings, Fatigue of Welded Structures Conference, Brighton, Paper No. 7, July, 1970, pp. 97-113.
61. Weibull, W.
FATIGUE TESTING AND ANALYSIS OF RESULTS, Pergamon Press, New York, 1961.
62. Wessel, E. T.
STATE OF THE ART OF WOL SPECIMEN FOR K_{IC} FRACTURE TOUGHNESS TESTING, Engineering Fracture Mechanics, Vol. 1, No. 1, June, 1968, pp. 77-104.
63. Wilhelm, D. P.
INVESTIGATION OF CYCLIC CRACK GROWTH TRANSITIONAL BEHAVIOR, Fatigue Crack Propagation, Special Technical Publication No. 415, ASTM, 1967, pp. 363-379.
64. Wilson, W. M.
FLEXURAL FATIGUE STRENGTH OF STEEL BEAMS, Bulletin No. 377, University of Illinois, Engineering Experiment Station, Urbana, Ill., 1948.

VITA

The author was born in Biel, Switzerland on August 13, 1942, the first child of Arthur and Victoria Hirt and older brother to his sister, Lieselotte. He was married to Hanneliese Mullhaupt in May 1970.

The author received his high school education at the Kantonsschule Solothurn where he graduated in 1961. He attended the Swiss Federal Institute of Technology in Zurich from October 1961 to December 1965. There he completed the requirements of the Department of Civil Engineering and was awarded the degree of a Dipl. Bau-Ing. ETH.

In January 1966 he joined Basler & Hofmann, Consulting Engineers, in Zurich, and was employed as a structural designer and analyst for one and one-half years.

He entered graduate school in September 1967 in the Department of Civil Engineering, Lehigh University, and worked as a half-time research assistant in Fritz Engineering Laboratory. He has been associated with research in fatigue which formed the basis for his doctoral work.